

THE EFFECT OF INTERFACE GEOMETRY ON FLOW LOSSES IN RIGHT-
ANGLED TEE JUNCTIONS

A Thesis

Presented in Partial Fulfillment of the Requirements for
the Degree Master of Science in the
Graduate School of The Ohio State University

By

Adam Michael Christian, B.S.M.E.

The Ohio State University
2003

Master's Examination Committee:

Dr. Ahmet Selamet, Adviser

Dr. Walter R. Lempert

Dr. Mohammad Samimy

Approved by

Adviser

Department of Mechanical Engineering

ABSTRACT

The present study investigates losses associated with the dividing flow at right-angle T-junctions. An experimental setup was constructed to measure the flow loss coefficients of T-junctions with circular through ducts and side branches of varying shape and cross-sectional area. Dividing flow experiments were conducted with twenty junction configurations on a steady-flow bench using air as the working fluid. Seven junctions with circular side branches were tested to determine the effects of: (1) interface radius equal to 0, 10, and 20% of the side branch diameter, (2) through duct to side branch area ratios of 1, 2.124, and 3.117, and (3) side branch taper including taper area ratios of 2.124 and 3.117. The last two categories employed 20% interface radii. Thirteen junctions with side branches of square, rectangular, and oval cross-section were investigated for area ratios of 1, 2.124, and 3.117 with 20% interface radii to quantify side branch shape effects. Junctions with rectangular and oval cross-section were also studied with side branch aspect ratios equal to 1/2 and 2. The total mass flow rate was also varied to examine the effect of Reynolds number on loss coefficients. Interface radii and primary runner taper were found to significantly reduce the losses. In the turbulent regime, loss coefficients were found to be independent of the through-duct Reynolds number. Side branch cross-sectional shape was found to have only a minor

effect on flow losses. A subset of results presented in this study was compared with the available literature.

Dedicated to my family

ACKNOWLEDGMENTS

I would like to thank my adviser, Dr. Ahmet Selamet, for his guidance and support. Throughout the entire work, never did he show any loss of confidence in my ability to do accurate work. I am grateful to the members of my committee, Dr. Walter Lempert and Dr. Mohammad Samimy for their review of this work and their suggestions.

I am sincerely grateful to the Powertrain Operations Division of Ford Motor Company for their support. Those who gave their very valuable time and resources include Jim Novak, Kevin Tallio, Ed Hernandez, Thomas Sanders, and Ken Tyrer. I would especially like to thank Keith Miazgowicz for his fantastic support of this project from its inception.

I would like to thank my coworkers at the Center for Automotive Research for their assistance and friendship during the last three years. I have been privileged to work with such talented people as Iljae Lee, Yale Jones, Cam Giang, William Erskine, Todd Howard, Andrew Madden, Jacques Paul, and Lauren Lecuru. I am particularly indebted to Dr. Nolan Dickey, who served many hours as an audience for my ideas and rants.

Finally I would like to thank my family and friends. Without their support, encouragement, and most importantly understanding, this would not have been possible. My sincerest gratitude goes to my fiancée, Amanda, who has sacrificed greatly to help me follow my dreams.

VITA

March 9, 1977Born – Columbus, Ohio

2000.....B.S. Mechanical Engineering,
The Ohio State University.

2000 - present.....Graduate Research Associate,
The Ohio State University

PUBLICATIONS

Research Publication

1. S. Merriman, A. Christian, R. Meyer, B. Kowalczyk, P. Palm, and I. V. Adamovich, "Studies of Conical Shockwave Modification by Nonequilibrium RF Discharge Plasma", paper 01-0347, presented at 39th AIAA aerospace sciences meeting and exhibit, Reno, NV, January 8-11, 2001
2. A. Christian, A. Selamet, K.D. Miazgowicz, and K.V. Tallio, "Flow Losses at Circular T-Junctions Representative of Intake Plenum and Primary Runner Interface", SAE paper 04Annual-821, 2004

FIELDS OF STUDY

Major Field: Mechanical Engineering

TABLE OF CONTENTS

	Page
Abstract.....	ii
Dedication.....	iii
Acknowledgments.....	iv
Vita.....	v
List of Tables	ix
List of Figures.....	x
Nomenclature.....	xi
Chapter	
1. Introduction.....	1
1.1 Background.....	1
1.2 Literature Survey	3
1.3 Objective.....	6
2. Losses In Internal Flows	10
2.1 Frictional Losses	10
2.2 Area-Pressure Relation	13
2.3 Dividing Flow Loss Coefficients.....	14
3. Experimental Setup.....	20

3.1	Flow Bench	20
3.2	Pressure Measurement	22
3.3	Straight Tube Setup.....	24
3.4	T-junction Setup.....	28
3.5	Sharp-Edged Orifice Flow Measurement	37
4.	Data Reduction and Analysis.....	42
4.1	Friction Factor Determination.....	42
4.2	T-Junction Loss Determination.....	46
5.	Results.....	50
5.1	Straight Tube.....	50
5.2	T-Junctions.....	53
5.2.1	Flow Loss Development Lengths	53
5.2.2	Reynolds Number Dependence and Curve Fitting	60
5.2.3	Comparisons with Published Data	67
5.2.4	Interface Radius, Area Ratio, and Side Duct Taper Effects	70
5.2.5	Side Branch Aspect Ratio and Shape Effects	77
6.	Concluding Remarks.....	87
Appendices		
A	Measured Loss Coefficients for Junctions with Noncircular or Tapered Side Ducts	92
B	Curve Fit Coefficients	106
	Bibliography	111

LIST OF TABLES

<u>Table</u>	<u>Page</u>
3.1 Average measured equivalent diameter for fabricated ducts.....	27
3.2 Equations for area and hydraulic diameter	27
3.3 Junctions with circular side branches tested	33
3.4 Junctions with tapered circular side branches.....	34
3.5 Junctions with square side branches	34
3.6 Junctions with rectangular side branches.....	35
3.7 Junctions with oval side branches.....	36
3.8 Approximate flow rate ranges for sharp-edged orifices	38
B.1 Curve fit coefficients for junctions with circular side branches.....	107
B.2 Curve fit coefficients for junctions with tapered circular side branches.....	108
B.3 Curve fit coefficients for junctions with square side branches	108
B.4 Curve fit coefficients for junctions with rectangular side branches.....	109
B.5 Curve fit coefficients for junctions with oval side branches.....	110

LIST OF FIGURES

<u>Figure</u>	<u>Page</u>
1.1 Combining and dividing flow types for right-angled tees.	2
2.1 Differential control volume for fully developed flow in a straight duct.....	11
2.2 Differential control volume for flow in a variable area duct.	14
2.3 Dividing flow control volumes	19
3.1 Compressor and flow nozzle arrangement.....	21
3.2 Triple-T piezometric ring.....	22
3.3 Straight duct friction factor setup	25
3.4 Cross-sections investigated: (a) circular, (b) square, (c) rectangular, (d) oval	28
3.5 Tee junction connections and common dimensions	29
3.6 T-junction dividing flow setup.....	31
3.7 Sharp-edged orifice installation	38
3.8 Flow orifice calibration: (a) $d_o = 22.86$ mm, (b) $d_o = 31.75$ mm.....	39
3.9 Flow orifice calibration: (a) $d_o = 41.91$ mm, (b) $d_o = 50.8$ mm.....	40
3.10 Flow orifice calibration: $d_o = 57.15$ mm	41
4.1 Pressure gradient in fully developed region.....	44
4.2 Pressure drop along combined or straight duct downstream of junction.....	47
5.1 Measured friction factor for varying duct shape: (a) circular, (b) square, (c) rectangular	51

5.2	Losses as a function of distance from interface of circular junction, $A_c/A_s=1$, $r=0$: (a) side duct, (b) straight duct	54
5.3	Losses as a function of distance from interface of circular junction, $A_c/A_s=1$, $r=0.1$ Ds: (a) side duct, (b) straight duct.....	55
5.4	Losses as a function of distance from interface of circular junction, $A_c/A_s=1$, $r=0.2$ Ds: (a) side duct, (b) straight duct	56
5.5	Losses as a function of distance from interface of circular junction, $A_c/A_s=2.124$, $r=0.2$ Ds: (a) side duct, (b) straight duct.....	58
5.6	Losses as a function of distance from interface of circular junction, $A_c/A_s=3.117$, $r=0.2$ Ds: (a) side duct, (b) straight duct	59
5.7	Losses for circular junction, $A_c/A_s=1$, $r=0$: (a) K_{cs} , (b) K_{cst}	61
5.8	Losses for circular junction, $A_c/A_s=1$, $r=0.1$ Ds: (a) K_{cs} , (b) K_{cst}	62
5.9	Losses for circular junction, $A_c/A_s=1$, $r=0.2$ Ds: (a) K_{cs} , (b) K_{cst}	63
5.10	Losses for circular junction, $A_c/A_s=2.124$, $r=0.2$ Ds: (a) K_{cs} , (b) K_{cst}	65
5.11	Combining and dividing flow types for right-angled tees.	66
5.12	Comparison of current results with published data for circular junction, $A_c/A_s=1$, $r=0$: (a) K_{cs} , (b) K_{cst}	68
5.13	Comparison of current measurements of K_{cs} with published data for circular junction, $A_c/A_s=1$: (a) $r=0.1$ Ds, (b) $r=0.2$ Ds.....	69
5.14	Effect of interface radius on losses for circular junction, $A_c/A_c=1$: (a) K_{cs} , (b) K_{cst}	72
5.15	Effect of A_c/A_s on losses for circular junction, $r=0.2$ Ds: (a) K_{cs} , (b) K_{cst}	74
5.16	Effect of side branch taper on losses for circular junction, $A_c/A_s=2.124$, $r=0.2$ Di: (a) K_{cs} , (b) K_{cst}	75

5.17	Effect of side branch taper on losses for circular junction, $A_c/A_s=3.117$, $r=0.2 D_i$: (a) K_{cs} , (b) K_{cst}	76
5.18	Effect of area ratio on losses for tapered circular junction, $r=0.2 D_i$, $A_c/A_i=1$: (a) K_{cs} , (b) K_{cst}	78
5.19	Effect of aspect ratio on losses for rectangular junction, $A_c/A_s=1$, $r=0.2 D_s$: (a) K_{cs} , (b) K_{cst}	79
5.20	Effect of side branch aspect ratio on losses for rectangular junction, $A_c/A_s=2.124$, $r=0.2 D_s$: (a) K_{cs} , (b) K_{cst}	80
5.21	Effect of side branch aspect ratio on losses for rectangular junction, $A_c/A_s=3.117$, $r=0.2 D_s$: (a) K_{cs} , (b) K_{cst}	81
5.22	Effect of side branch shape on losses for all junctions with $A_c/A_s=1$ and $r=0.2 D_s$: (a) K_{cs} , (b) K_{cst}	83
5.23	Effect of side branch shape on losses for all junctions with $A_c/A_s=2.124$ and $r=0.2 D_s$: (a) K_{cs} , (b) K_{cst}	84
5.24	Effect of side branch shape on losses for all junctions with $A_c/A_s=3.117$ and $r=0.2 D_s$: (a) K_{cs} , (b) K_{cst}	85
A.1	Losses for tapered circular junction, $A_c/A_i=1$, $A_c/A_s=2.124$, $r=0.2 D_s$: (a) K_{cs} , (b) K_{cst}	93
A.2	Losses for tapered circular junction, $A_c/A_i=1$, $A_c/A_s=3.117$, $r=0.2 D_s$: (a) K_{cs} , (b) K_{cst}	94
A.3	Losses for square junction, $A_c/A_s=1$, $r=0.2 D_s$: (a) K_{cs} , (b) K_{cst}	95
A.4	Losses for square junction, $A_c/A_s=2.124$, $r=0.2 D_s$: (a) K_{cs} , (b) K_{cst}	96
A.5	Losses for square junction, $A_c/A_s=3.117$, $r=0.2 D_s$: (a) K_{cs} , (b) K_{cst}	97
A.6	Losses for rectangular junction, $A_c/A_s=2.124$, $W/H=2$, $r=0.2 D_s$: (a) K_{cs} , (b) K_{cst}	98

A.7	Losses for rectangular junction, $A_c/A_s=3.117$, $W/H=2$, $r=0.2 D_s$: (a) K_{cs} , (b) K_{cst}	99
A.8	Losses for rectangular junction, $A_c/A_s=1$, $W/H=1/2$, $r=0.2 D_s$: (a) K_{cs} , (b) K_{cst}	100
A.9	Losses for rectangular junction, $A_c/A_s=2.124$, $W/H=1/2$, $r=0.2 D_s$: (a) K_{cs} , (b) K_{cst}	101
A.10	Losses for rectangular junction, $A_c/A_s=3.117$, $W/H=1/2$, $r=0.2 D_s$: (a) K_{cs} , (b) K_{cst}	102
A.11	K_{cst} for oval junction, $W/H=2$, $r=0.2 D_s$: (a) $A_c/A_s=2.124$, (b) $A_c/A_s=3.117$	103
A.12	K_{cst} for oval junction, $W/H=1/2$, $r=0.2 D_s$: (a) $A_c/A_s=1$, (b) $A_c/A_s=2.124$	104
A.13	K_{cst} for oval junction, $A_c/A_s=3.117$, $W/H=1/2$, $r=0.2 D_s$	105

NOMENCLATURE

a	square or rectangular duct height
A	duct cross-sectional area
b	rectangular duct width, curve fit coefficient
c	curve fit coefficient
d	pressure tap diameter, duct diameter
D	duct diameter
e	fluid internal energy
f	Fanning friction factor
g	acceleration due to gravity
H	side branch height
K	flow loss coefficient
\dot{m}	mass flow rate
M	Mach number
p	static pressure
\mathcal{P}	duct wetted perimeter
\dot{Q}	heat transfer rate
Q	volumetric flow rate
Re	Reynolds number

S	kinematic viscosity curve fit coefficient
T	fluid temperature
U	mean fluid velocity
W	work done by fluid, side branch width
x	distance along duct longitudinal axis
z	fluid height

Greek symbols

γ	ratio of specific heats
Δ	difference
μ	kinematic viscosity
ρ	fluid density
σ	stress
τ	shear stress

Subscripts

a	ambient
c	combined duct

<i>CS</i>	control surface
<i>CV</i>	control volume
<i>e</i>	equivalent
<i>f</i>	friction
<i>h</i>	hydraulic
<i>i</i>	tap location index, side branch interface, orifice inlet
<i>in</i>	junction inlet
<i>j</i>	downstream duct index
<i>l</i>	local
<i>o</i>	orifice
<i>s</i>	side duct
<i>st</i>	straight duct
<i>t</i>	total
<i>w</i>	wall

CHAPTER 1

INTRODUCTION

1.1 Background

A flow loss can be described as the conversion of fluid kinetic and/or potential energy into heat by the way of friction and turbulent mixing. They occur whenever an internal viscous flow encounters mixing, separation, or shear. In engineering applications, flow losses typically result in a decrease in system efficiency due to the increased work required to move the fluid. Due to the turbulent, unsteady nature of flow losses with separation, it is often difficult to predict the performance of many flow configurations analytically. Their performance can be estimated, however, by the use of nondimensionalized loss coefficients determined experimentally.

A common flow loss component in engineering applications is a junction, which is formed by the intersection of three or more ducts at their ends and separated by an angle between their longitudinal axes. Tee junctions are a subset of three branch junctions in which two ducts of equal cross-section form a single through duct that is intersected at its midpoint by the third duct or side branch. There are a total of four unique flow configurations for right-angled tees as shown in Figure 1.1. These configurations can be categorized as two combining and two dividing flow types. For

junctions with through duct to side branch angle other than 90° there are two additional configurations (one combining and one dividing) due to the asymmetry of the junction.

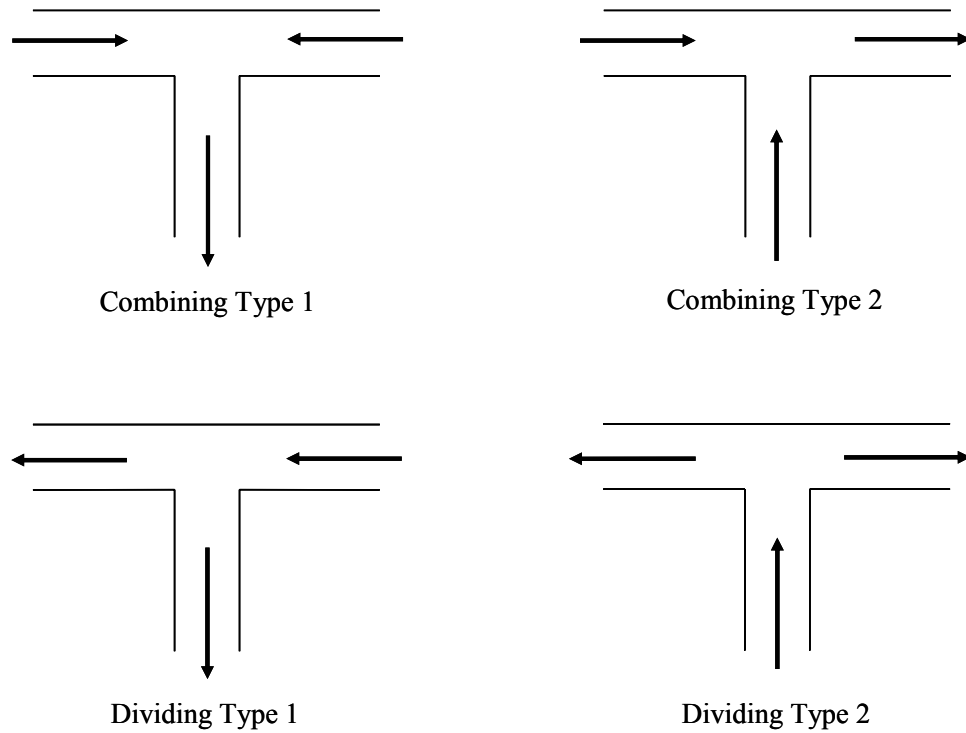


Figure 1.1: Combining and dividing flow types for right-angled tees.

Many loss components, such as bends or diffusers, can be described by a single loss coefficient for a given geometry, while junction flow losses are more complicated in that they require separate coefficients to describe losses between each pair of ducts, which are also functions of the relative flow in the branches of the junction. Some predominate parameters for T-junction geometry are the through duct to side branch area ratio, angle between the through duct and branch, duct cross-sectional shapes, and

modifications of the junction interface by radii or chamfers. Such an extensive set of parameters makes a comprehensive experimental determination of junction performance rather difficult. In fact, in spite of research on the topic since the early 1900's there has yet to be a truly systematic and complete experimental study of even a small subset of possible geometries.

1.2 Literature Survey

Some of the earliest experimental work (Vogel, 1926,1928; Petermann, 1929; Kinne, 1931) was conducted by a group led by D. Thoma at the hydraulic laboratory of the Technical University of Munich. Vogel (1926, 1928) performed experiments with right-angled circular junctions of varying interface radius, area ratio, and side branch taper. Using water flowing in iron pipes with through-duct diameter $D=43$ mm, dividing type 1 and combining type 2 (Recall Figure 1.1) loss coefficients were measured for all geometries tested. For junctions with all three branches of equal diameter, Vogel showed that both interface radius and area ratio had significant effects on junction losses. Loss coefficients were also found to be independent of flow rate for incompressible flow in the turbulent regime.

The work of Vogel was continued by Petermann (1929) for junctions with side branch angle of 45° and varying area ratio, radius, and branch taper. During Petermann's work it was found that: (1) the frictional losses in the ducts used by Vogel had changed due to oxidation of the iron material; and (2) the frictional losses in the sections of iron pipe were large in relation to those caused by the junction. To improve accuracy, the setup was remade with junctions and tubes made of smooth brass and although not

specified explicitly, higher flow rates were used to increase the measured pressure drops. Petermann found that branch angle and side branch taper had significant effects on junction losses.

Kinne (1931) continued experiments using the experimental setup of Petermann for junctions with area ratios, branch tapers, and interface radii equal to those studied by Petermann, with branch angles of 60° . The measurements made by Vogel for right-angled junctions with area ratio of unity and varying interface radius of 0, 0.1, and 0.2 D were also repeated by Kinne using the more accurate experimental setup.

Experiments similar to those performed at Munich were conducted by a group at the State University of Iowa under the leadership of J.S. McNown (1954) with a more thorough investigation of a smaller test matrix than that of the Munich group. With water as the working fluid, these experiments quantified the effect of area ratio on combining type 2 and dividing type 1 loss coefficients for sharp-edged, circular, right-angled tees with through-duct diameters of $D=52$ mm.

Combining type 2 and dividing type 1 flows were also studied by Gardel (1957) using water flowing in circular junctions made of asbestos concrete with through-duct diameters of $D=150$ mm. Experiments were conducted with Reynolds number ranging from 2.5×10^5 to 3.4×10^5 in the duct carrying the combined flow. The effects of branch angle on losses in junctions of area ratio equal to unity, and of area ratio on right angled junctions were studied using 11 junction geometries. While interface radii were used on nearly all junctions tested, their size was not precisely controlled, giving a somewhat random sample of radius effects. Using these results, as well as those published by the Munich group, Gardel presents empirical equations for losses as functions of flow ratio,

area ratio, interface radius, and branch angle. The experiments were repeated by Gardel *et al.* (1971) with a focus on increased accuracy. The experimental setup was similar to that in 1957 and the test matrix was expanded to measure losses for all four flow configurations in 33 geometries. The junction fabrication was also more closely controlled yielding junctions with area ratio of unity and varying interface radius of 0, 0.1, and 0.2 D.

An investigation of radius effects on junction losses was performed by Ito *et al.* (1973) for circular, right-angled junctions with area ratio of unity. Using water as the working fluid in ducts of diameter $D=35$ mm, flow loss coefficients were found for all four flow configurations in tees with side branch to through duct interface radii equal to 0, 0.091, 0.188 and 0.502 D. Experiments were conducted with Reynolds number equal to 1×10^5 and 2×10^5 in the duct carrying the combined flow. Empirical equations were presented for the flow losses as functions of interface radius and flow ratio.

A review of several published works was performed by Miller (1971) in addition to experimental work quantifying the performance of junctions with square through ducts of width $D=305$ mm and square or circular side branches. Using air as the working fluid, several right-angled junctions were tested for all flow configurations with through duct to side branch area ratios of 1, 1.27, and 2.86, and side branch interface chamfers of 1, 1/2, and 1/8 D. This work, combined with other published data, was later compiled (Miller, 1990) and curve fit providing numerous charts for junction flow losses as functions of area ratio, branch angle, interface radius or chamfer, and flow ratio. Not covered in these charts, however, are junctions both of area ratio other than unity and interface radii larger than 10% of the side branch diameter.

Analytical relations predicting the performance of dividing flows in junctions of varying branch angle and fixed area ratio of unity were presented by Hager (1984). The primary assumptions used in this work were that the flow stagnates on the far edge of the branch interface, and that the flow entering the branch deviates from the axis of the through duct by an angle equal to 1/4th that of the branch angle. The predictions were found to correlate well with published experimental data. This work was extended by Basset et al. (1999) by the addition of variable area ratio and branch taper, and additional relations for the remaining flow configurations. The predictions show the correct directional trends for the effects of area ratio and branch angle. However, a major parameter identified by experimental studies, junction interface radius or chamfer, is not represented in these relations.

1.3 Objective

The objective of the thesis is to experimentally determine the flow losses associated with dividing type 1 flow in right-angled junctions of varying geometry. Experiments will be conducted using air flowing at varying through-duct flow rates to investigate any dependence of junction loss coefficients on through-duct Reynolds number. The development of flow after separation at the junction interface will also be measured to determine the distance necessary for loss coefficients to be fully realized. Twenty junction configurations will be examined to determine the effects of: (1) through to side duct interface radius, (2) through to side duct area ratio, (3) side duct taper, and (4) side duct shape.

Despite the volume of work on the subject of flows in three-branch junctions, there is still a lack of understanding in the performance of junctions flowing air over a wide range of through-duct velocities. Several researchers have found that junction loss coefficients are independent of through-duct flow rate for Reynolds numbers above $Re=10^5$. However, the high Reynolds flows were typically reached using water as the working fluid, or air in large ducts flowing at relatively low velocities. The current work investigates velocity effects with air flowing at Mach number $M=0.04-0.28$ ($Re=6 \times 10^4 - 3.8 \times 10^5$) in the combined duct.

The original works were usually performed with the intended application of the results to large piping systems, where long lengths of straight pipe are connected by junctions. In such applications the flow in the downstream ducts becomes fully developed, with the flow losses due to the junction being fully realized. In many engineering applications however, the sections of straight duct can be very short, before connecting to some other loss generating component. In the current work pressure measurements will be made over a length of approximately 5 to 35 pipe diameters from the junction interface in the downstream ducts to investigate the formation of losses after separation.

A common test configuration in earlier works is the junction with all ducts of circular cross-section, area ratio equal to unity, and varying interface radius. This configuration will be examined here for radii equal to 0, 10 and 20% of the branch diameter for comparison of the current experimental setup with those of previous works. Area ratio effects have been studied extensively for right circular junctions with sharp-edged interfaces and radii equal to 10% of the branch diameter. These results often do

not agree well, however, and there is little data on junctions with larger radii. As a new contribution, junctions with through to side duct area ratios of 1, 2.124, and 3.117 and interface radii equal to 20% of the branch diameter will be studied. Side branch taper effects will also be studied by testing two junctions with side branches with diameters that are equal to the through duct, and then taper to an area ratio of 2.124 and 3.117. Both junctions employ 20% interface radii.

Miller (1990) asserts that duct cross-sectional shape has only a small effect on junction losses; however a conclusive study of shape effects has not been performed. In the current work, junctions with side branches of circular, square, rectangular, and oval cross-section will be studied for through duct to side branch area ratios of 1, 2.124, and 3.117 and interface radii equal to 20% of the side branch diameter. In the case of junctions with rectangular and oval side branches, aspect ratio effects will be studied by rotating the side branch by 90° along its longitudinal axis.

In Chapter 2, theory for flow losses in T-junctions is described. The losses are divided into two general categories, those caused by the junction itself, and by wall friction. Frictional effects must be subtracted from static pressure measurements in order to quantify the effects of the junction geometry alone. A compressible formulation for static pressure drop in a moving gas due to duct wall friction is presented, as well as formulations for the two incompressible loss coefficients used to describe type 1 dividing flow.

The experimental setup is discussed in Chapter 3. The flow bench and pressure measurement techniques are described first. The experimental setup and procedure for duct friction measurements are outlined, along with the description of all duct cross-

sections studied. The experimental setup for dividing type 1 flow loss measurement is then given with a description of all junction geometries investigated.

The approaches used to reduce experimental data are outlined in Chapter 4. The reduction and analysis of straight duct friction measurements is described first. Corrections are made for the change in static pressure measurements due to cross-sectional area variation in the fabricated ducts. Junction flow loss coefficient calculations are then described, where multiple measurements are averaged to reduce experimental error.

Results of all experiments are discussed in Chapter 5. Friction factor measurement results are discussed first. Comparisons are made with the theoretical predictions of Prandtl for fully developed turbulent flow in a circular duct. T-junction loss coefficient results are presented next. The redevelopment of flow in the ducts downstream of the junction interface is shown in the form of pressure measurements along the duct longitudinal axis for junctions with varying interface radius and area ratio. The dependence of fully developed loss coefficients on through-duct Reynolds number for the same junctions is then presented, followed by the comparison of current results with those available in literature. The effects of junction geometry parameters, interface radius, area ratio, side duct taper, and side duct shape are then discussed. Finally, concluding remarks are provided in Chapter 6 with recommendations for future work.

CHAPTER 2

LOSSES IN INTERNAL FLOWS

2.1 Frictional Losses

In order to determine the losses due to the division of flow at the junction only, it is necessary to accurately define and subtract the effect of wall friction from experimental data. Consider a fully developed one-dimensional flow in a duct of constant cross-section as shown in Figure 2.1. Applying the momentum equation to the control volume (CV) of length dx yields

$$A \frac{d}{dx} (\rho U^2) + A \frac{dp}{dx} + \tau_w \mathcal{P} = 0, \quad (2.1)$$

where ρ is the fluid density, A the duct cross-sectional area, U the mean fluid velocity, τ_w the wall shear stress, and \mathcal{P} the duct wetted perimeter. The wall shear can be expressed as the product of the dynamic pressure in the duct and a Fanning friction factor f :

$$\tau_w = \frac{1}{2} \rho U^2 f. \quad (2.2)$$

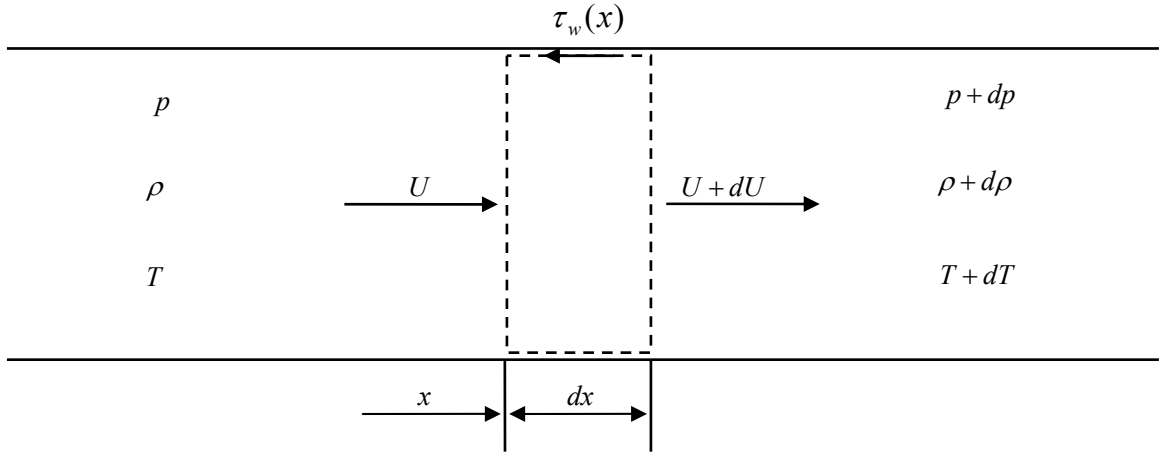


Figure 2.1: Differential control volume for fully developed flow in a straight duct.

It is also convenient to introduce D_h as the duct hydraulic diameter defined by

$$D_h = \frac{4A}{\mathcal{P}}. \quad (2.3)$$

Combining Eqs. (2.1) through (2.3)

$$U^2 \frac{d\rho}{dx} + 2\rho U \frac{dU}{dx} + \frac{dp}{dx} + \frac{1}{2} \rho U^2 \frac{4f}{D_h} = 0. \quad (2.4)$$

When combined with the continuity equation,

$$A \frac{d}{dx}(\rho U) = 0, \quad (2.5)$$

Eq. (2.4) becomes

$$-U^2 \frac{d\rho}{dx} + \frac{dp}{dx} + \frac{1}{2} \rho U^2 \frac{4f}{D_h} = 0. \quad (2.6)$$

If the fluid is assumed incompressible, $\frac{d\rho}{dx} = 0$, reducing Eq. (2.4) to

$$\frac{dp}{dx} = -\frac{1}{2}\rho U^2 \frac{4f}{D_h}. \quad (2.7)$$

Equation (2.7) is commonly used to calculate the pressure gradient in flows of incompressible fluids or of gases with Mach numbers less than 0.3 where compressibility effects are negligible.

In the case of gaseous flows with Mach number greater than 0.3 compressibility effects cannot be ignored. Application of the energy equation to the CV in Figure 2.1 for adiabatic flow yields

$$A \frac{d}{dx}(\rho U e) + p A \frac{dU}{dx} - \tau_w \mathcal{P} U = 0, \quad (2.8)$$

where e is the internal energy of the fluid. Using ideal gas relations the internal energy can be defined as

$$e = \frac{p}{(\gamma - 1)\rho}, \quad (2.9)$$

where γ is the ratio of specific heats. Combining Eqs. (2.2), (2.3), (2.5), (2.8), and (2.9) yields

$$\frac{1}{(\gamma - 1)} \frac{dp}{dx} - \frac{p}{\rho} \left(\frac{\gamma}{\gamma - 1} \right) \frac{d\rho}{dx} - \frac{1}{2} \rho U^2 \frac{4f}{D_h} = 0. \quad (2.10)$$

Next, combine Eqs. (2.10) and (2.6) to eliminate $\frac{d\rho}{dx}$:

$$\frac{dp}{dx} = -\frac{1}{2} \left[1 + \frac{1}{\frac{p}{\rho U^2} - \frac{1}{\gamma}} \right] \rho U^2 \frac{4f}{D_h}. \quad (2.11)$$

Equation (2.11) is similar in form to Eq. (2.7), but differs in that ρ , p , U , and f are functions of x .

2.2 Area-Pressure Relation

Any variation in duct cross-sectional area will result in a corresponding variation in static pressure. In order to determine the losses due to the division of flow at the junction only, it is necessary to accurately define and subtract the effect of duct cross-sectional area variation from experimental data. Consider a fully developed, steady, and quasi one-dimensional flow in a duct of varying area as shown in Figure 2.2. Applying the momentum equation to a control volume of length dx while neglecting friction yields

$$d(\rho AU^2) + Adp = 0. \quad (2.12)$$

The differential form of the continuity equation becomes

$$d(\rho AU) = 0. \quad (2.13)$$

Combining Eqs. (2.12) and (2.13) yields

$$-U^2 Ad\rho - \rho U^2 dA + Adp = 0. \quad (2.14)$$

If the flow is considered incompressible, Eq. (2.14) reduces to

$$dp = \rho U^2 \frac{dA}{A}. \quad (2.15)$$

Eq. (2.15) shows that the change in static pressure for an incompressible flow is proportional to product of the fluid dynamic pressure and fractional change in duct cross-sectional area.

For compressible flow $\frac{d\rho}{dx} \neq 0$, which requires an additional equation to solve for

the change in static pressure due to area change.

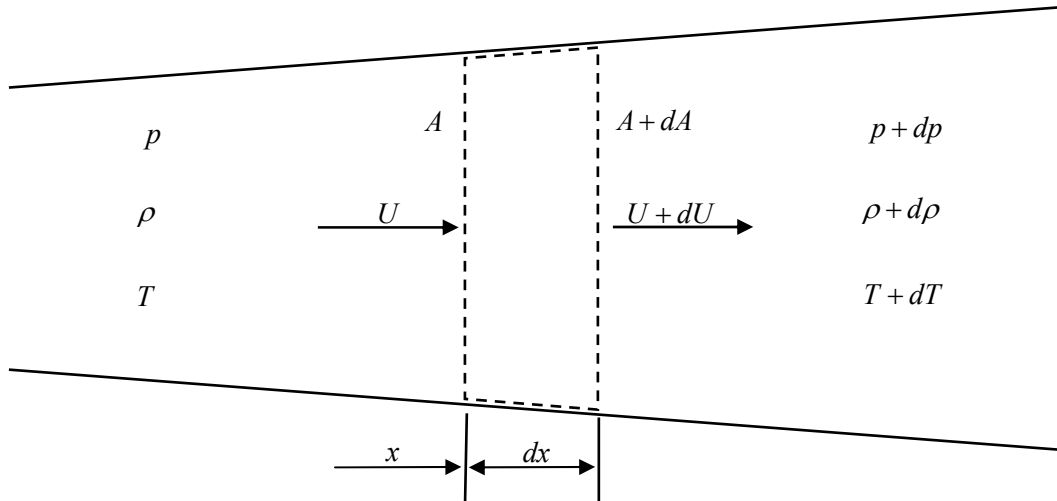


Figure 2.2: Differential control volume for flow in a variable area duct.

Application of the energy equation to the CV in Figure 2.2 for adiabatic flow yields

$$d(\rho A U e) + p d(A U) = 0. \quad (2.16)$$

Next combine Eqs. (2.9), (2.13), (2.14) and (2.16) to eliminate e , de , $d\rho$, and dU :

$$dp = \left[\frac{\rho U^2}{1 - \frac{\rho U^2}{p\gamma}} \right] \frac{dA}{A}. \quad (2.17)$$

Equation (2.17) differs from (2.15) in that $\frac{dp}{dA} < 0$ for flows with Mach number greater than $M=1$.

2.3 Dividing Flow Loss Coefficients

For a CV containing a moving compressible fluid, the first law of thermodynamics (see, for example, Fox *et al.*, 1998) gives

$$\dot{Q} - \dot{W} = \frac{\partial}{\partial t} \int_{CV} e_t \rho dV + \int_{CS} e_t \rho \vec{U} \cdot d\vec{A}, \quad (2.18)$$

where \dot{Q} is the rate of heat transferred to the CV, \dot{W} the rate of work done by the fluid on its surroundings, V the fluid volume, and e_t the specific total energy defined as

$$e_t = e + \frac{U^2}{2} + gz, \quad (2.19)$$

with e being the specific internal energy, g the acceleration due to gravity, and z the height of the fluid above some datum.

Provided the fluid is not used to generate mechanical work, such as in a turbine, the rate of work done by the CV can be conveniently subdivided as

$$\dot{W} = \dot{W}_{normal} + \dot{W}_{shear}, \quad (2.20)$$

where

$$\dot{W}_{normal} = - \int_{CS} \sigma d\vec{A} \cdot \vec{U} \quad (2.21)$$

represents the rate of work done by normal stress

$$\sigma = -p \quad (2.22)$$

at the control surfaces (CS) neglecting the impact of viscous effects on σ_{nn} .

$$\dot{W}_{shear} = - \int_{CS} \vec{\tau} \cdot \vec{U} dA \quad (2.23)$$

is the work out of the CV due to shear stress τ acting in the plane of dA at the CS. The surfaces of the CV can be categorized as either being solid, preventing fluid from passing through it, or open, allowing fluid flow. Assuming the no-slip condition exists at the solid walls of the control volume, the fluid velocity and therefore shear work will be zero.

If the flow is also considered one-dimensional, the open surfaces can easily be made

perpendicular to the flow and so the dot product in Eq. (2.23) will be zero. As a result, the right hand side of Eq. (2.23) will equal zero and there will be no shear work done on the control volume.

For steady, adiabatic flow, Eqs. (2.18) through (2.23) can be combined to give

$$0 = \int_{CS} \left(e + \frac{p}{\rho} + \frac{U^2}{2} + gz \right) \rho \vec{U} \cdot d\vec{A}. \quad (2.24)$$

Assuming one-dimensional flow, integration of Eq. (2.24) between an upstream location 1 and a downstream location 2 yields

$$0 = \rho_2 U_2 A_2 \left(e_2 + \frac{p_2}{\rho_2} + \frac{U_2^2}{2} + gz_2 \right) - \rho_1 U_1 A_1 \left(e_1 + \frac{p_1}{\rho_1} + \frac{U_1^2}{2} + gz_1 \right). \quad (2.25)$$

For steady, one-dimensional flow, the mass flow rate at both locations must be equal

$$\rho_2 U_2 A_2 = \rho_1 U_1 A_1 = \dot{m}, \quad (2.26)$$

where \dot{m} is the mass flow rate through the CV. For no variation in the fluid height between locations 1 and 2, Eqs. (2.25) and (2.26) readily yield

$$e_2 - e_1 = \left(\frac{p_1}{\rho_1} + \frac{U_1^2}{2} \right) - \left(\frac{p_2}{\rho_2} + \frac{U_2^2}{2} \right), \quad (2.27)$$

where $e_2 - e_1$ represents the irreversible conversion of mechanical to thermal energy between these two locations. This is due to both uniform losses caused by duct friction and local losses caused by flow separation. The change in internal energy between points 1 and 2 is thus

$$e_2 - e_1 = \Delta e_f + \Delta e_l, \quad (2.28)$$

where Δe_f and Δe_l are the components due to friction and local losses, respectively.

Combining Eqs. (2.27) and (2.28) for the mechanical energy loss, and

nondimensionalizing with respect to $\frac{1}{2}U_1^2$ yield,

$$\frac{\Delta e_l}{\frac{1}{2}U_1^2} = \frac{p_1}{\frac{1}{2}\rho_1 U_1^2} - \frac{p_2}{\frac{1}{2}\rho_2 U_1^2} - \left(\frac{U_2}{U_1}\right)^2 + 1 - \frac{\Delta e_f}{\frac{1}{2}U_1^2}. \quad (2.29)$$

For incompressible flow, $\rho_1 = \rho_2 = \rho$, thus Eq. (2.29) reduces to

$$K_{12} = \frac{p_1 - p_2}{\frac{1}{2}\rho U_1^2} - \left(\frac{U_2}{U_1}\right)^2 + 1 - \frac{\Delta e_f}{\frac{1}{2}U_1^2}, \quad (2.30)$$

where K_{12} is the incompressible loss coefficient.

Assuming that at least several diameters after the loss generating component are required for the flow to become fully redeveloped, the uniform friction [the last term in Eq. (2.30)] can have a significant effect on the total losses measured. Assuming frictional losses exist only in a duct of constant cross-section leading from the component, and the flow is incompressible, the change in internal energy due to uniform losses can be written as

$$\Delta e_f = \frac{\Delta p_f}{\rho}, \quad (2.31)$$

where Δp_f is the change in static pressure due to frictional losses between the outlet of the component and location 2.

Substituting Eq. (2.31) into (2.30) and applying a CV designated by 1 in Figure 2.3, where all flow entering the volume from the combined duct on the right exits through the bottom to the side branch, yield

$$K_{cs} = \frac{p_c - p_s}{\frac{1}{2}\rho U_c^2} - \left(\frac{U_s}{U_c}\right)^2 + 1 - \frac{\Delta p_f}{\frac{1}{2}\rho U_c^2}, \quad (2.32)$$

with the subscripts c and s representing the combined and side ducts, respectively.

If p_c is taken as the pressure in the combined duct just upstream of the junction, the frictional losses will then be due to flow in the side branch only. Thus, when flow in the side branch is zero, frictional losses will also be zero. If the static pressure in the side branch is assumed to be equal to that of the combined duct, K_{cs} will be unity. This assumption is reasonable provided that the combined and straight duct cross-sectional areas are equal, and the junction geometry is such that the flow from the combined to the straight duct is not disturbed greatly by the side branch to straight duct interface.

Similarly, a loss coefficient for CV 2, where all flow entering the volume at the right from the combined duct exits at the left to the straight branch, can be formed as

$$K_{cst} = \frac{p_c - p_{st}}{\frac{1}{2}\rho U_c^2} - \left(\frac{U_{st}}{U_c}\right)^2 + 1 - \frac{\Delta p_f}{\frac{1}{2}\rho U_c^2}, \quad (2.33)$$

where the subscript st is for quantities in the straight duct.

If the cross-sectional area of the straight duct is equal to that of the combined duct, their average velocities will be equal when there is zero flow into the side branch. If the flow is not disturbed greatly by the common duct to side branch interface, then the

static pressure drop between the combined and straight ducts is purely due to frictional losses, and K_{cst} will equal zero.

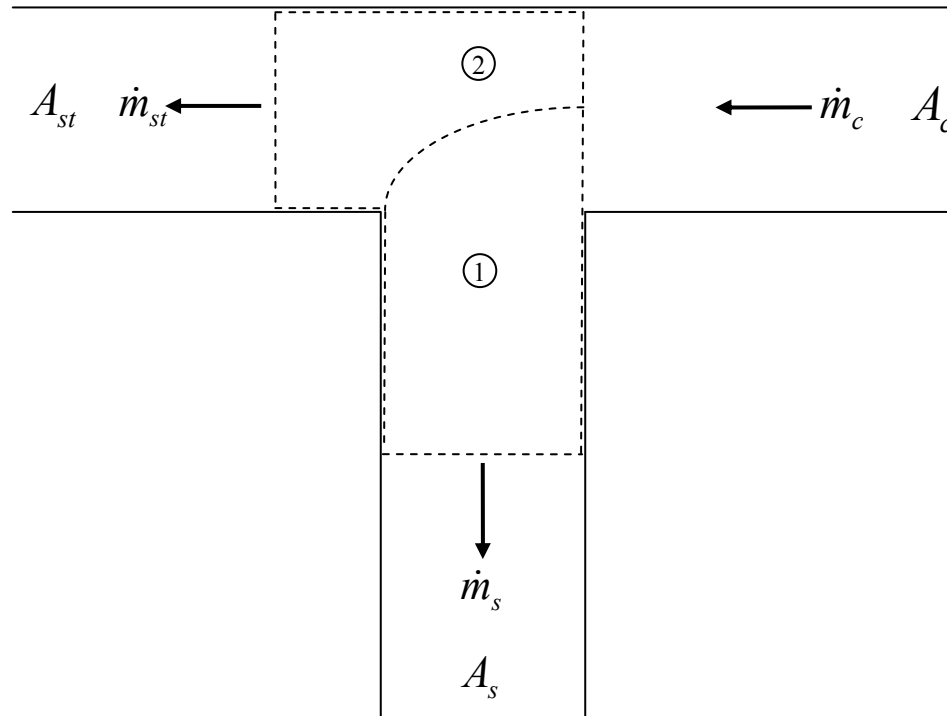


Figure 2.3: Dividing flow control volumes

The tendency of K_{cs} to approach unity and K_{cst} to zero as the flow in the side branch is reduced to zero has been predicted by others (Basset *et al.*, 1999; and Hager, 1984) using hydraulic theory with the assumptions of incompressible, inviscid flow. The trend has also been observed experimentally (Ito *et al.*, 1973; and McNown, 1954) for several geometries with some reduction of K_{cs} for tees with combined and side ducts of equal area and radiused interfaces.

CHAPTER 3

EXPERIMENTAL SETUP

3.1 Flow Bench

All experiments were performed on a flowbench donated by Ford Scientific Laboratories using air as the working fluid. Figure 3.1 shows a simplified schematic of the bench, which is arranged in a pull-through configuration with the test specimens placed upstream of the inlet. A vacuum is created by a Spencer Turbine Company turbo compressor rated at $0.389 \text{ m}^3/\text{s}$ (825 CFM) powered by a 30 kW (40 hp) electric motor. The bench is capable of generating a maximum flow rate of 0.63 kg/s (1150 SCFM) with pressure drops across the test piece of up to 8.72 kPa (35 in H₂O) and a flow rate of 0.19 kg/s (350 SCFM) at a maximum pressure drop of 22.42 kPa (90 in H₂O).

The flow rate is controlled by a pair of 6 in. and 2 in. diameter butterfly valves for gross adjustment and fine tuning, respectively. The valves are arranged such that the compressor sees a nearly constant flow rate while the ratio of air being pulled through the test piece and an auxiliary air inlet is varied. Each pair of valves is positioned by a Milwaukee Controls 0A15M-025-96015 actuator. The actuators are controlled by two

analog output channels of a National Instruments AT-MIO-16 DAQ board mounted in a PC running Windows NT operating system and LabVIEW data acquisition software.

Flow rate through the test piece is measured by a set of 7 custom fabricated converging nozzles with throat diameters ranging from 7.94 to 88.90 mm that were calibrated at standard conditions of 300 K (80 F) and 100.58 kPa (29.7 in Hg) with a set of four NIST traced flow nozzles. An individual or combination of nozzles can be used to match flow rate demands. The nozzle inlet absolute pressure and temperature is measured by a Mensor model 11900-402 digital pressure gauge and Ω EOMEGA digital temperature sensor, respectively. Pressure drop across the nozzles is measured by a Meriam Instrument model A699B inclined water manometer with a range of 0-1.49 kPa (0-6 in H₂O). Nozzle inlet air density compensation is accomplished by altering the manometer inclination angle.

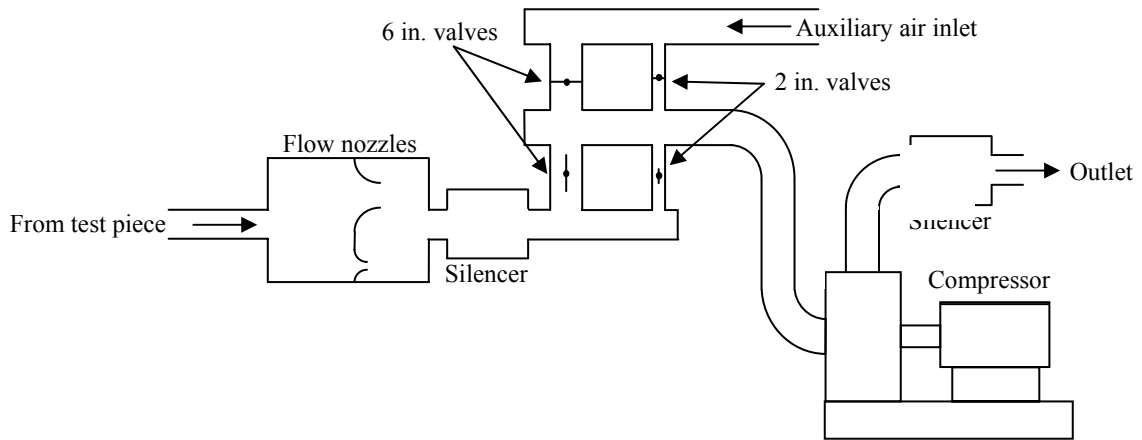


Figure 3.1: Compressor and flow nozzle arrangement

3.2 Pressure Measurement

All duct pressure tap locations consisted of four taps separated by 90° in a piezometric ring arrangement as described by Blake (1976). All holes were 1 mm in diameter and drilled perpendicular to the tube axis. Each hole was then deburred and sanded from the inside of the tube. A smooth burr free finish was found to be very important in achieving acceptable measurement accuracy. Bungs were fabricated and bonded or glued to the tube outer surface and connected by equal lengths of Tygon tubing in a triple-T configuration yielding the average pressure of the four taps. An example of a typical pressure tap arrangement is shown in Figure 3.2.

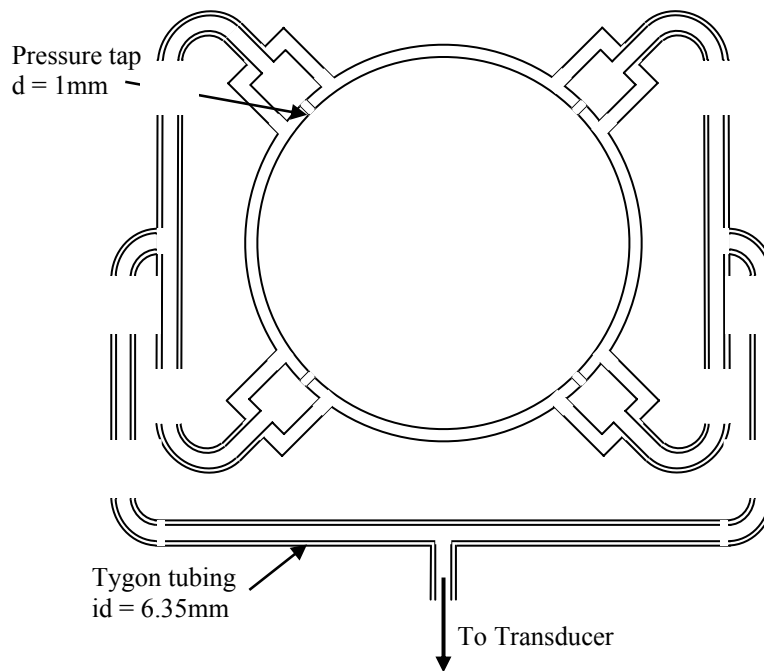


Figure 3.2: Triple-T piezometric ring

The laboratory ambient pressure measurements were made using a Meriam model 311EG10WM mercury manometer. All differential pressures in the setup were measured with Validyne model P55D differential pressure transducers within a quoted accuracy of $\pm 0.25\%$ of full scale, including non-linearity, hysteresis and non-repeatability. The transducer range was adjusted to match the pressure drops encountered during experiment by the use of replaceable pressure diaphragms of varying thickness. Four different diaphragms with full scale pressures of 0.87, 3.49, 8.72, and 22.42 kPa (corresponding to 3.5, 14, 35, and 90 in H₂O) were used to provide the highest possible accuracy, while still meeting the pressure drop requirement encountered during the experiment.

Transducer calibrations for full scale pressures of 0.87 and 3.49 kPa were performed with a 4.98 kPa (20 in H₂O) Meriam model 34FB2TM water micromanometer with an accuracy of ± 0.50 Pa. Calibrations for full scale pressures of 8.72 and 22.42 kPa were performed using a model 351 Meriam smart manometer with a full scale pressure of 49.82 kPa (200 in H₂O) and accuracy of ± 12.45 Pa. All transducer calibrations of same full scale pressure were performed simultaneously to minimize transducer to transducer variation.

Pressure transducer output signals were measured by a Keithley model KPCI-3116 DAQ board configured to provide 16 differential analog channels. LabVIEW data acquisition software was used to collect all signals and user input including, test piece volumetric flow rate, and ambient temperature and pressure. Input signals were averaged for approximately 30 seconds before all experimental values were saved simultaneously to a text file for later manipulation.

3.3 Straight Tube Setup

Straight tube experiments were performed first to determine the uniform losses in each tube used in the T-junction experiments. A typical straight tube experimental setup is shown in Figure 3.3. Air was drawn through a circular duct of diameter $D=63.32$ mm, and allowed to develop for $55 D$ before flowing through a transition piece that gradually changed the shape and area to that of the test duct. The development duct size was chosen so that the cross-sectional area during transition would remain constant or reduce from the development duct to test section to minimize any flow disturbance. Ten tap locations were used to measure the pressure drop due to redevelopment downstream of the transition piece and the subsequent pressure gradient due to wall friction in the fully developed region. The first pressure tap location was used to measure the drop in pressure from ambient to the beginning of the test section. All downstream taps were referenced from this location, allowing the use of more sensitive transducers to measure the relatively small changes in static pressure along the test section. Transducer calibrations were modified during the experiment with each duct to match the pressures encountered. The flow rate through the test section was varied over the entire range expected in the T-junction experiments, and the fully developed pressure gradient was used to find the friction factor of the duct.

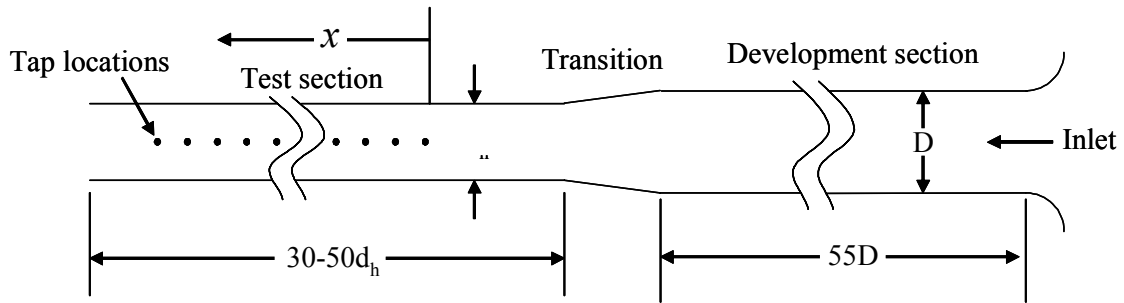


Figure 3.3: Straight duct friction factor setup

Four duct shapes were studied, including circular, square, rectangular, and oval as shown in Figure 3.4, for three cross-sectional areas corresponding to those later used in the tee experiments. The cross-sectional area, and equivalent and hydraulic diameters for each shape are listed in Table 3.2. All rectangular and oval ducts were constructed with an aspect ratio $b/a=2$. All test ducts were between 30 and 50 hydraulic diameters long and were made without seams perpendicular to the tube axis to minimize flow disturbances.

Several materials were used in duct fabrication to attain the desired shapes and sizes. Two of the circular ducts were made of cast acrylic tube, while a third was of grey PVC. The cast acrylic was optically transparent, allowing easy inspection of the pressure taps along the test section. The inner surface of the cast acrylic appeared to be very smooth and straight, while some very slight waviness could be seen in the PVC tubes.

All square and rectangular ducts were fabricated from pieces of 12.7 mm thick clear acrylic sheet that were bonded together at their edges using solvent. All pieces were milled to dimension along their entire length on a horizontal milling machine. During

bonding, the pieces were placed in a fixture to ensure they were perpendicular and straight.

Oval ducts were made from 3.175 mm thick ABS plastic sheet that was heated and formed around a mandrel of desired shape and size. Each tube was comprised of two sheets formed in the shape of a J that were welded together along the tube axis at tangents to the circular sections as shown in Figure 3.4. This formed a pair of seams on the inner surface of the ducts that were sanded smooth. The ABS sheet also had some surface roughness that was visible on the inner surface of the ducts.

As a result of the various methods and materials used in duct fabrication, the actual fabricated dimensions differ somewhat from the specified nominal dimensions. Measurements were made to find the actual cross-sectional area along the length of each duct. Table 3.1 lists the resulting average equivalent diameter as defined in Table 3.2 and the maximum variance for each duct.

Shape	Material	Average Equivalent Diameter \bar{D}_e (mm)
Circular	Acrylic	63.32 ± 0.46
		43.57 ± 0.46
	PVC	35.87 ± 0.64
Square	Acrylic	63.13 ± 0.40
		43.45 ± 0.67
36.37 ± 0.49		
Rectangular		64.36 ± 0.71
		44.21 ± 0.37
	36.76 ± 0.35	
Oval	ABS	64.49 ± 0.89
		43.83 ± 0.37
		36.07 ± 0.51

Table 3.1: Average measured equivalent diameter for fabricated ducts.

Shape	Area	Equivalent Diameter D_e	Hydraulic Diameter D_h
Circular	$\frac{\pi d^2}{4}$	d	d
Square	a^2	$\frac{2a}{\sqrt{\pi}}$	a
Rectangular	ab	$2\sqrt{\frac{ab}{\pi}}$	$\frac{2ab}{a+b}$
Oval	$(b-a)a + \frac{\pi a^2}{4}$	$\sqrt{\frac{4(b-a)a}{\pi} + a^2}$	$\frac{4ab + (\pi - 4)a^2}{2b + (\pi - 2)a}$

Table 3.2: Equations for area and hydraulic diameter

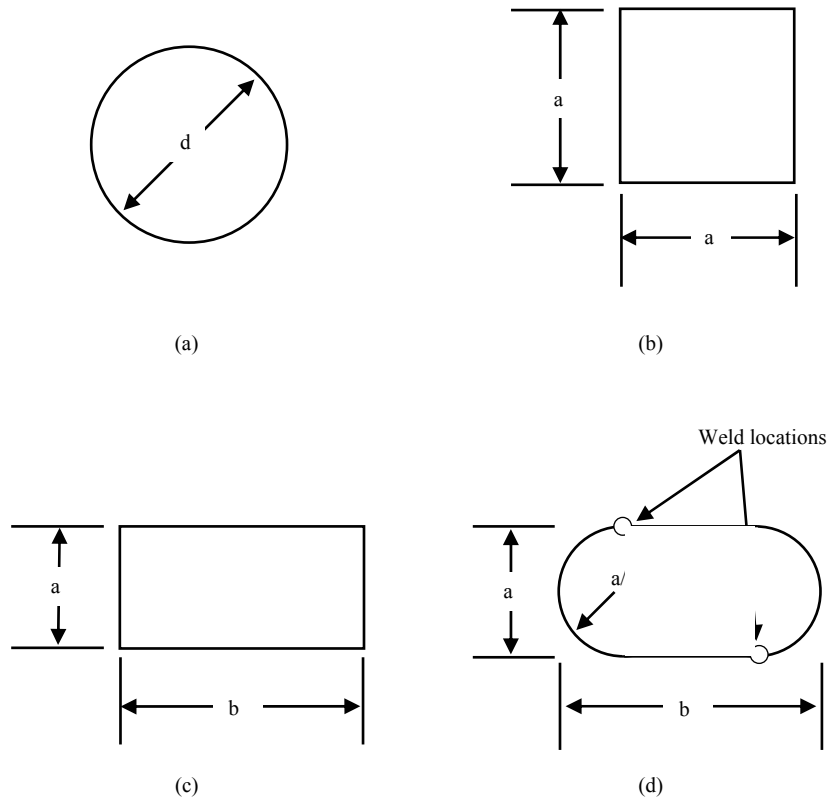


Figure 3.4: Cross-sections investigated: (a) circular, (b) square, (c) rectangular, (d) oval

3.4 T-junction Setup

All T-junctions were designed in SDR3 IDEAS CAD software prior to fabrication. Figure 3.5 shows the common dimensions of all tees used in this study. Laser stereolithography was used to generate plastic three-dimensional models from the CAD data. The technique uses UV light produced by a laser to trace the cross section of the part onto the surface of a liquid photopolymer pool. The photopolymer hardens with exposure to the UV light forming a slice of the part approximately 0.08 mm thick. The solidified layer is then lowered to a depth of 0.08 mm below the liquid surface and the

next layer is formed on top of it. Successive layers are built up to form the entire part. The finished part is then placed under a UV lamp to cure any remaining photopolymer. The resultant part has excellent dimensional tolerance with some surface roughness due to the layers forming the part. No sanding was done to remove this roughness from the junction inner surface as it was decided that the overall shape of the junction and the radius of the interface were more important than the surface finish. This combination of design and fabrication methods allowed testing of geometries previously too complex to define or fabricate accurately.

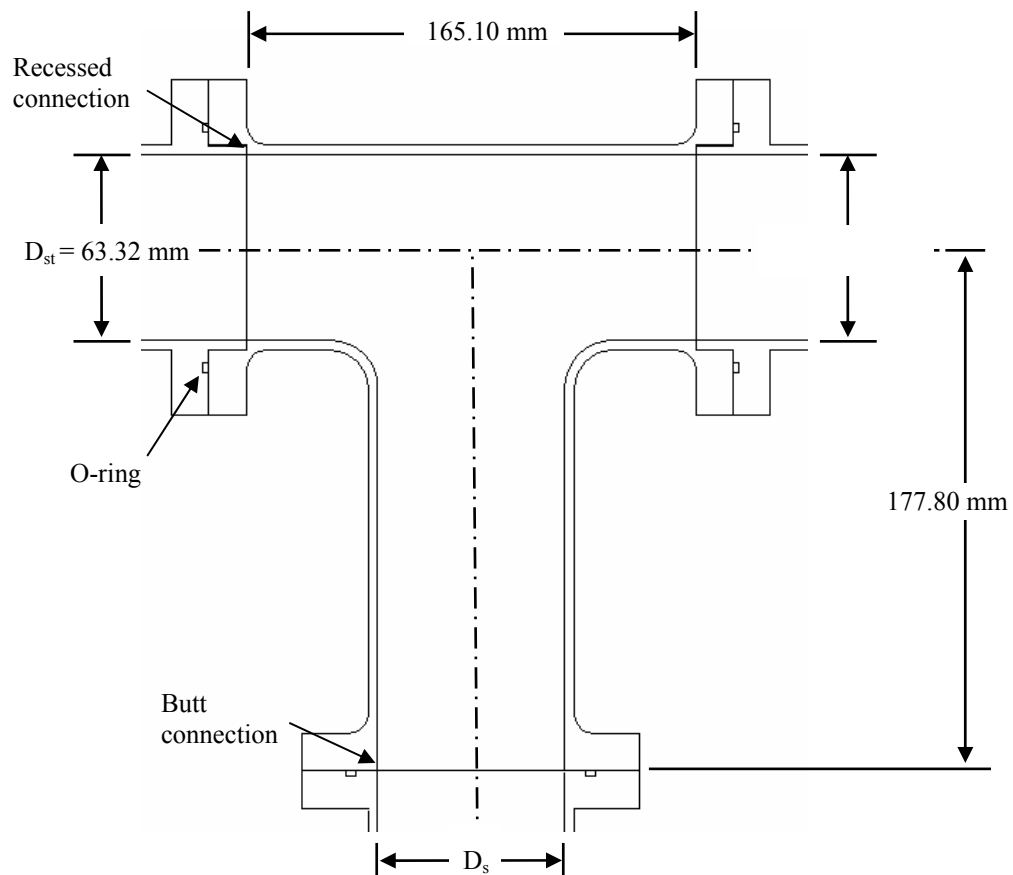


Figure 3.5: Tee junction connections and common dimensions

All connections of circular ducts to the tees were made with recessed flanges as shown in Figure 3.5. This allowed a gap-free, concentric fit between the test piece and ducts. Due to the difficulty of controlling the outer tube dimensions, all noncircular ducts were connected with a simple butt flange. All connections were sealed with o-rings between mating flanges.

Test pieces were attached to the flow bench in the configuration depicted in Figure 3.6. Flow first entered the combined duct through a bellmouthed entrance of radius $0.2D_c$ and was allowed to develop for $30D_c$ before entering the tee. A dividing flow was established by connecting both the straight duct and side branch to the flow bench inlet. Flow rates in the side and straight ducts were controlled with a pair of butterfly valves located downstream of the test sections. Data sweeps were performed by varying the side branch flow rate, while keeping that of the combined duct fixed to vary the side to main duct flow ratio from zero to 100% in increments of approximately 3%. Multiple sweeps were made for various main duct flow rates to find any effect of combined duct Reynolds number on flow loss coefficients.

A single pressure tap, labeled as P_{in} in Figure 3.6, was placed $1.81 D_c$ upstream of the tee to attain the tee inlet static pressure and provide a reference for all downstream taps. Ten pressure transducers were used to measure the pressure drop from the tee inlet to the side and straight ducts. Similar to the straight duct measurements, transducer calibration was again varied to match the maximum pressure drop encountered during each experiment in order to reduce errors.

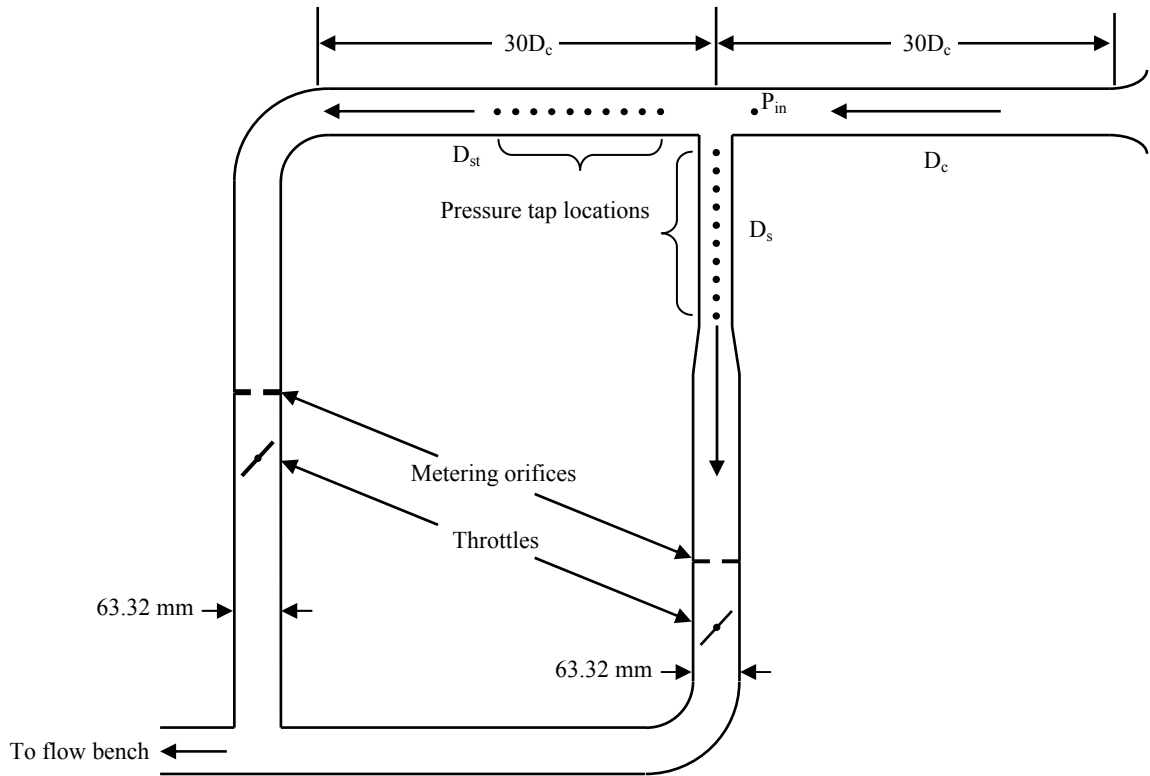


Figure 3.6: T-junction dividing flow setup

Seven junctions with all ducts of circular cross-section were fabricated to study the effects of area ratio (A_c/A_s), interface radius (r), and side branch taper area ratio (A_i/A_s). The junctions with circular side branches of constant area and their defining characteristics are listed in Table 3.3. Three junctions with $A_c/A_s=1$ were fabricated with varying radii of 0 , 0.1 , and $0.2 D_s$ to study radius effects. Because it is typically desirable to minimize flow losses in engineering applications, and that area ratio effects for junctions with sharp edged interfaces ($r = 0$) have been extensively covered, an interface radius of $0.2 D_s$ was adopted in the current experiments for all remaining junctions with

side branches of uniform area. Two additional junctions were fabricated with $A_c/A_s=2.124$ and 3.117 to determine area ratio effects for junctions with generous radii.

Table 3.4 lists junctions with side branches that began with cross-sectional areas at the junction interface equal to that of the through duct ($A_c/A_s=1$), that then tapered down to give a final area ratio of $A_c/A_s=2.124$ and 3.117 . The side branch taper began at a distance of $D_c/2$ from the through-duct centerline, and tapered to the final dimension over a length of $2D_c$. The radii for both junctions were equal to 20% of the side branch diameter at the junction interface.

To quantify side branch cross-sectional shape effects, thirteen junctions with branches of square, rectangular, and oval cross-sections as shown in [Tables 3.5 through 3.7](#) were tested for $A_c/A_s=1$, 2.124 , and 3.117 . Junctions with rectangular and oval side branches were made with duct aspect ratios $b/a=2$ as defined in Figure 3.4 which were rotated 90° to create two junction aspect ratios of $W/H=1/2$ and 2 for $A_c/A_s>1$. Junctions with $A_c/A_s=1$ and $W/H=2$ were not possible, due to W being greater than D_c . All junctions with non-circular branch cross-sections employed interface radii equal to 20% of the diameter for a circular duct with equal area of the side duct.

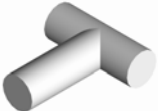




Tee	A_c/A_s	r/D_s
	1	0
		0.1
		0.2
	2.124	
	3.117	

Table 3.3: Junctions with circular side branches tested



Tee	A_c/A_i	A_c/A_s	r/D_i
	1	2.124	0.2
		3.117	

Table 3.4: Junctions with tapered circular side branches


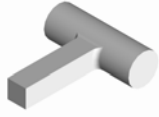
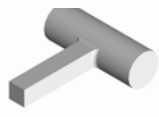
Tee	A_c/A_s	r/D_s
	1	0.2
	2.124	
	3.117	

Table 3.5: Junctions with square side branches


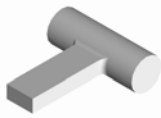

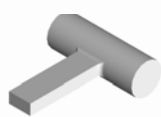

Tee	A_c/A_s	W/H	r/D_s
	1	$\frac{1}{2}$	0.2
	2.124	$\frac{1}{2}$	
	2.124	2	
	3.117	$\frac{1}{2}$	
	3.117	2	

Table 3.6: Junctions with rectangular side branches




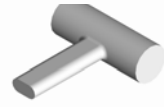
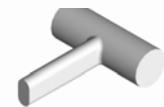
Tee	A_c/A_s	W/H	r/D_s
	1	$\frac{1}{2}$	0.2
	2.124	$\frac{1}{2}$	
	2.124	2	
	3.117	$\frac{1}{2}$	
	3.117	2	

Table 3.7: Junctions with oval side branches

3.5 Sharp-Edged Orifice Flow Measurement

Sharp edged orifices were used to measure the flow through the straight and side branches of the tees independently. A total of four orifice sizes with diameters of 22.86, 31.75, 41.91, 50.8, and 57.15 mm (0.90, 1.25, 1.65, 2.00, and 2.25 in.) were used to provide acceptable accuracy over the required flow range. The orifices were fabricated by Piping Technology & Products, Inc. of Houston, Texas and made of 3.18 mm thick 304 stainless steel and chamfered at 45° from the outlet side to a depth of 2.22 mm. The orifices were installed in D=63.32 mm ducts that were downstream of the straight and side branch test sections (Figure 3.6). Pressure taps were located 1D before and 0.625D after the orifice inlets (Figure 3.7). The plates were located by recessed flanges and sealed with o-rings as described for the T-junction connections.

Each orifice size was calibrated against the Ford flow bench over a pressure drop range of 0-8.70 kPa and with inlet absolute pressures ranging from 81.95 to 98.88 kPa. Sweeps were performed by holding the upstream absolute pressure constant while varying the drop across the orifices. A curve fit of the form

$$\dot{m} = a\Delta p^b \quad (3.1)$$

was found for each sweep, where \dot{m} is the mass flow rate, Δp is the pressure drop across the orifice, and a and b are fit coefficients. Figures 3.8-3.10 show the measured and curve-fit orifice mass flow rate versus pressure drop for the five sizes used during tee experiments, while Table 3.8 provides the approximate flow range covered by each orifice.

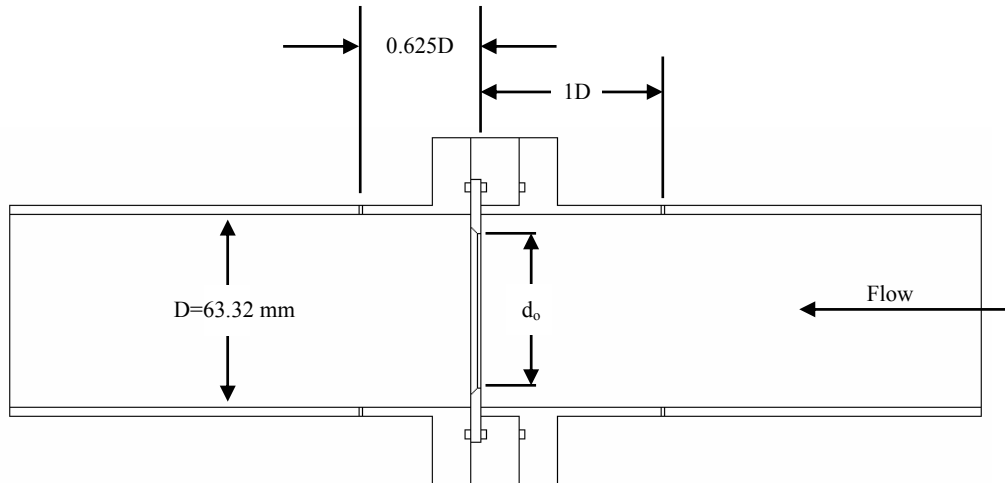


Figure 3.7: Sharp-edged orifice installation

d_o (mm)	Flow rate range (kg/s)
22.86	0-0.035
31.75	0.035-0.070
41.91	0.070-0.128
50.8	0.128-0.228
57.15	0.228-0.425

Table 3.8: Approximate flow rate ranges for sharp-edged orifices

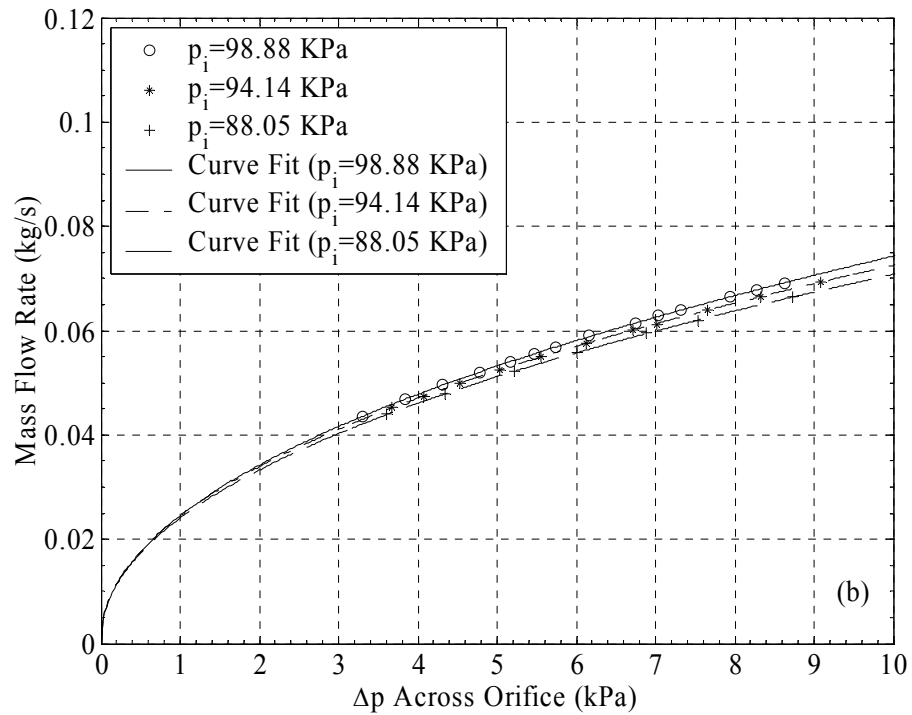
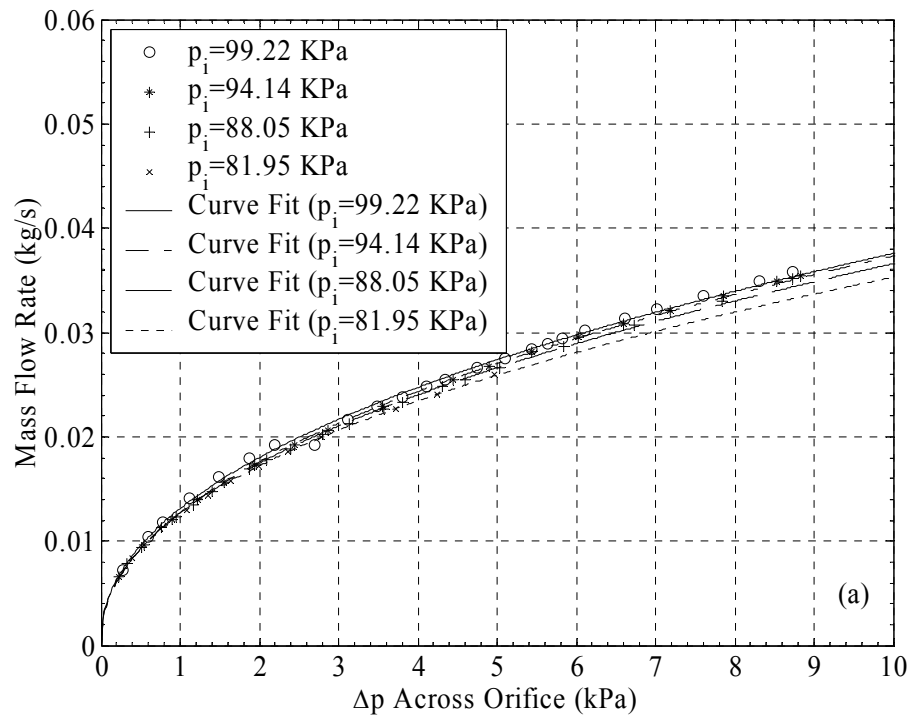


Figure 3.8: Flow orifice calibration: (a) $d_o = 22.86$ mm, (b) $d_o = 31.75$ mm

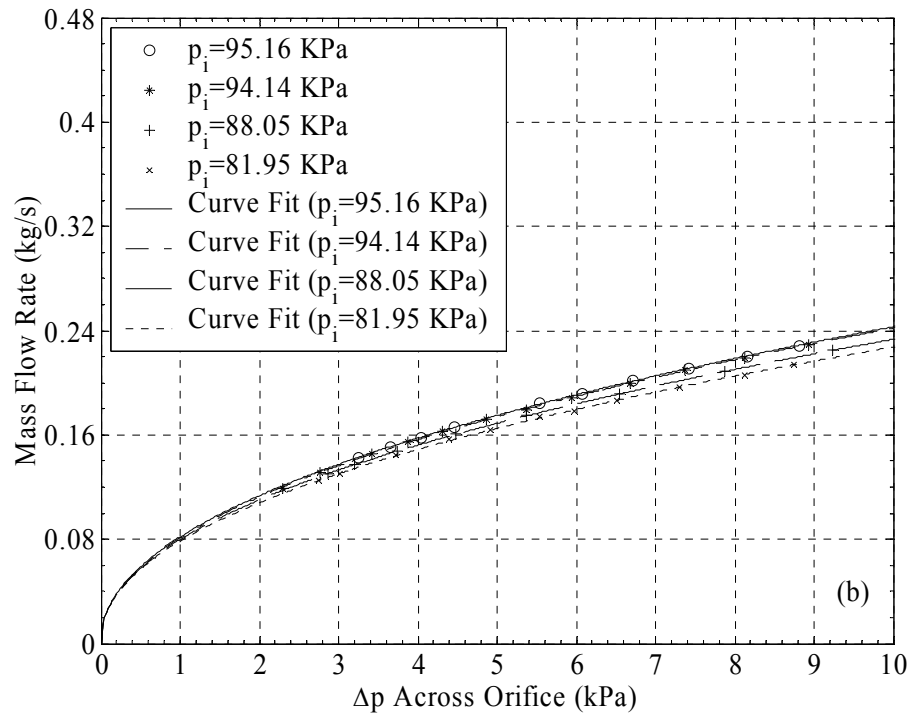
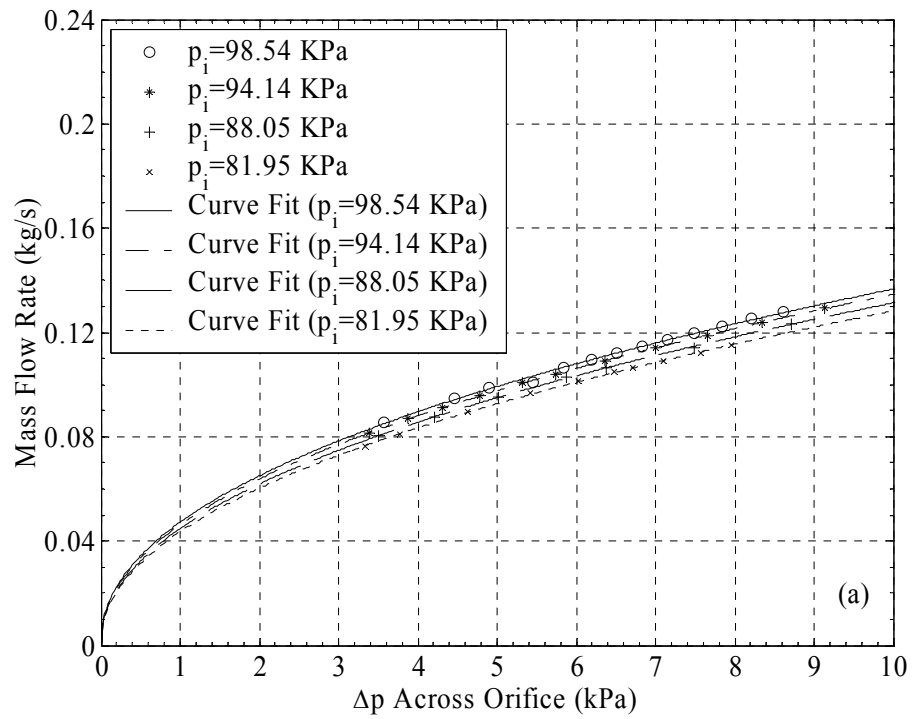


Figure 3.9: Flow orifice calibration: (a) $d_o = 41.91$ mm, (b) $d_o = 50.8$ mm

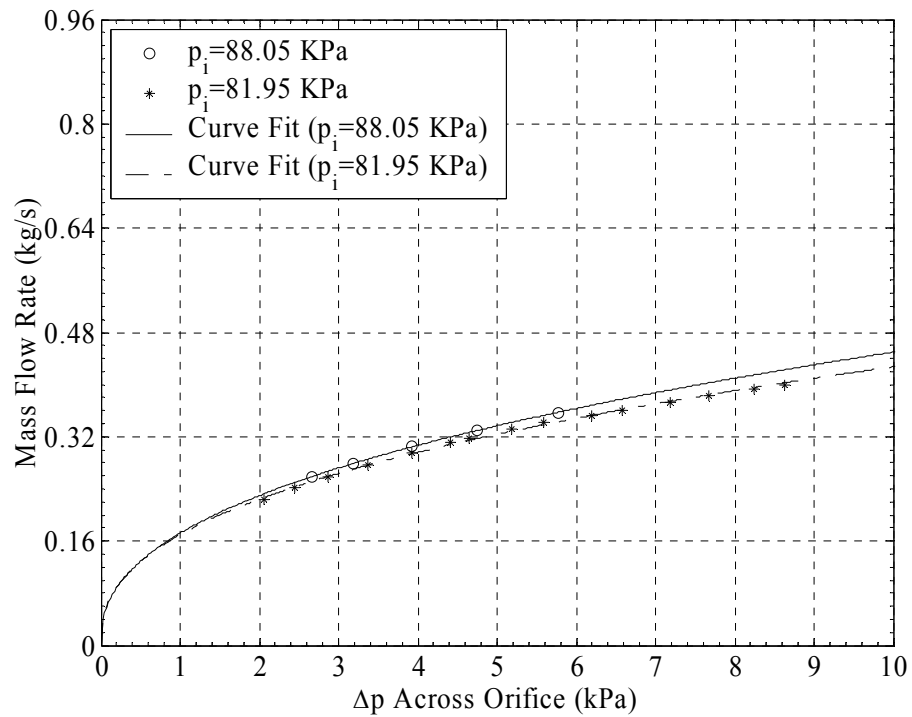


Figure 3.10: Flow orifice calibration: $d_o = 57.15$ mm

During T-junction experiments, the mass flow rate was determined from the curve fits at the measured pressure drop and linear interpolation to correct for upstream absolute pressure. Due to the relatively constant laboratory temperature, a compensation for temperature was not performed. The sum of the mass flow rates measured by the orifices was compared to that of the flow bench during experiment as an error check. Disagreement between the two measurements was found to never exceed $\pm 5\%$ and was typically less than $\pm 2\%$, varying inversely with combined duct flow rate.

CHAPTER 4

DATA REDUCTION AND ANALYSIS

4.1 Friction Factor Determination

Straight duct flow experiments for each side branch shape and size were conducted to determine the friction factor as a function of Reynolds number to be used in T-junction experiments. Pressure measurements were made in the fully developed region, identified by linearly varying static pressure with longitudinal distance along the duct. The exact region measured varied from duct to duct, with a typical length of 25 to 35 hydraulic diameters.

The differential control volume described in Section 2.1 is applied to the test section shown in Figure 3.3. Average values of measured properties such as p , ρ , and U are used in Eq. (2.11) to find the duct friction factor. Since the pressure is assumed to vary linearly across the differential control volume, a least squares fit of the pressure gradient in the fully developed region shown in Figure 4.1 is found in the form

$$p = c_1 \left(\frac{x}{D_h} \right) + c_2, \quad (4.1)$$

where x is the distance from the first pressure tap in the test section (see Figure 3.3), D_h is the hydraulic diameter of the duct, and c_1 and c_2 are coefficients. The compressible

formulation in Section 2.1 is used to find the friction factor due to the high flow velocities encountered during T-junction tests. Although the pressure gradient in compressible flow is a function of distance, it is assumed constant over the test length. This is reasonable given the short length of the test section and the relatively low Mach number of the flow ($M < 0.5$). The average pressure in the fully developed region is defined as

$$\bar{p} = c_1 \left(\frac{\bar{x}}{D_h} \right) + c_2, \quad (4.2)$$

where \bar{x} is half the distance between the first and last pressure taps in the fully developed region.

Temperature measurements along the duct were not performed during experiment, and so the gas temperature and resulting density are estimated by assuming the flow from ambient to the test section to be isentropic. Although the process may be between isentropic and isothermal, the assumption of isentropic flow is reasonable given the low thermal conductivity of the duct materials and relatively short duct lengths. Using isentropic relations, the average density in the test section is

$$\bar{\rho} = \rho_a \left(\frac{\bar{p}}{p_a} \right)^{\frac{1}{\gamma}}, \quad (4.3)$$

where the subscript a represents ambient quantities. The average velocity in the middle of the fully developed region is equal to

$$\bar{U} = \frac{\dot{m}}{\bar{\rho}A}, \quad (4.4)$$

where \dot{m} is the mass flow rate in the duct and \bar{A} is the average measured duct cross-sectional area.

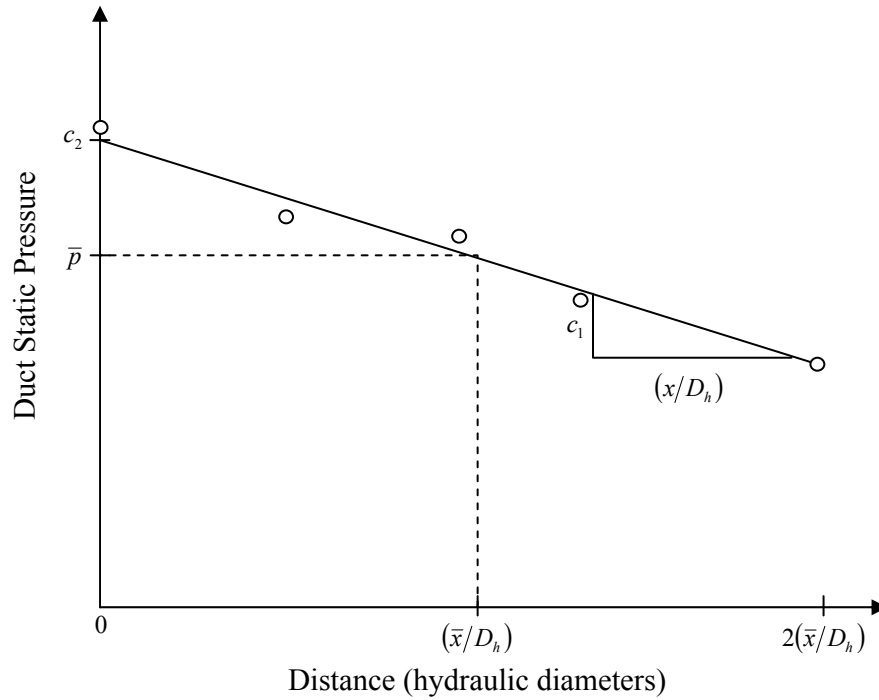


Figure 4.1: Pressure gradient in fully developed region

The average quantities in Eqs. (4.3) and (4.4) are used to find the Reynolds number in the duct yielding

$$\bar{\text{Re}} = \frac{\bar{\rho} \bar{U} D_h}{\bar{\mu}}, \quad (4.5)$$

where $\bar{\mu}$ is the kinematic viscosity of the fluid in the middle of the fully developed region that is found with the empirical correlation by Sutherland (see, for example, page 700 in Fox *et al.*, 1998):

$$\bar{\mu} = \frac{b\bar{T}^{\frac{1}{2}}}{1 + \frac{S}{\bar{T}}}, \quad (4.6)$$

where

$$b = 1.458 \times 10^{-6} \frac{\text{kg}}{\text{m} \cdot \text{s} \cdot \text{K}^{\frac{1}{2}}},$$

$$S = 110.4\text{K},$$

and \bar{T} is the temperature in the middle of the fully developed region. Under the assumption of isentropic flow the temperature can be found by

$$\bar{T} = T_a \left(\frac{\bar{p}}{p_a} \right)^{\left(\frac{\gamma-1}{\gamma} \right)}. \quad (4.7)$$

Due to the methods employed in the fabrication of the test ducts, some area variation over the duct lengths exists and so the relation presented in Eq. (2.17) is used to correct for the resulting variation in static pressure. The change in static pressure at an individual tap location j due to area variation is estimated by

$$dp_j = \left[\frac{\bar{\rho}\bar{U}^2}{1 - \frac{\bar{\rho}\bar{U}^2}{\bar{p}\gamma}} \right] \frac{A_j - \bar{A}}{\bar{A}} \quad (4.8)$$

A corrected static pressure is then found by

$$p'_j = p_j - dp_j, \quad (4.9)$$

which is then used to find a new least squares linear fit of the corrected pressure gradient in the duct

$$p' = c_3 \left(\frac{x}{D_h} \right) + c_4. \quad (4.10)$$

Using the compressible friction factor relation presented in Eq. (2.11) an average corrected friction factor can be found for the flow in the fully developed region of the straight duct yielding

$$\bar{f} = \frac{1}{2} \left(\frac{1 - \frac{\bar{p}\gamma}{\bar{\rho}\bar{U}^2}}{\bar{p}\gamma + (\gamma - 1)\bar{\rho}\bar{U}^2} \right) c_3. \quad (4.11)$$

4.2 T-Junction Loss Determination

In order to quantify the losses due to the division of flow at the T-junction, pressure measurements were made in the fully developed region of each duct. Junction inlet properties are based on a single pressure measurement $1.81 D_c$ upstream of the junction interface in the combined duct. Up to ten pressure tap locations were used in the straight and side ducts to measure the redevelopment of flow after separation. The tap locations varied for each experiment, but were typically located between 5 and $35 D_h$ from the junction interface.

To reduce error, averages of quantities measured in the fully developed region of the downstream ducts are used in Eqs. (2.32) and (2.33). A least squares fit of form similar to equation (4.1) is found for five pressure taps in each of the straight and side duct fully developed regions giving

$$p_i = c_{1i} \left(\frac{x_i}{D_{hi}} \right) + c_{2i}, \quad (4.12)$$

where the subscript i represents values for the straight or side ducts and x is the distance from the junction interface.

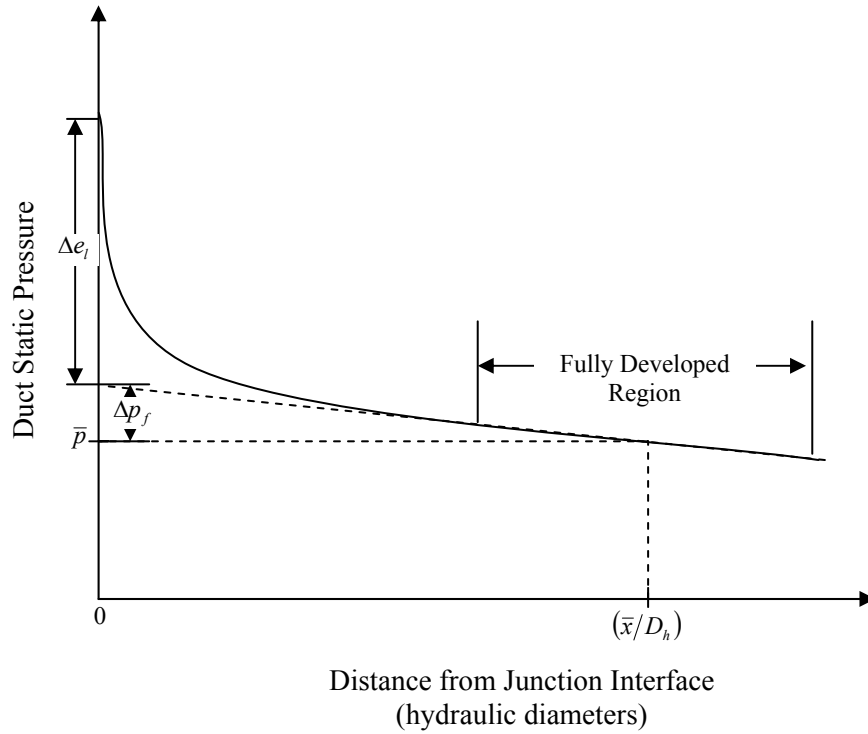


Figure 4.2: Pressure drop along combined or straight duct downstream of junction

The average pressure in the fully developed region of each duct is found by evaluating equation (4.12):

$$\bar{p}_i = c_{1i} \left(\frac{\bar{x}_i}{D_{hi}} \right) + c_{2i}, \quad (4.13)$$

where \bar{x} is the distance from the junction interface to the middle of the fully developed region. Equations (4.3) through (4.7) based on isentropic relations are used to find the fluid density, velocity, and Reynolds number for each duct.

The losses due to frictional effects in the downstream ducts are estimated by finding the corresponding friction factor calculated in section 4.1 for the given duct shape, size, and Reynolds number using a linear interpolation between friction measurement data points. The pressure drop due to friction at location j of duct i the can be found by rearranging equation (2.11) as

$$\Delta p_{fij} = 2 \left[\frac{\bar{p}_i \gamma + (\gamma - 1) \bar{\rho}_i \bar{U}_i^2}{1 - \frac{\bar{p}_i \gamma}{\bar{\rho}_i \bar{U}_i^2}} \right] \left(\frac{x_{ij}}{D_{hi}} \right) \bar{f}_i. \quad (4.14)$$

The corresponding drop in static pressure between the junction interface and the middle of the fully developed region of duct i is

$$\Delta \bar{p}_{fi} = 2 \left[\frac{\bar{p}_i \gamma + (\gamma - 1) \bar{\rho}_i \bar{U}_i^2}{1 - \frac{\bar{p}_i \gamma}{\bar{\rho}_i \bar{U}_i^2}} \right] \left(\frac{\bar{x}_i}{D_{hi}} \right) \bar{f}_i. \quad (4.15)$$

A correction for duct area variation in junction experiments is performed just as in the straight duct friction experiments in section 4.1. The change in static pressure at location j of duct i is estimated by

$$dp_{ij} = \left[\frac{\bar{\rho}_i \bar{U}_i^2}{1 - \frac{\bar{p}_i \gamma}{\bar{\rho}_i \bar{U}_i^2}} \right] \frac{A_{ij} - \bar{A}_i}{\bar{A}_i} \quad (4.16)$$

which is used to give a corrected static pressure

$$p'_{ij} = p_{ij} - dp_{ij}. \quad (4.17)$$

A least squares fit of $p'_i D_{hi}/x_i$ is then found and used to calculate a corrected static pressure in the middle of the fully developed region in each duct

$$\bar{p}'_i = c_{3i} \left(\frac{\bar{x}_i}{D_{hi}} \right) + c_{4i} \quad (4.18)$$

Replacing p_2 with \bar{p}'_i and Δp_f with $\Delta \bar{p}_{fi}$ in Eqs. (2.30) and (2.31), the mean loss coefficient for flow between the combined duct and downstream duct i is

$$K_{ci} = \frac{p_c - \bar{p}'_i}{\frac{1}{2} \rho_c U_c^2} - \left(\frac{\bar{U}_i}{U_c} \right)^2 + 1 - \frac{\Delta \bar{p}_{fi}}{\frac{1}{2} \rho_c U_c^2}. \quad (4.19)$$

Equation (4.19) is used to find the losses due to the division of flow at the junction interface and subsequent transition to fully developed flow in the downstream duct with frictional effects subtracted. It is an average of the losses measured at all pressure tap locations in the fully developed region. If the measured loss coefficient as a function of duct length is of any interest, such losses between the junction interface and a single tap location j in downstream duct i can be found by

$$K_{cij} = \frac{p_c - p'_{ij}}{\frac{1}{2} \rho_c U_c^2} - \left(\frac{\bar{U}_i}{U_c} \right)^2 + 1 - \frac{\Delta p_{fij}}{\frac{1}{2} \rho_c U_c^2}. \quad (4.20)$$

Note that the average quantities are still used for ρ , U , and p in the friction term, and for U in the dynamic pressure term of Eq. (4.20). Although it would be preferable to use quantities evaluated at each tap location, the relatively short ducts, low velocity, and assumption of incompressibility on which the loss coefficient formulation is based reduce the effect of the change in these terms to less than that of experimental error.

CHAPTER 5

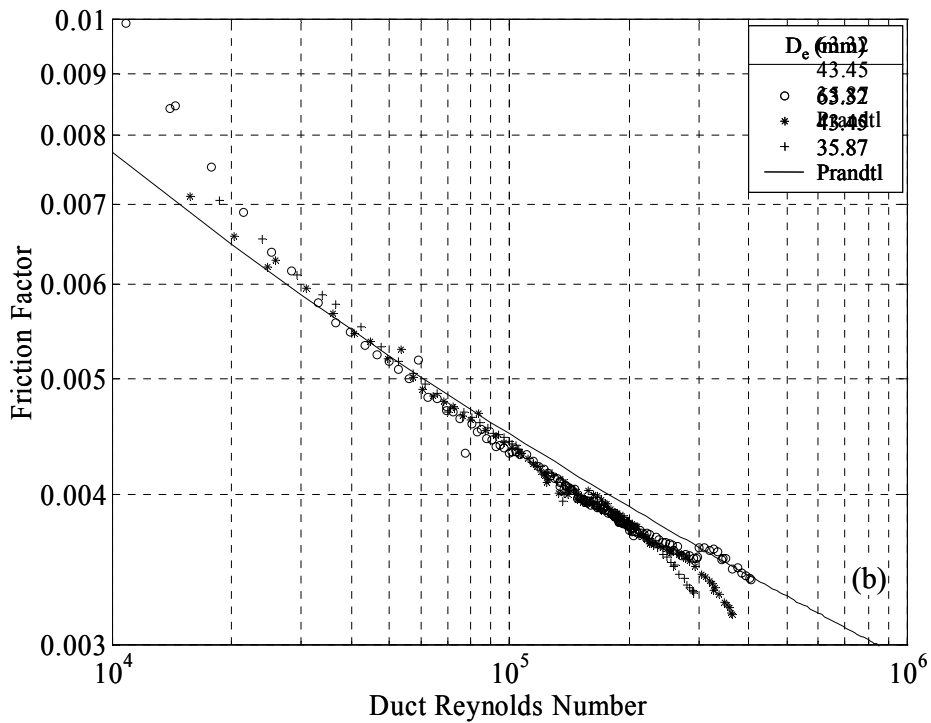
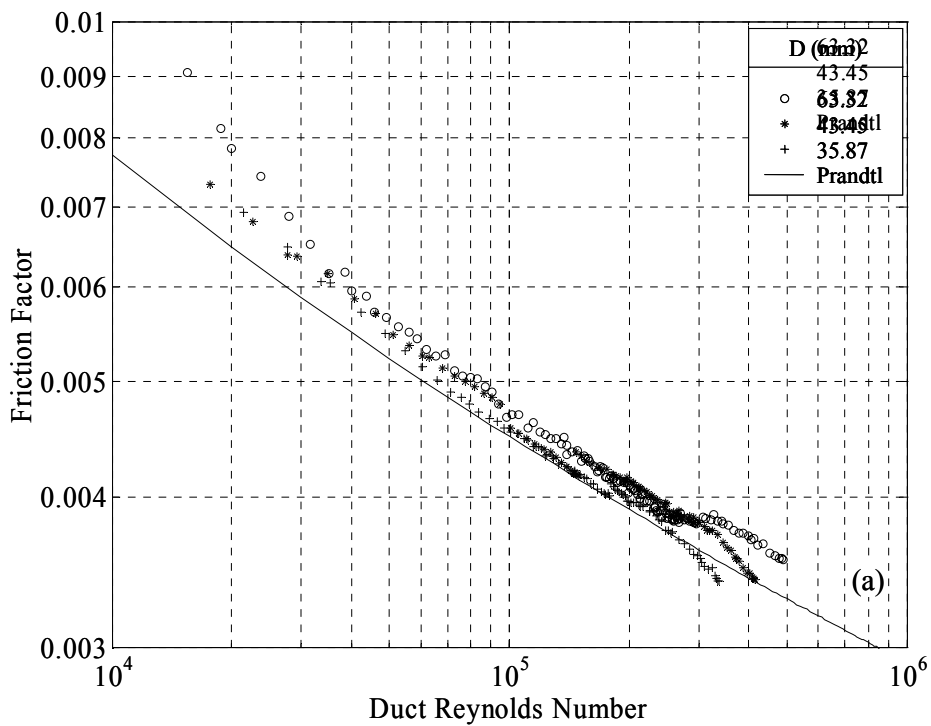
RESULTS

5.1 Straight Tube

Twelve ducts were tested with varying shape and cross-sectional area to determine flow losses due to friction. The measured Fanning friction factors in circular, square, and rectangular ducts are depicted as a function of duct Reynolds number in Figure 5.1 (a), (b), and (c), respectively. Also included is the friction factor by Prandtl (see Benedict, 1980) for turbulent flow in a hydraulically smooth pipe:

$$\frac{1}{\sqrt{4f}} = 2 \log(\text{Re} \sqrt{4f}) - 0.8. \quad (5.1)$$

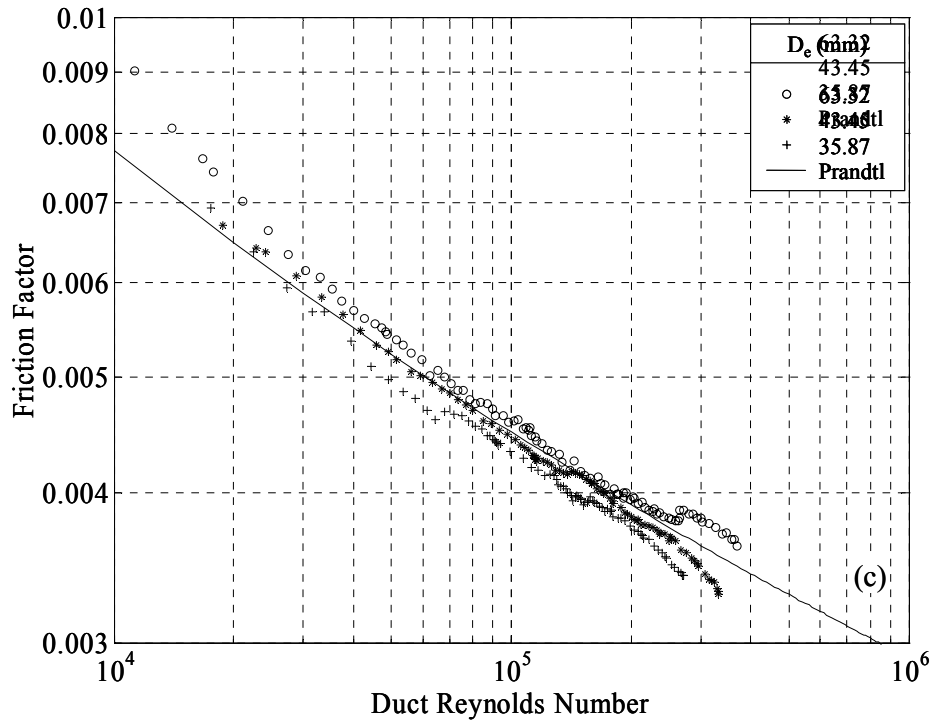
The widest possible range of flow rates was tested for each duct in order to insure that friction data would be available for all conditions encountered in junction experiments. The largest deviations from Prandtl occur at the highest and lowest flow rates tested. For the range of Re used in the T-junction experiments ($\text{Re}_c = 6 \times 10^4 - 4 \times 10^5$), however, the measured friction for all ducts closely follows the Prandtl estimates. The deviation at the lowest flow rates is attributed primarily to pressure measurement inaccuracies. This is most evident for the largest ducts tested, in which the total pressure drop over the entire test section at the lowest flow rate was typically around 7 Pa (0.028 in H₂O only, which



Continued

Figure 5.1: Measured friction factor for varying duct shape: (a) circular, (b) square, (c) rectangular

Figure 5.1 continued



corresponds to 0.8% of the full scale reading for the most sensitive transducer calibration used of 872 Pa (3.5 in H₂O). The increasingly negative slopes at $Re > 3 \times 10^5$ for the two smaller duct sizes tested are the result of flow measurement error due to the high system pressure drops encountered in this range. Total system pressure drops reached the maximum attainable by the flow bench, equal to 22.42 kPa (90 in H₂O). The flow nozzle absolute inlet pressure was at the very limit of the manometer compensation range, resulting in a higher indicated mass flow rate.

The measurements of friction factor for all three sizes of circular ducts tested resulted in measured friction factors slightly higher than the predictions of Prandtl over the range of $Re = 6 \times 10^4 - 4 \times 10^5$. This is to be expected, as the ducts tested were not

perfectly smooth. The measurements for rectangular ducts are about the same as Prandtl, whereas those of square ducts are consistently below. This is in agreement with the trend of increasing friction factor with duct aspect ratio observed by Hartnett *et al.* (1962).

Upon completion of straight duct experiments, it was found that the measured friction factor for the oval ducts was significantly higher than all other ducts tested. Further investigation revealed that the type and thickness of construction materials used in oval duct fabrication was not sufficient to prevent deformation of the duct cross-sections under the level of vacuum generated during experiment. The reduction in cross-sectional area caused an increase in mean velocity, resulting in a higher measured pressure gradient. Since the error due to duct deformation was a function of test piece pressure drop, there was no justifiable way to correct the experimental data, and so no measurements for oval ducts are presented here.

5.2 T-Junctions

Experiments were first performed with the circular junctions to: (1) determine flow development lengths required to accurately measure loss coefficients, (2) study loss coefficient dependence on combined duct Reynolds number, and (3) verify the accuracy of the test setup.

5.2.1 Flow Loss Development Lengths

The measured loss coefficients K_{cs} and K_{cst} in junctions with $A_c/A_s=1$ and varying r are shown in Figures 5.2-5.4 as a function of distance from the junction interface for varying Q_s/Q_c and for the highest combined duct flow rates tested. The depicted

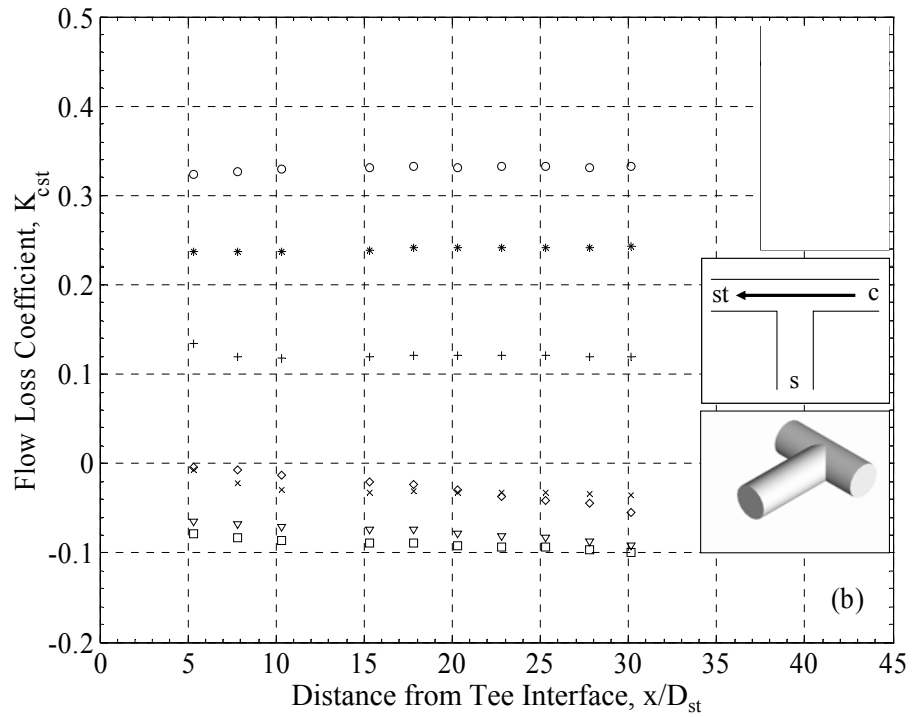
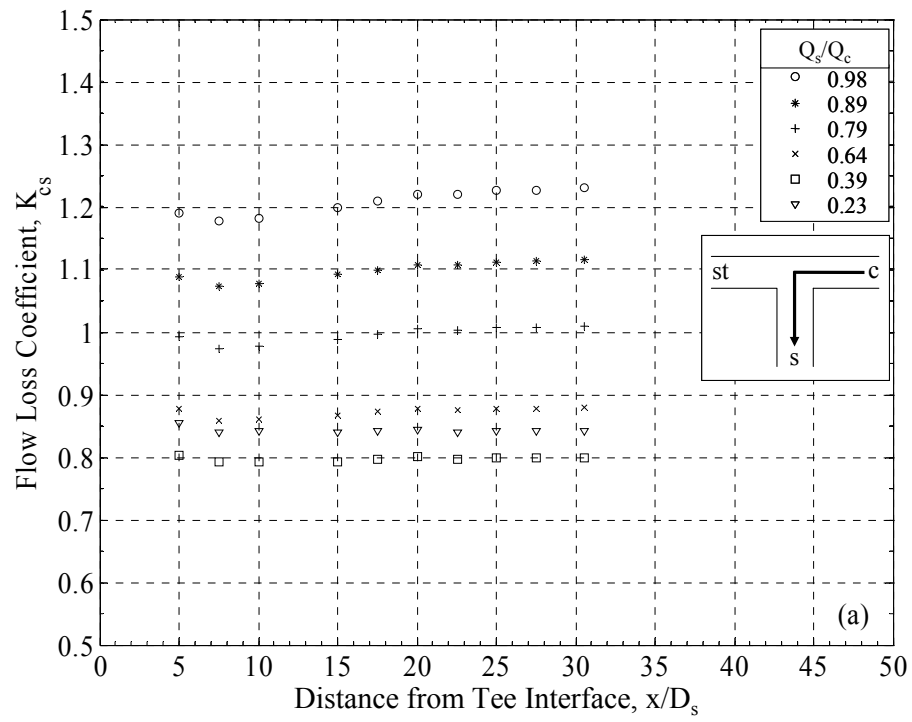


Figure 5.2: Losses as a function of distance from interface of circular junction, $A_c/A_s=1$, $r=0$: (a) side duct, (b) straight duct

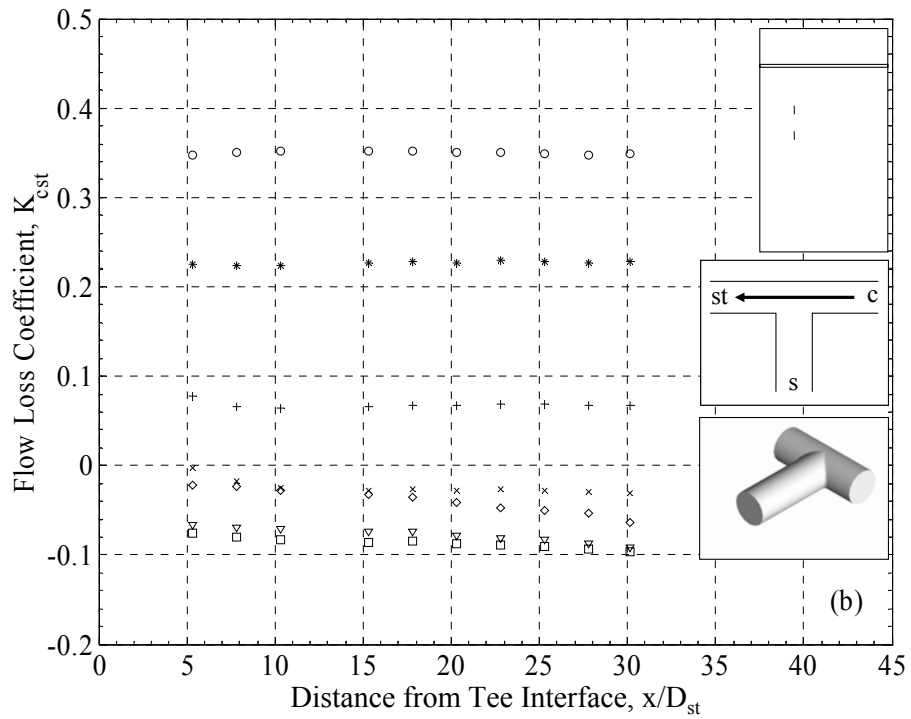
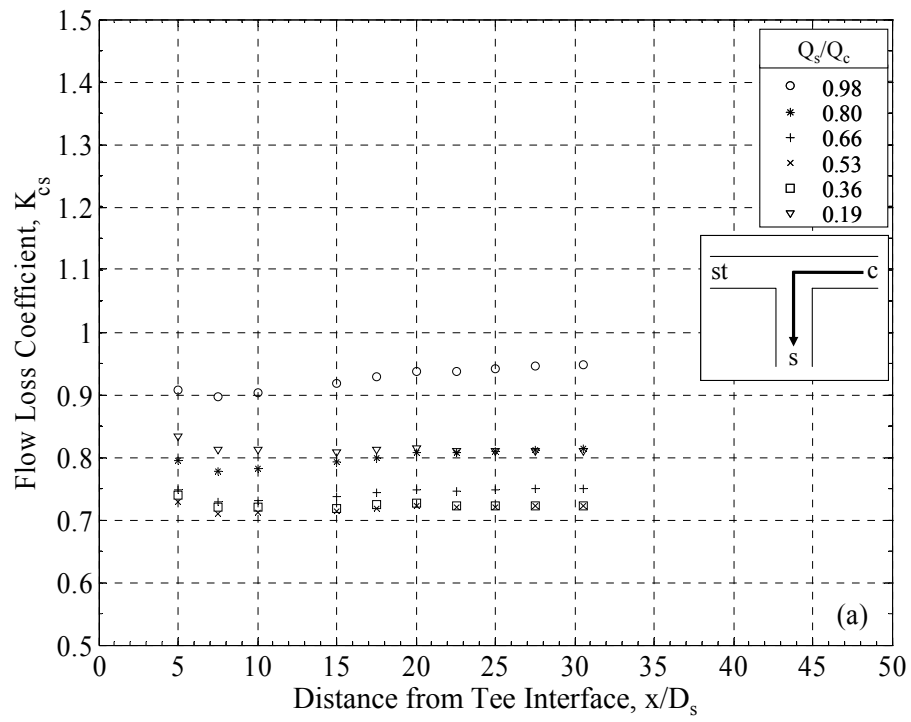


Figure 5.3: Losses as a function of distance from interface of circular junction, $A_c/A_s=1$, $r=0.1 D_s$: (a) side duct, (b) straight duct

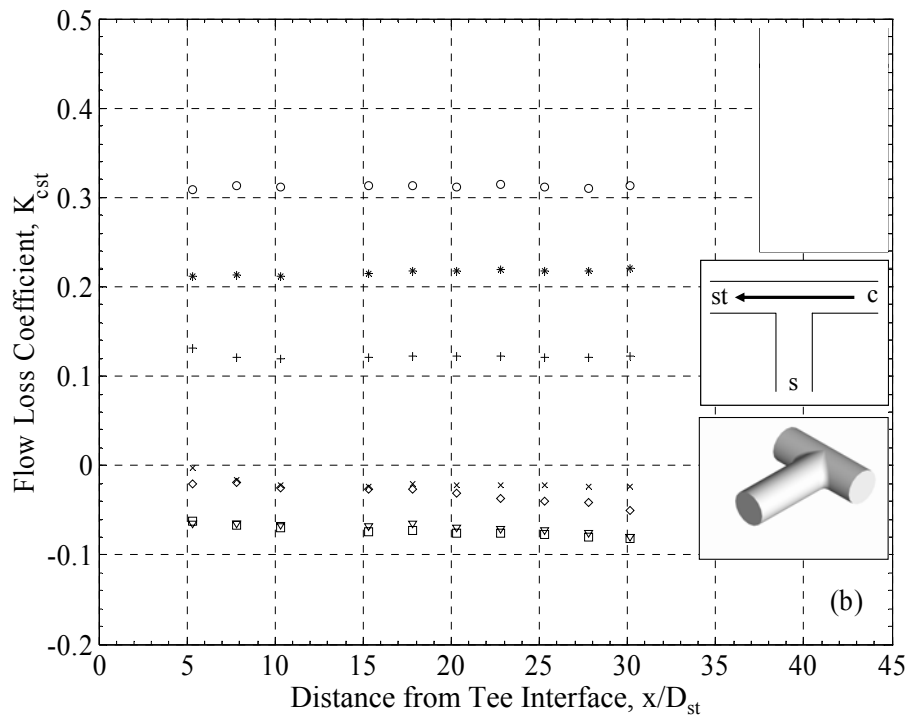
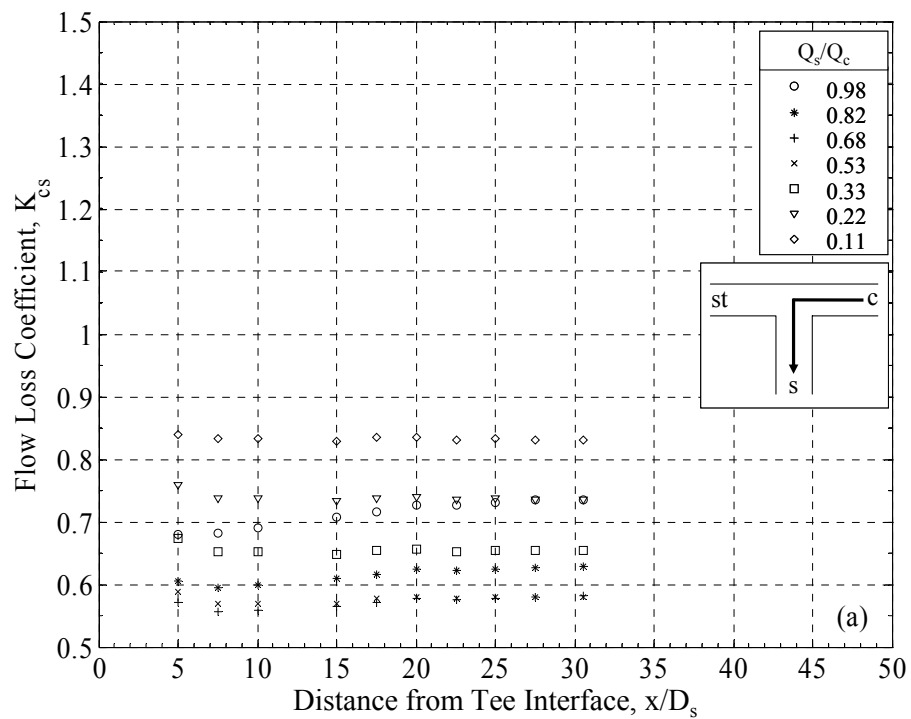


Figure 5.4: Losses as a function of distance from interface of circular junction, $A_c/A_s=1$, $r=0.2 D_s$: (a) side duct, (b) straight duct

behavior is typical of all combined flow rates used. The primary uses of such plots are to evaluate the accuracy of the friction data used in determining the loss coefficient, and to find the minimum length required for the measured loss coefficient to reach a constant value with distance from the junction interface, indicating fully developed flow. The near constant value of K_{cs} (Figures 5.2a, 5.3a, and 5.4a) over the length $x/D_s=20 - 30$ indicates that both the frictional effects are correctly accounted for, and that the flow has become fully developed. Although there is some variation in K_{cs} over the length $x/D_s=5 - 20$, the majority of flow losses are realized within the first tap location of $x/D_s=5$ for all three junctions. The development of K_{cs} is also relatively independent of junction interface radius over a range of: $r=0 - 0.2 D_s$ for $A_c/A_s=1$.

The measured loss coefficients K_{cs} and K_{cst} in junctions with $r=0.2 D_s$ and $A_c/A_s=2.124$ and 3.117 are shown in Figures 5.5 and 5.6, respectively, as a function of distance from the junction interface for varying Q_s/Q_c and for the highest combined duct flow rates tested. The depicted behavior is typical of all combined flow rates used. The majority of flow losses in the side branch (Figures 5.5a and 5.6a) are realized within the first tap location of $x/D_s=5$ for side branch velocities up to those of the combined duct, occurring at flow ratios of $Q_s/Q_c=0.47$ and 0.32 for $A_c/A_s=2.124$ and 3.117 , respectively. Both the shape and length of development for K_{cs} at side duct velocities above those in the combined duct are consistent with the experimental results of Barbin *et al.* (1963) and Wang *et al.* (1974) for the entry length of circular ducts. Measurements of K_{cs} for both junctions are relatively flat over the length $x/D_s=20-35$ for flow ratios up to $Q_s/Q_c=0.75$. At higher flow ratios, K_{cs} decreases in the case of $A_c/A_s=2.124$, and increases for $A_c/A_s=3.117$, with increasing distance from the junction interface. This may be attributed

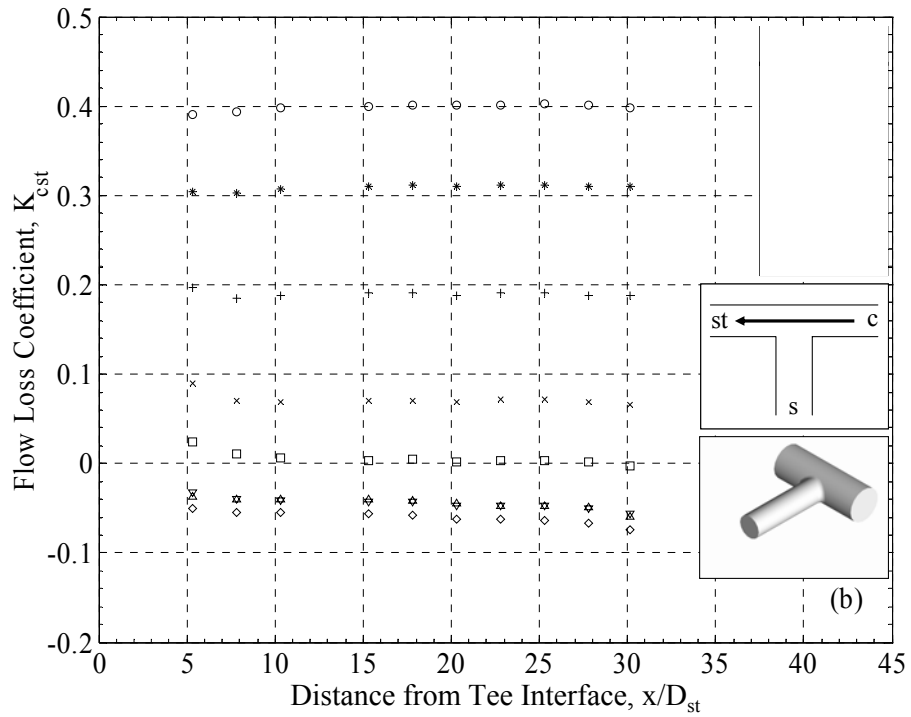
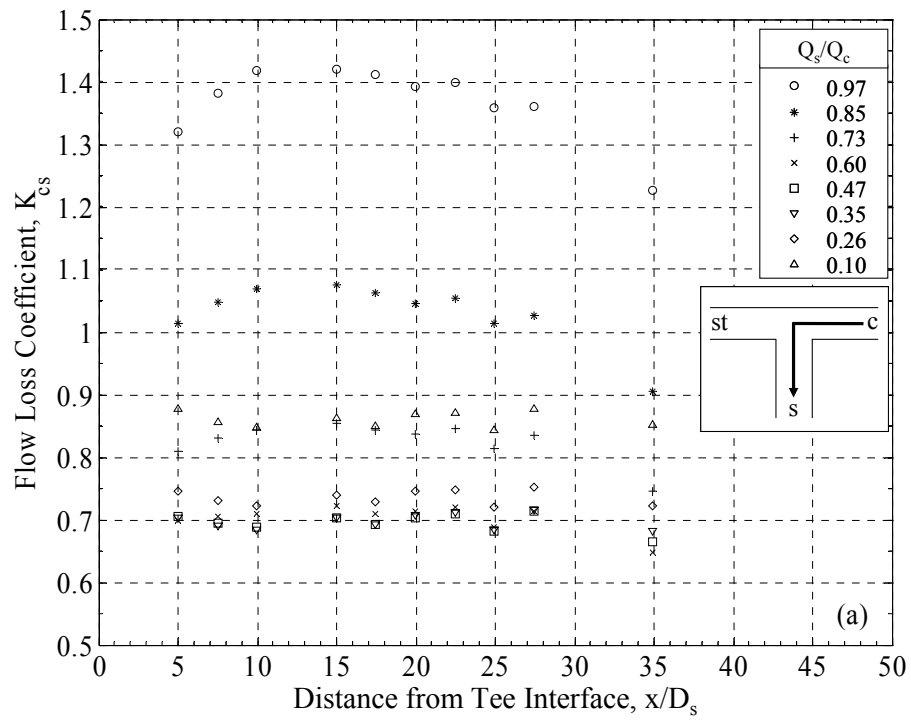


Figure 5.5: Losses as a function of distance from interface of circular junction, $A_c/A_s=2.124$, $r=0.2 D_s$: (a) side duct, (b) straight duct

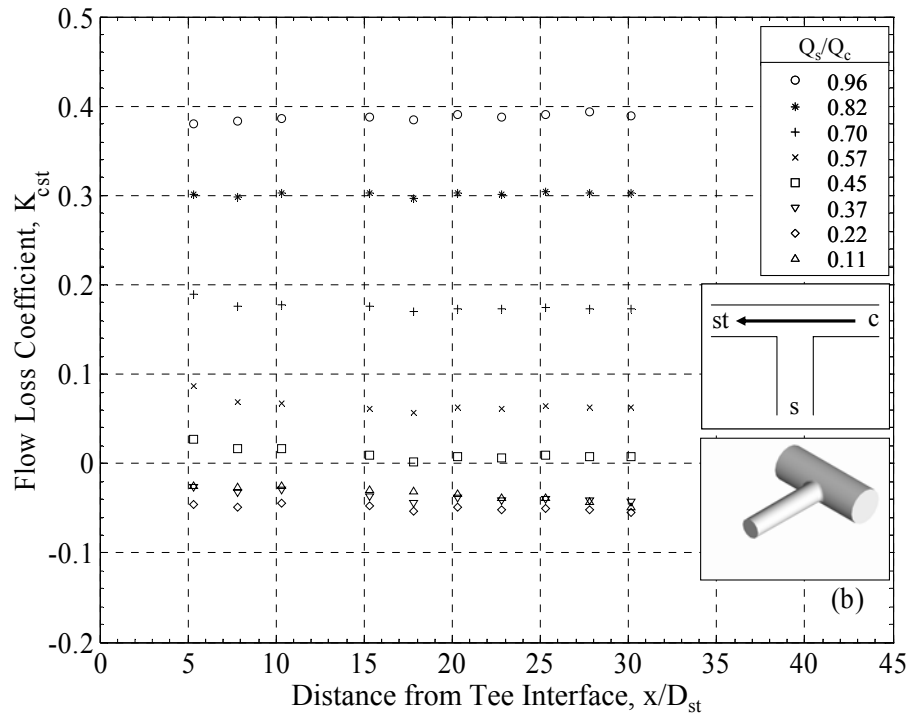
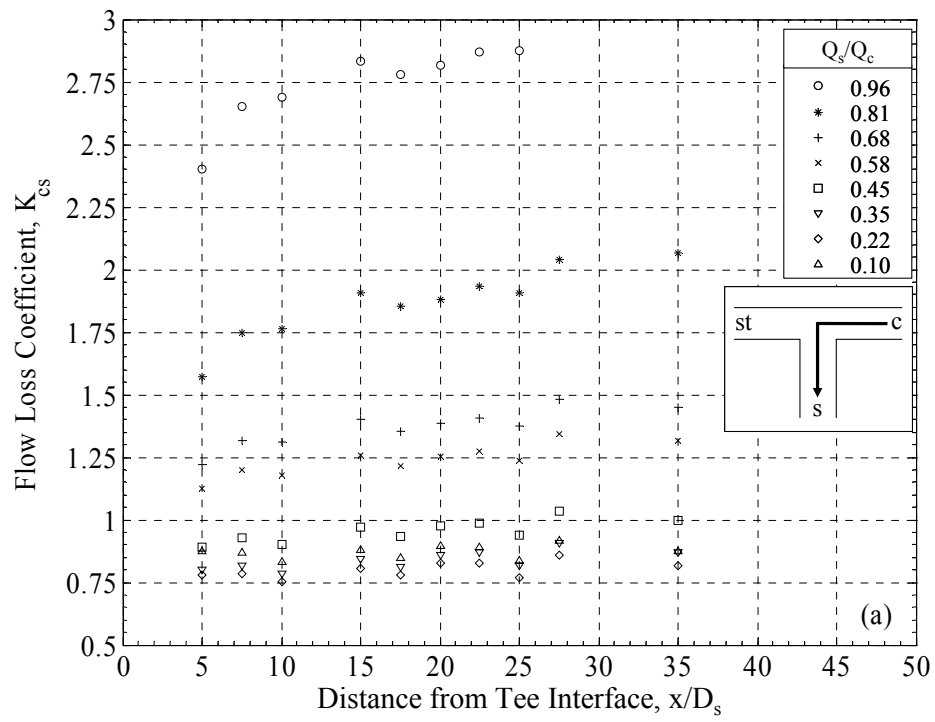


Figure 5.6: Losses as a function of distance from interface of circular junction,

$A_c/A_s=3.117$, $r=0.2 D_s$: (a) side duct, (b) straight duct

to an increased measurement error resulting from higher A_c/A_s . The amount of static pressure drop between the common duct and side branch due to acceleration of the fluid increases as A_c/A_s is increased, as do the frictional losses in the side branch for a given combined-duct flow rate, due to the higher fluid velocity in the side branch. The result is a smaller part of the total static pressure drop being due to junction flow losses. As an example, K_{cs} accounts for approximately 65% of the measured static pressure drop in the case of $A_c/A_s=1$ and $r=0.2D_s$, and only approximately 15% in the case of $A_c/A_s=3.117$ and equal interface radius.

K_{cst} is nearly constant over the entire test length of $x/D_{st}=5 - 30$, for all five circular junctions tested (Figures 5.2b, 5.3b, 5.4b, 5.5b, and 5.6b) indicating that the flow quickly redevelops in the straight duct after the junction interface. The development of K_{cst} is relatively unaffected by junction interface radius, or area ratio for all junctions tested.

5.2.2 Reynolds Number Dependence and Curve Fitting

The measured loss coefficients K_{cs} and K_{cst} for circular junctions are shown in Figures 5.7-5.9 for $A_c/A_s=1$ and varying r . K_{cs} is independent of Re_c over the entire range of combined-duct flow rates tested, $Re_c=6.19 \times 10^4 - 3.75 \times 10^5$ ($M_c=0.04 - 0.28$) in junctions with $r=0$ (Figure 5.7a) and $0.1 D_s$ (Figure 5.8a). For the junction with $r=0.2 D_s$ (Figure 5.9a), K_{cs} decreases asymptotically with increasing Re_c , becoming nearly constant for $Re_c > 2 \times 10^5$. K_{cst} is independent of Re_c (Figures 5.7b, 5.8b, and 5.9b) in all junctions and flow rates measured.

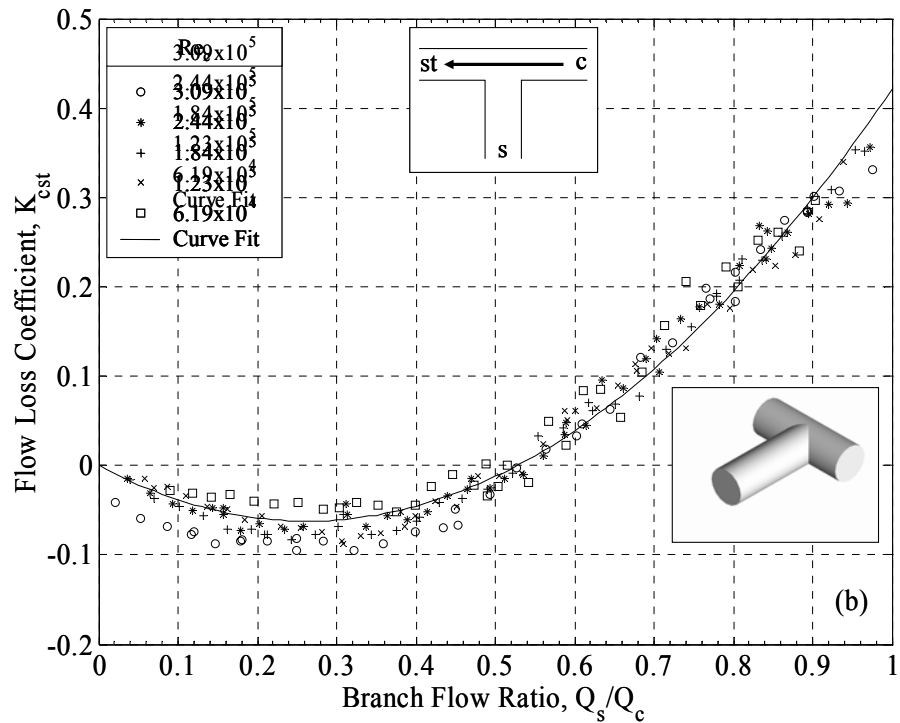
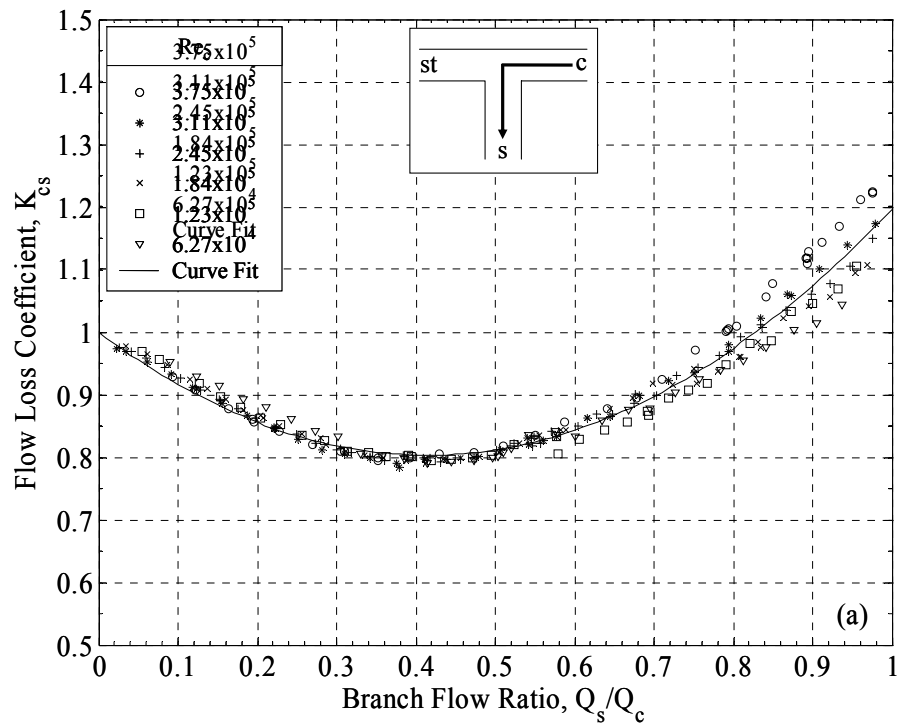


Figure 5.7: Losses for circular junction, $A_c/A_s=1$, $r=0$: (a) K_{cs} , (b) K_{cst}

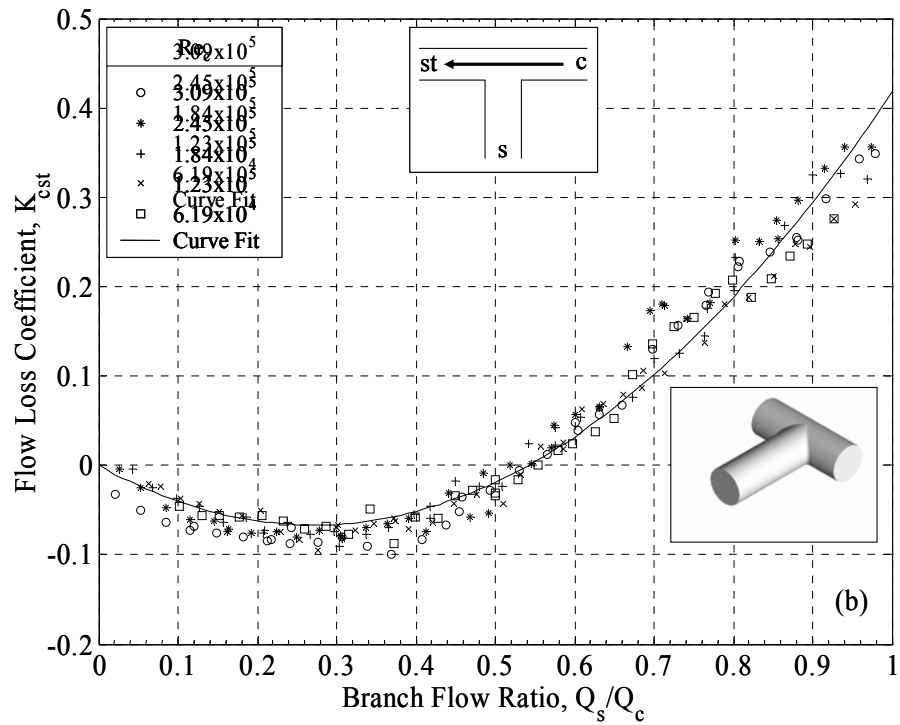
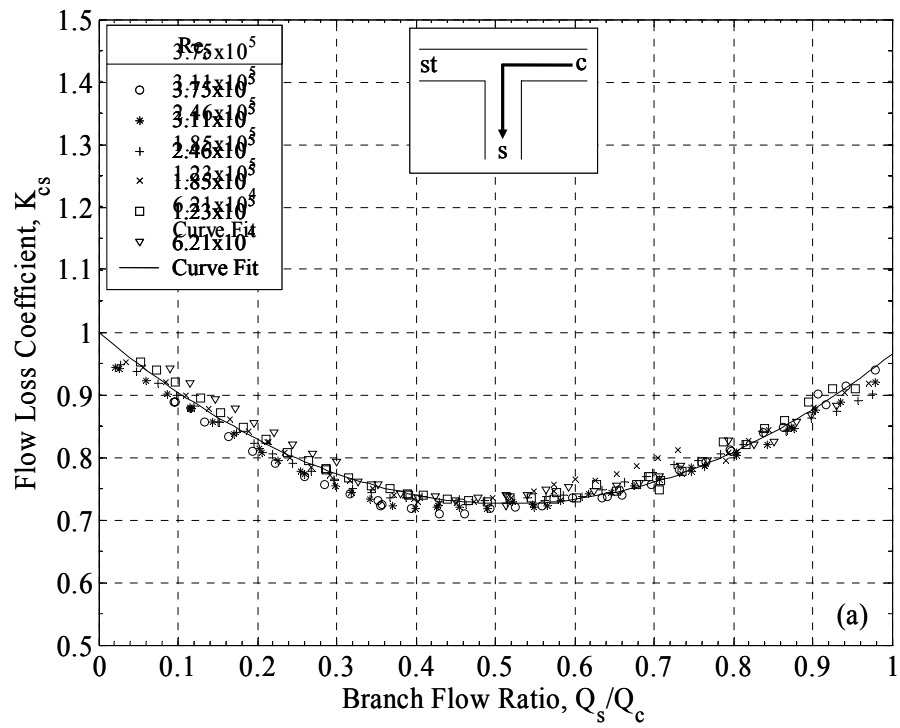


Figure 5.8: Losses for circular junction, $A_c/A_s=1$, $r=0.1 D_s$: (a) K_{cs} , (b) K_{cst}

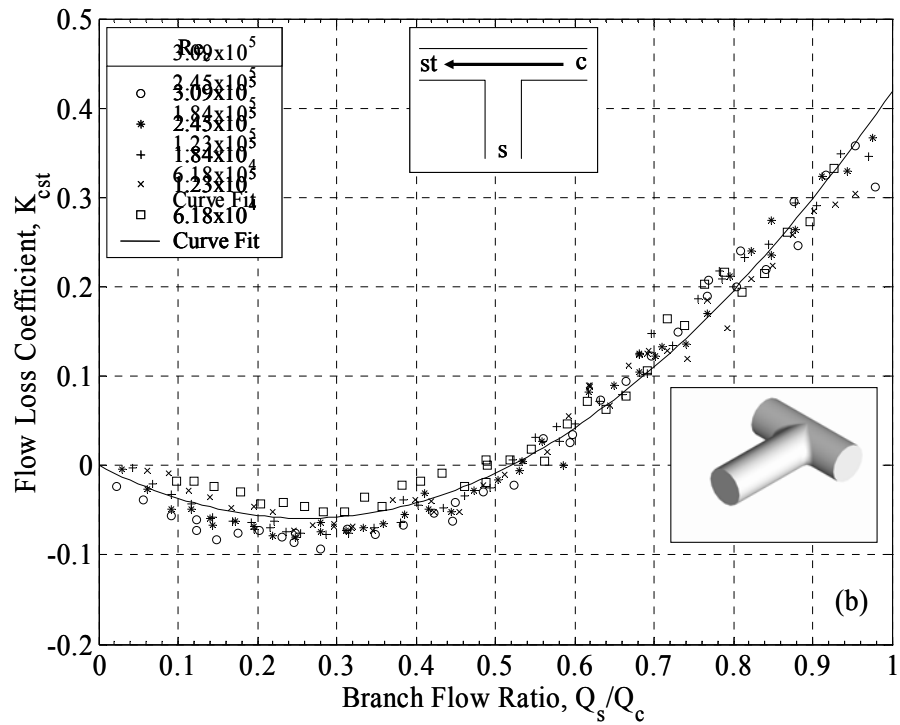
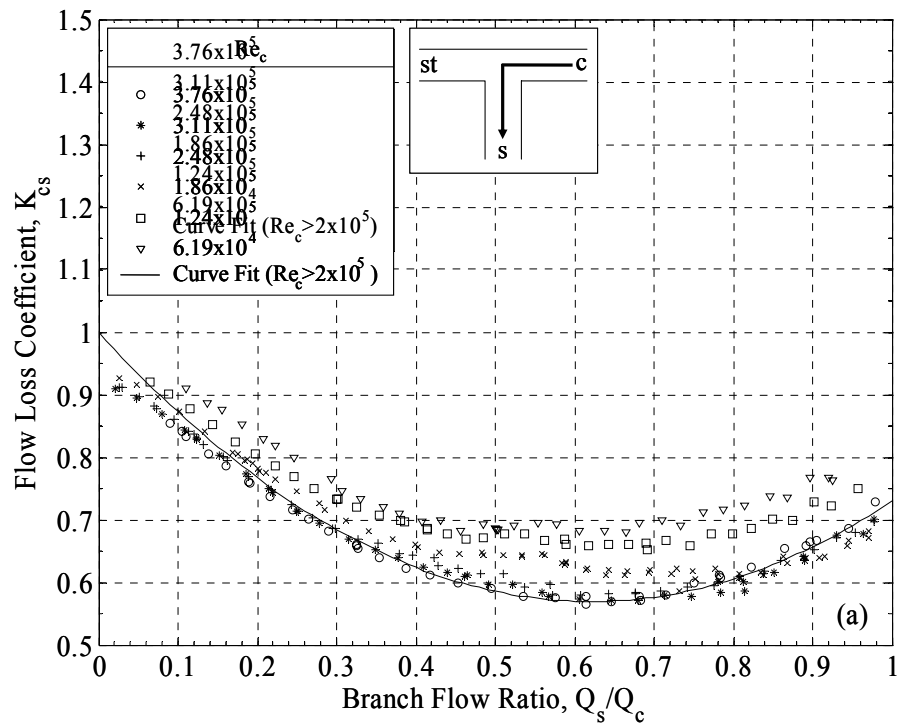


Figure 5.9: Losses for circular junction, $A_c/A_s=1$, $r=0.2 D_s$: (a) K_{cs} , (b) K_{cst}

Loss coefficients for circular junctions with $A_c/A_s=2.124$ and 3.117 are shown in Figures 5.10 and 5.11, respectively. Although both junctions employ radii of $r=0.2 D_s$, and there is some spread in measurements of K_{cs} (Figures 5.10a and 5.11a), there is no discernable dependence on Re_c . The increased scatter of K_{cs} relative to junctions with $A_c/A_s=1$ is due to the higher measurement error described earlier for junctions with $A_c/A_s > 1$. K_{cst} (Figures 5.10b and 5.11b) does not exhibit any increase in measurement error, however, as the straight duct diameter is equal to that of the combined duct in all junctions tested. K_{cst} also shows no dependence on Re_c for $A_c/A_s > 1$.

For $Q_s/Q_c=0$, there is no drop in static pressure due to friction in the side branch since $U_s=0$, therefore the static pressure along its length must be constant. Because the combined and side ducts are connected, their static pressures must be equal at the interface. Provided the interface does not significantly influence the combined duct flow, this will result in $K_{cs}=1$ in Eq. (2.32). Also for $Q_s/Q_c=0$, the flow rate in the straight duct is equal to that in the combined duct. Because $A_c=A_{st}$, the change in static pressure between the combined and straight ducts should then be due to friction only, resulting in $K_{cst}=0$ in Eq. (2.33). The tendency of K_{cs} to head to unity and K_{cst} to zero as Q_s/Q_c approaches zero has been predicted by Hager (1984), along with a second order dependence of both loss coefficients on Q_s/Q_c . Thus, second order fits with y-intercepts of unity for K_{cs} and zero for K_{cst} are presented in Figures 5.7-5.11. All data points are used in the curve fitting with the exception of K_{cs} in the junction with $A_c/A_s=1$ and $r=0.2 D_s$, (Figure 5.9a) which includes only points with $Re_c > 2 \times 10^5$. The quality of fit with equations of this form is good, with the largest discrepancy being in the case of $A_c/A_s=1$ and $r=0.2 D_s$, whose y-intercept appears to be slightly below unity at approximately 0.95.

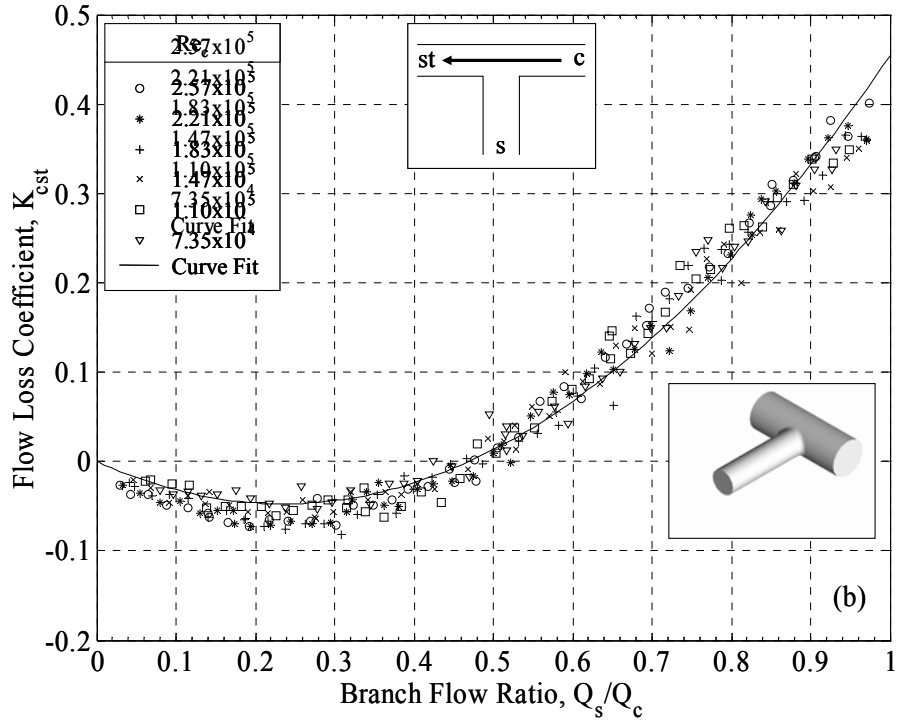
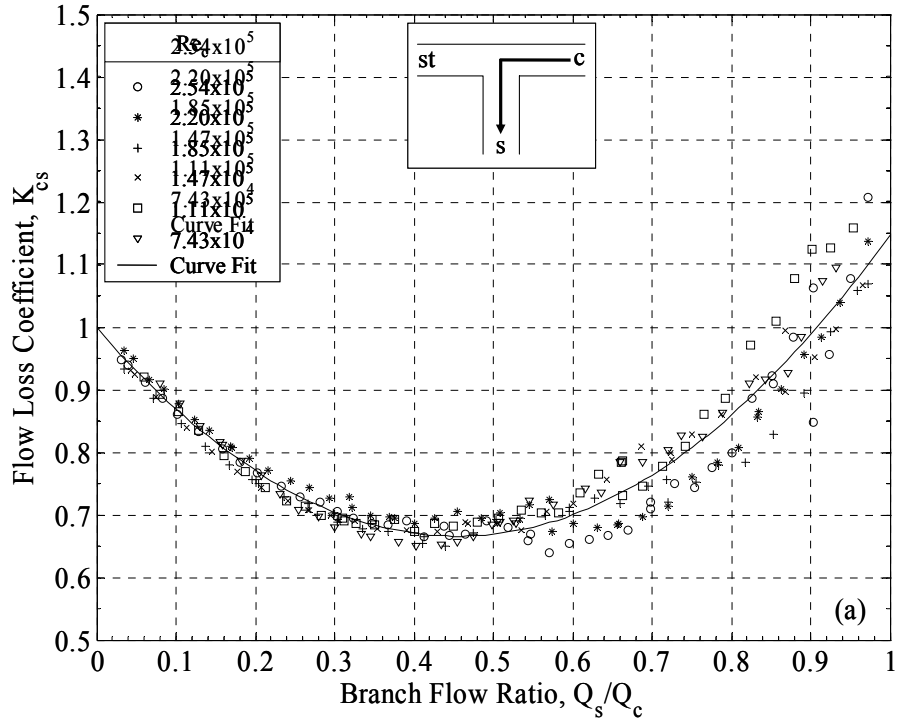


Figure 5.10: Losses for circular junction, $A_c/A_s=2.124$, $r=0.2 D_s$: (a) K_{cs} , (b) K_{cst}

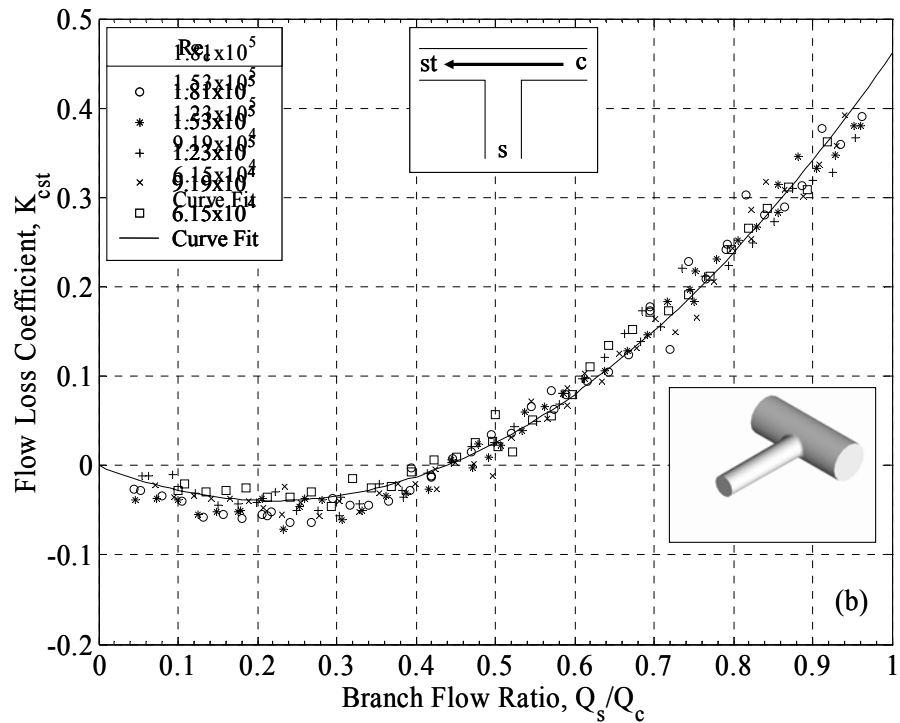
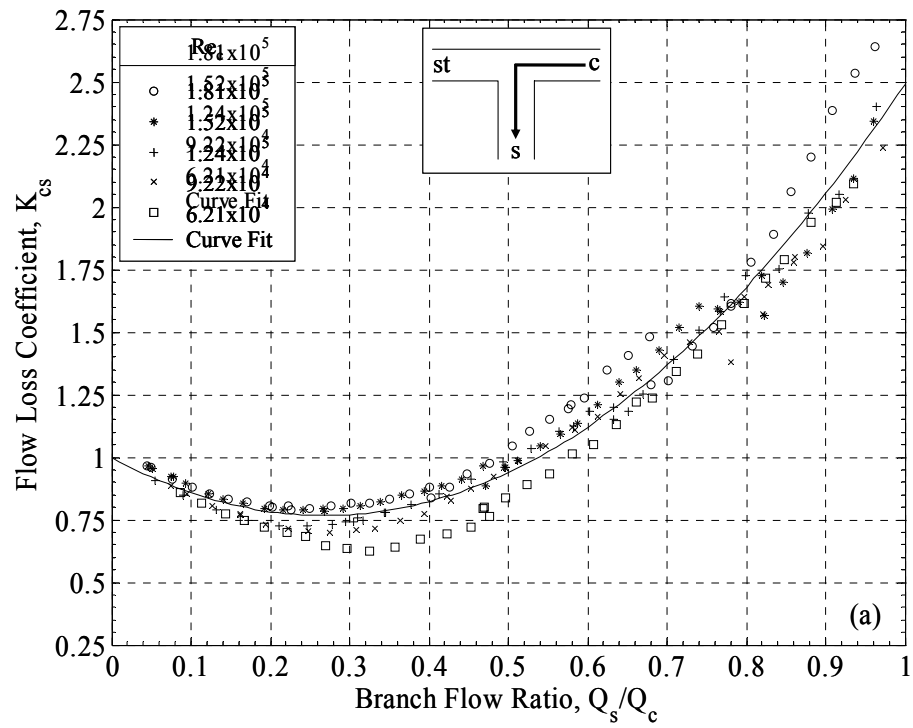


Figure 5.11: Losses for circular junction, $A_c/A_s=3.117$, $r=0.2 D_s$: (a) K_{cs} , (b) K_{cst}

5.2.3 Comparisons with Published Data

Comparisons of the results for circular junctions with those available in the literature for identical junction configurations are shown in Figures 5.12-5.13 for $A_c/A_s=1$ and varying r . For the values of A_c/A_s used in the current work, direct comparisons are only available for the junctions with $A_c/A_s=1$. It should be noted that air was used as the working fluid in the current study, while water was used in all of the previous works. The curve fit of K_{cs} for $A_c/A_s=1$ and $r=0$ is compared in Figure 5.12a to the published results of Kinne (1931), McNown (1954), Gardel *et al.* (1971), and Ito *et al.* (1973). The results of the current study fall in between those of Kinne and Gardel *et al.*, while showing good agreement with Ito *et al.* The current results for K_{cst} for the same junction (Figure 5.12b) are also somewhat bounded by those of Kinne and Gardel *et al.*, while those of Ito *et al.* are slightly higher. All results show K_{cst} being negative at low to mid Q_s/Q_c . An in-depth study of this phenomenon was performed by McNown (1954), who attributed the apparent gain in energy between the combined and straight ducts to the inaccuracy in the assumption of uniform flow made in the formulation of Eq. (2.30), leading to the neglect of radial variation of fluid velocity. At low Q_s/Q_c mostly slower moving fluid from the wall of the combined duct is drawn into the side branch. As a result, the fluid that continues on to the straight duct has a higher average kinetic energy than that in the combined duct.

The current results also fall somewhat in the middle of the published data for K_{cs} for $A_c/A_s=1$ and $r=0.1$ and $0.2 D_s$ in Figures 5.13a and 5.13b, respectively. There is some discrepancy at flow ratios below $Q_s/Q_c=0.35$, which is primarily due to the choice of

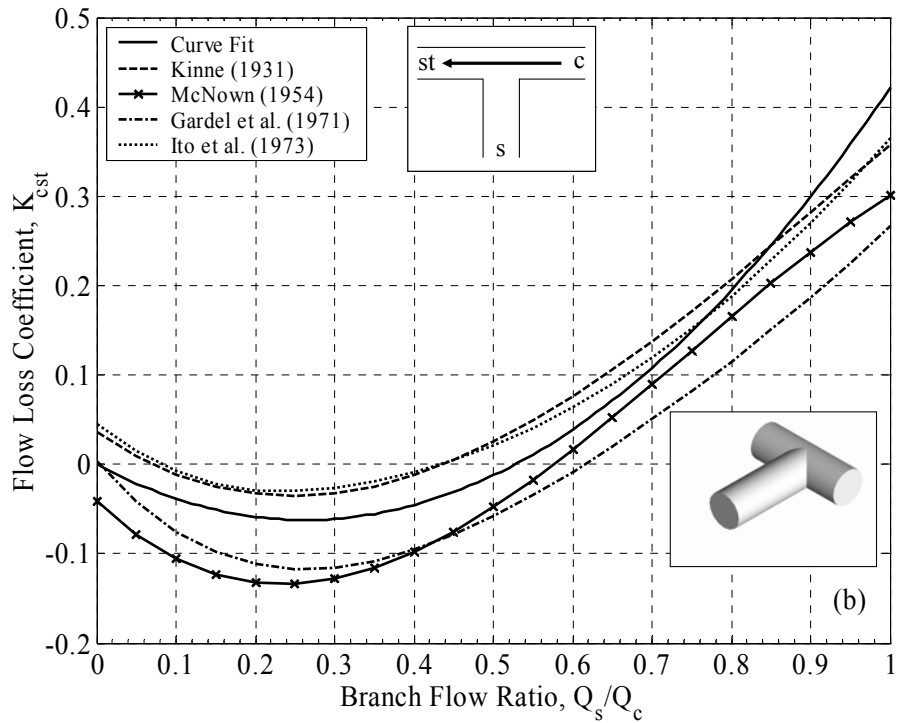
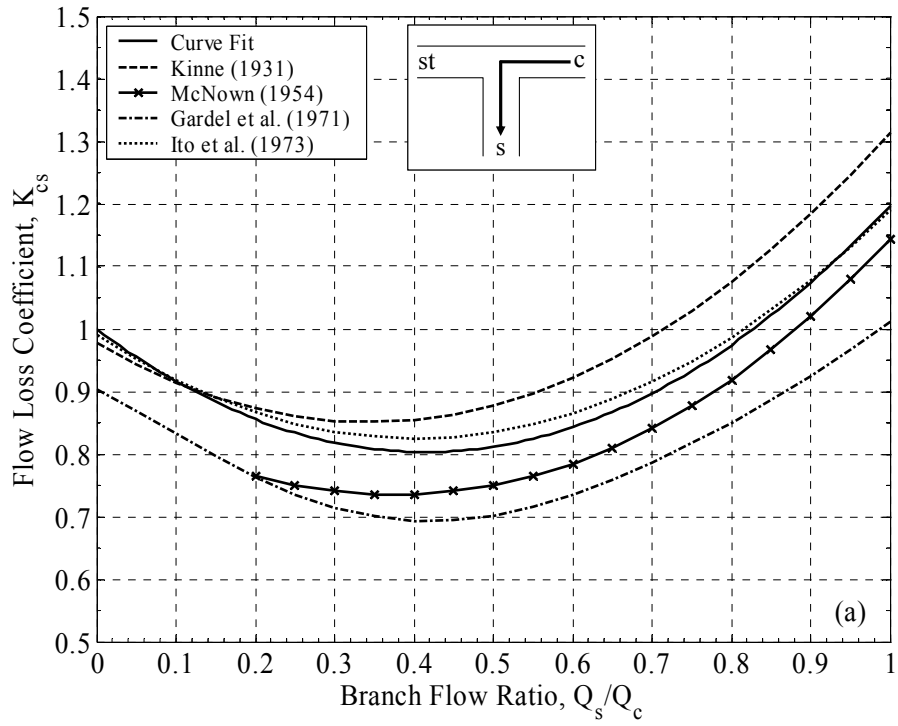


Figure 5.12: Comparison of current results with published data for circular junction, $A_c/A_s=1$, $r=0$: (a) K_{cs} , (b) K_{cst}

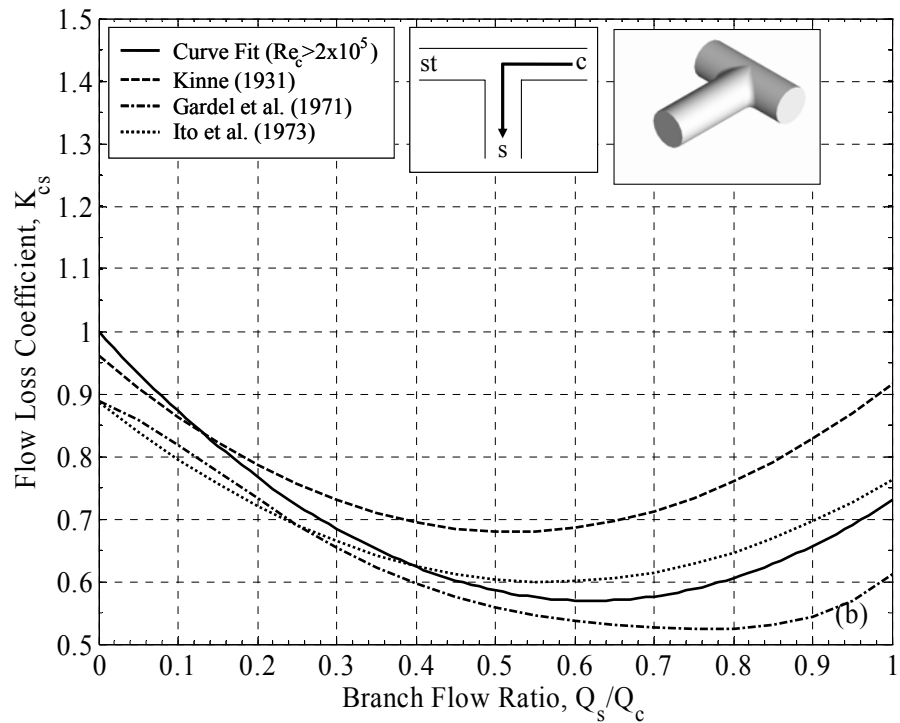
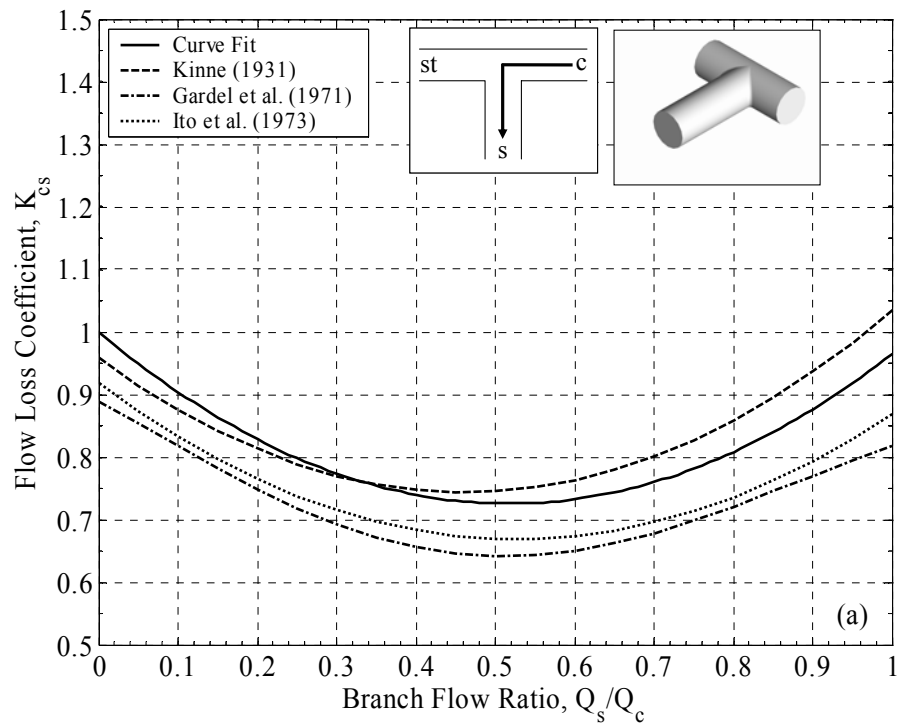


Figure 5.13: Comparison of current measurements of K_{cs} with published data for circular junction, $A_c/A_s=1$: (a) $r=0.1 D_s$, (b) $r=0.2 D_s$

curve fit. The results of the current work for $r=0.2 D_s$ (Figure 5.13b) agree best with Ito *et al.* Although the spread in results for $r=0.2 D_s$ is not any greater than those for other r , some of the discrepancy could be attributed to the Reynolds number dependency observed in the current work for this geometry. The experiments were conducted with combined duct Reynolds numbers of $Re_c=1 \times 10^5$ and 2×10^5 by Ito *et al.* and 2.5×10^5 - 3.4×10^5 by Gardel *et al.*, while no combined duct flow rate is explicitly defined by Kinne. Overall, the results of the current work appear to be within the experimental variation presented by the published data.

5.2.4 Interface Radius, Area Ratio, and Side Duct Taper Effects

With preliminary experiments exploring development length and Reynolds number dependence completed, a test strategy was determined for the remaining junctions. In all subsequent tests, five pressure tap locations were used in the fully developed region (typically $x/D_h=20-45$) of each downstream duct allowing the simultaneous measurement of both loss coefficients with the available number of pressure transducers. While development effects could be avoided completely by taking pressure measurements a great distance from the junction interface, an increase in measurement error would result from the higher frictional losses contributing to the total static pressure drop, and the effect of error in friction factor measurements on loss coefficient calculation would be compounded by the increased duct length. Due to the independence of both loss coefficients to Re_c in all but one junction configuration, the number of combined duct flow rates tested was reduced to approximately half of that tested in the preliminary experiments, while still covering the same overall range. Curve

fits previously described in Section 5.2.2 are used in the remaining figures in this chapter for discussion purposes. Experimental results for all junctions with noncircular or tapered side branches are presented in Appendix A, while the curve fits used for all junctions are defined explicitly in Appendix B.

The effects of interface radius on K_{cs} and K_{cst} for $A_c/A_s=1$ are shown in Figure 5.14. The addition of a radius of only $r=0.2 D_s$ (Figure 5.14a) reduces K_{cs} by nearly 40% at $Q_s/Q_c=1$. As r is increased, the location of the minima in K_{cs} moves to higher Q_s/Q_c . The current experiments show an increasing rate of reduction in K_{cs} with increasing radius. This is contrary to the results of both Kinne (1931) and Ito *et al.* (1973), who show a reducing rate of reduction. The trend in the results of Gardel *et al.* (1971) is somewhat between these two extremes, showing a constant rate of reduction with increasing radius. A possible cause for this discrepancy is the high sensitivity of K_{cs} on r , combined with the relative difficulty in defining the magnitude of r around the entire perimeter of the interface. The method used in the current work for junction construction allowed the interface radius to be precisely defined and controlled, thereby making this an unlikely source of error. The layering technique used in junction construction resulted in a somewhat rough surface finish on the junction inner surface, which is in contrast to the highly polished metal pieces used in the works of Kinne and Ito *et al.* The surface finish of junctions used in the work of Gardel *et al.* (1971) was likely somewhere in between, as they were made of cast asbestos concrete. Given the high sensitivity of K_{cs} to interface radius size, it is likely that there is also a sensitivity to surface roughness. K_{cst} is independent of interface radius in the current experiments (Figure 5.14b), which is in agreement with the findings of Ito *et al.*, while Kinne shows some variation. All three

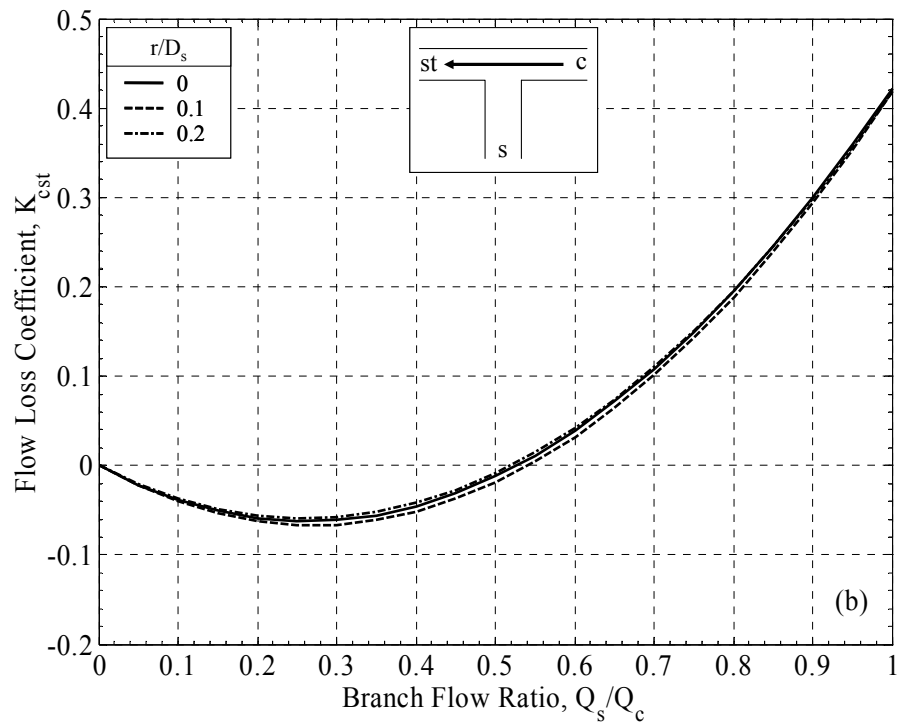
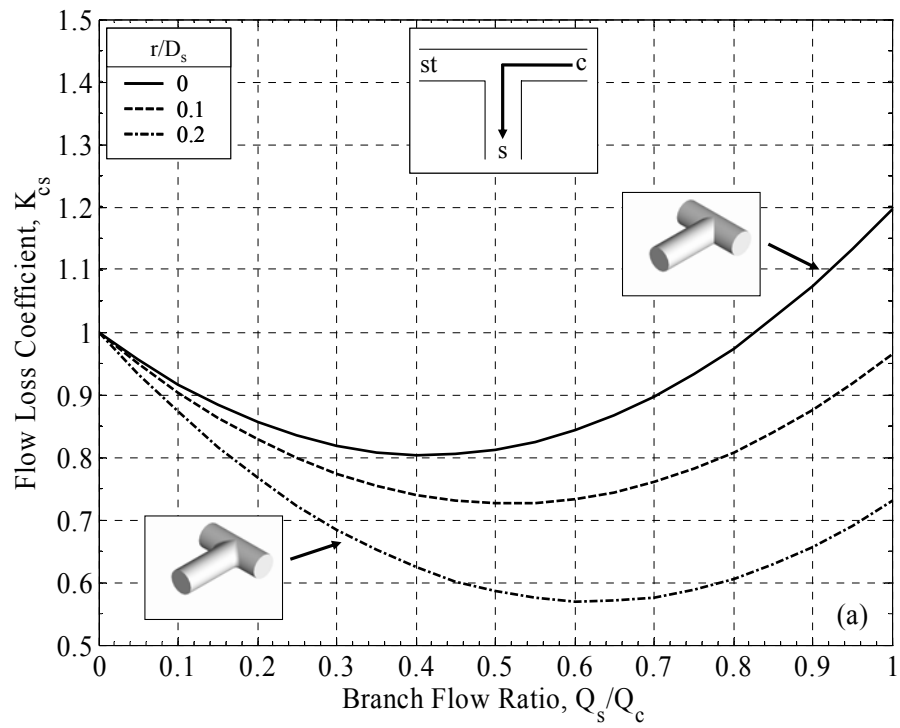


Figure 5.14: Effect of interface radius on losses for circular junction, $A_c/A_c=1$: (a) K_{cs} ,
 (b) K_{cst}

curve fits of K_{cst} for varying radius are nearly identical, showing the repeatability of the current experimental approach.

The effects of A_c/A_s on loss coefficients in junctions with $r=0.2 D_s$ are shown in Figure 5.15. K_{cs} increases strongly with A_c/A_s , (Figure 5.15a) which is consistent with the results of Vogel (1926), McNown (1954), and Gardel *et al.* (1971). As A_c/A_s is increased, the location of the minima in K_{cs} moves to lower Q_s/Q_c . Because the current experiments do not include junctions with $A_c/A_s > 1$ and $r \neq 0.2 D_s$, they cannot be used to determine if the effect of interface radius on K_{cs} is also a function of A_c/A_s . The work of Gardel *et al.* (1971) does include junctions with $A_c/A_s > 1$ and varying interface radius, however, showing that the relative reduction in K_{cs} with increasing r is independent of A_c/A_s . In Figure 5.15b, K_{cst} is shown to increase slightly with A_c/A_s , and is in agreement with the trend presented by McNown (1954). Although the effect is small, the repeatability of K_{cst} measurements demonstrated in junctions with $A_c/A_s=1$ and varying r suggests that it cannot be attributed to experimental error.

The effects of side branch taper on loss coefficients are shown in Figures 5.16 and 5.17 for $A_c/A_s=2.124$ and 3.117, respectively. Both tapered junctions included interface radii that were equal to 20% of the side branch diameter at the junction interface. Included are the results for non-tapered junctions with $r=0.2 D_s$ and $A_c/A_s=1$ or that of the tapered junction. This in effect shows the limits where the length of taper in the junction is infinitely long ($A_c/A_s=1$), or infinitely short ($A_c/A_s=2.124$ or 3.117). The addition of a taper significantly reduces K_{cs} (Figures 5.16a and 5.17a) for both A_c/A_s tested. At low to mid flow ratios K_{cs} is actually lower in the tapered junctions than the junction with $A_c/A_s=1$ and $r=0.2 D_s$. This could be due to the combination of more efficient turning

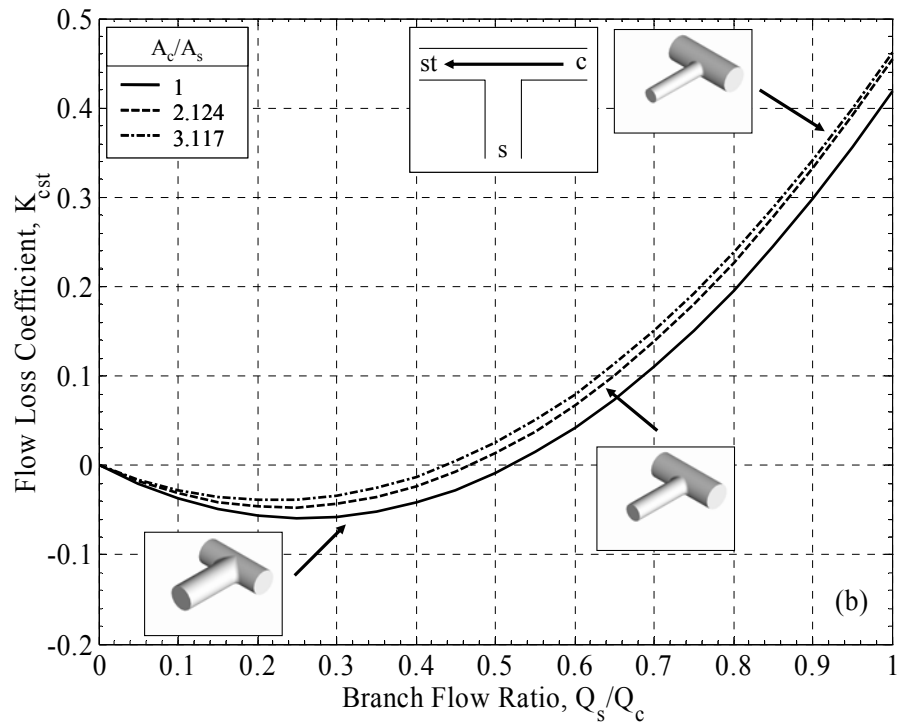
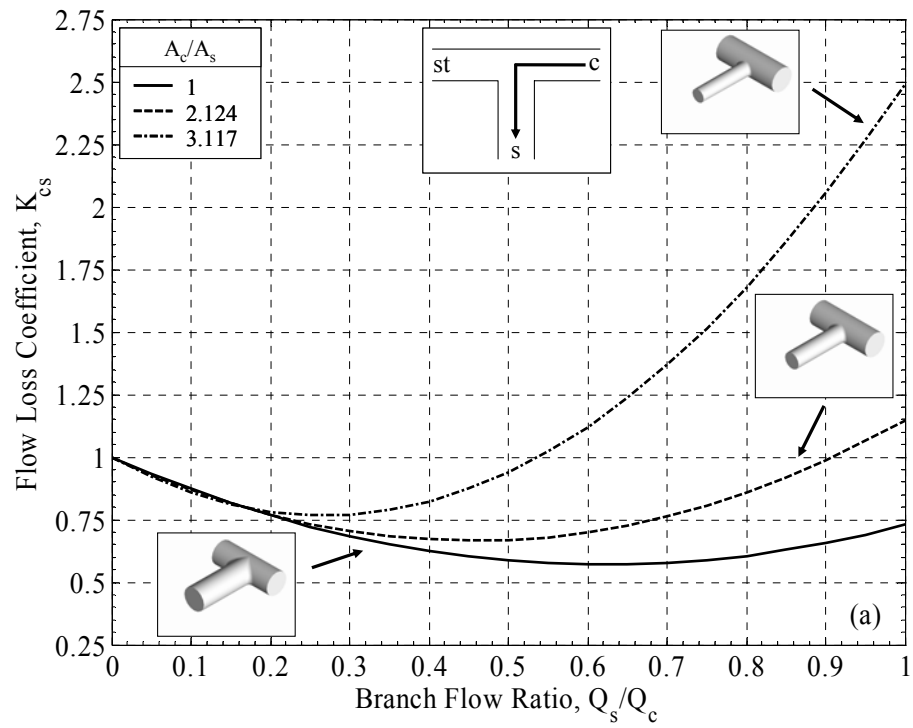


Figure 5.15: Effect of A_c/A_s on losses for circular junction, $r=0.2 D_s$: (a) K_{cs} , (b) K_{cst}

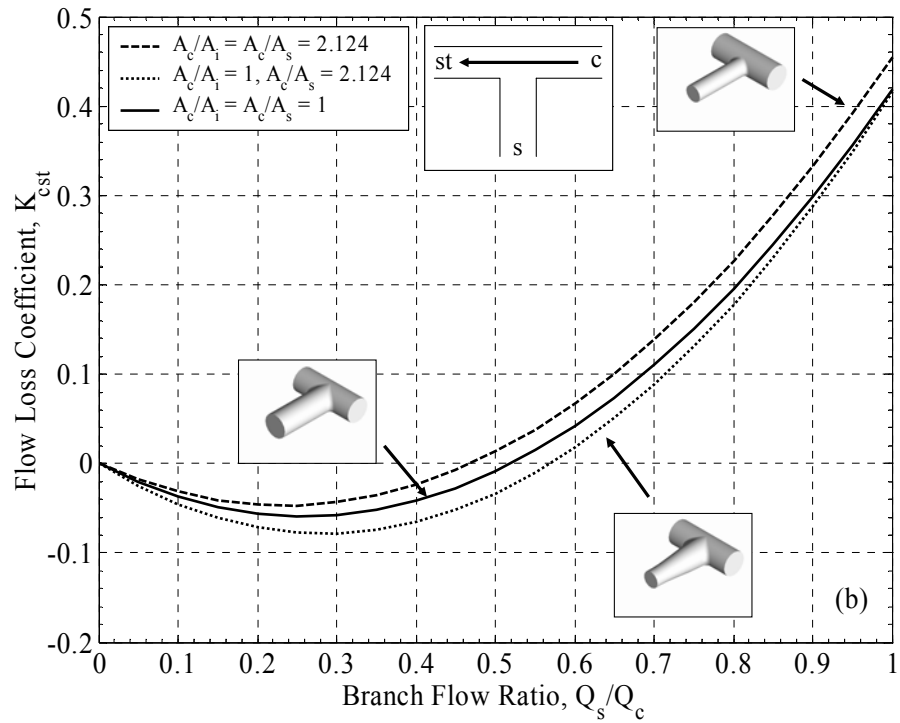
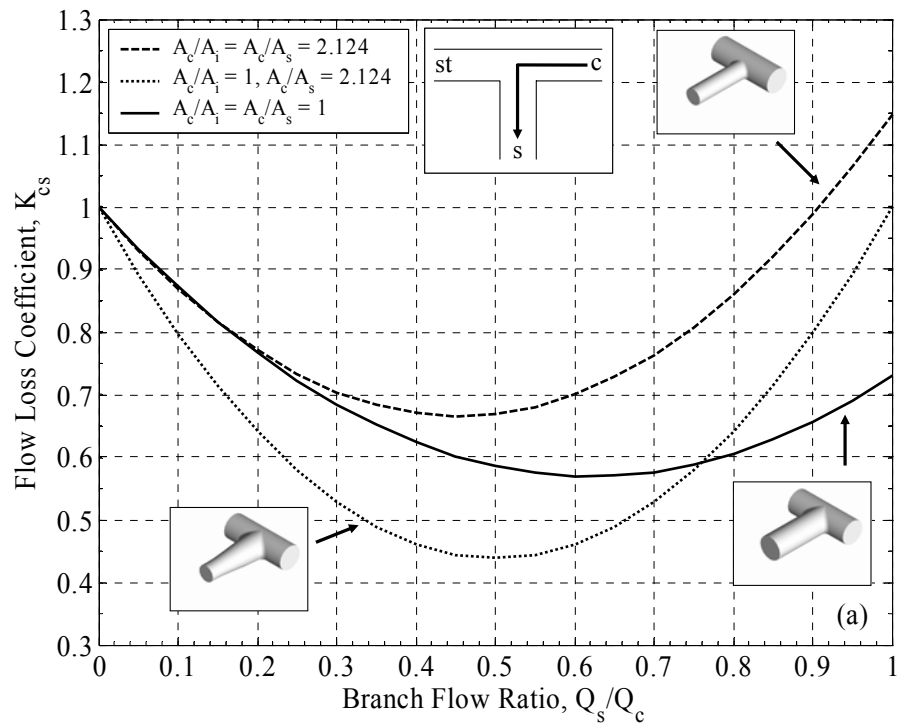


Figure 5.16: Effect of side branch taper on losses for circular junction, $A_c/A_s=2.124$, $r=0.2 D_1$: (a) K_{cs} , (b) K_{cst}

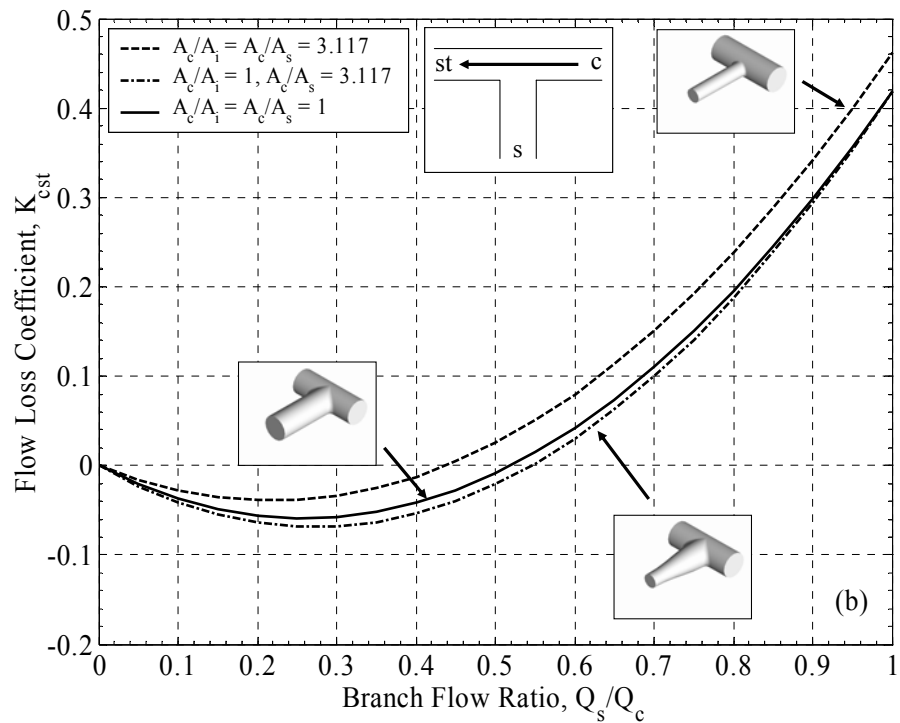
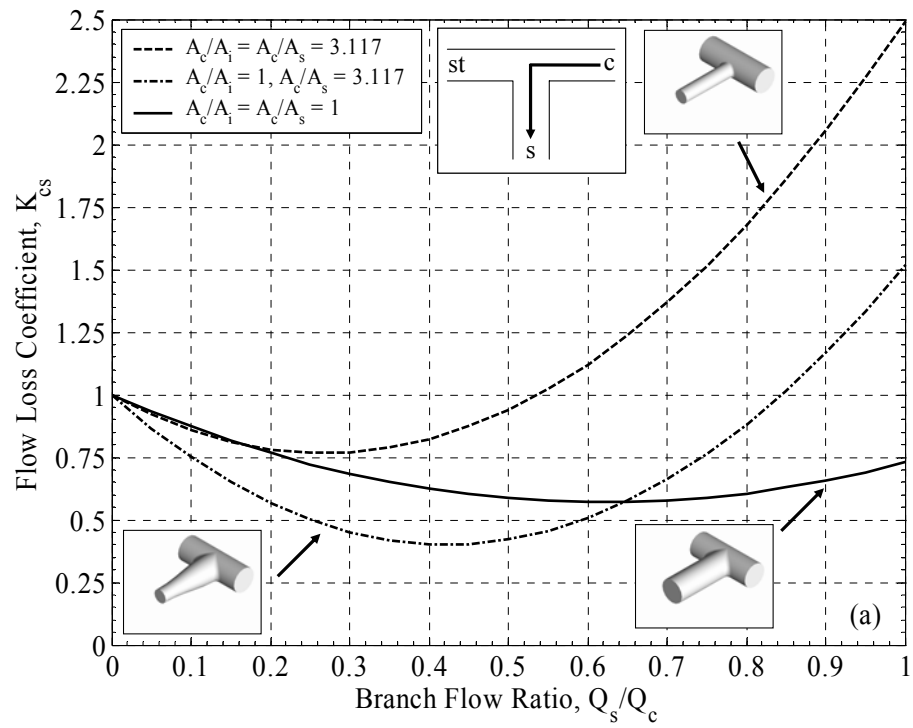


Figure 5.17: Effect of side branch taper on losses for circular junction, $A_c/A_s=3.117$,

$r=0.2 D_i$: (a) K_{cs} , (b) K_{cst}

of the flow with the larger interface and radius, and the reduced deceleration of flow between the combined and side duct needed at low flow ratios in junctions with $A_c/A_s > 1$. The addition of a side branch taper also shifts the location of the minima in K_{cs} to higher Q_s/Q_c , occurring in both junctions at side branch velocities above that of the combined duct. The amount of reduction in K_{cs} for the two junctions tested shows an increasing effect of side duct taper with increasing taper area ratio A_i/A_s .

Figure 5.18 shows the effect of A_c/A_s in tapered junctions with interface area ratio $A_c/A_i=1$. Interestingly, the junction with $A_c/A_s=1$ is not the configuration for lowest K_{cs} (Figure 5.18a) at all flow ratios. Instead, it is roughly the junction whose side duct velocity is nearest that of the combined duct. The strong increase in K_{cs} at $Q_s/Q_c=1$ shown in Figure 5.15a also occurs in the tapered junctions, although at a much slower rate. K_{cst} (Figure 5.18b) is only slightly reduced by the tapered side duct at intermediate Q_s/Q_c , while it is unchanged at $Q_s/Q_c=1$.

5.2.5 Side Branch Aspect Ratio and Shape Effects

The effects of side branch aspect ratio are shown in Figures 5.19, 5.20, and 5.21 for varying $A_c/A_s=1, 2.124,$ and $3.117,$ respectively. Included are the results for rectangular junctions with aspect ratios of $W/H=1/2$ and $2,$ as well as those for square junctions ($W/H=1$). The high aspect ratio junctions ($W/H=2$) have the long side of their rectangular side duct cross-section perpendicular to the combined duct flow direction, providing a wide base for the flow to turn about. The centerline radius of the turning flow must be very short for this junction however, as the height of the side branch is reduced. In contrast, the low aspect ratio junction ($W/H=1/2$) provides a very narrow

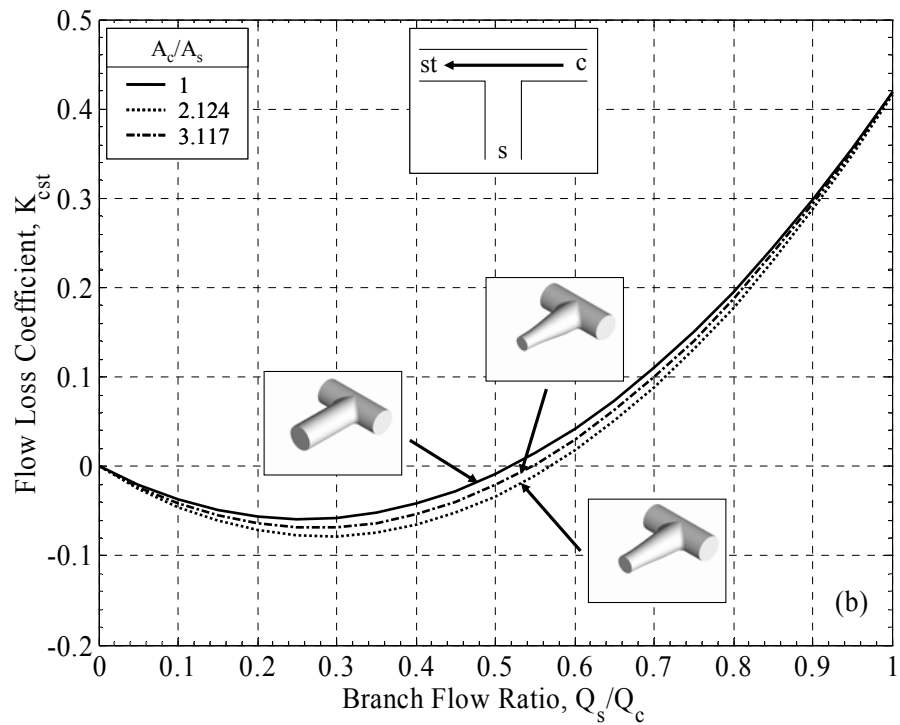
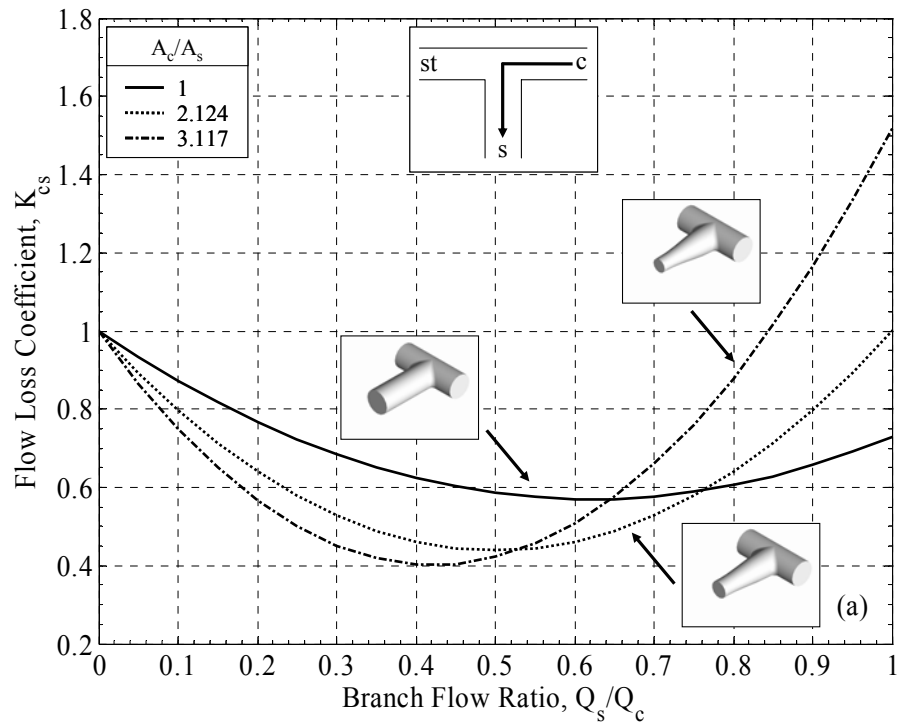


Figure 5.18: Effect of area ratio on losses for tapered circular junction, $r=0.2 D_i$, $A_c/A_i=1$:
 (a) K_{cs} , (b) K_{cst}

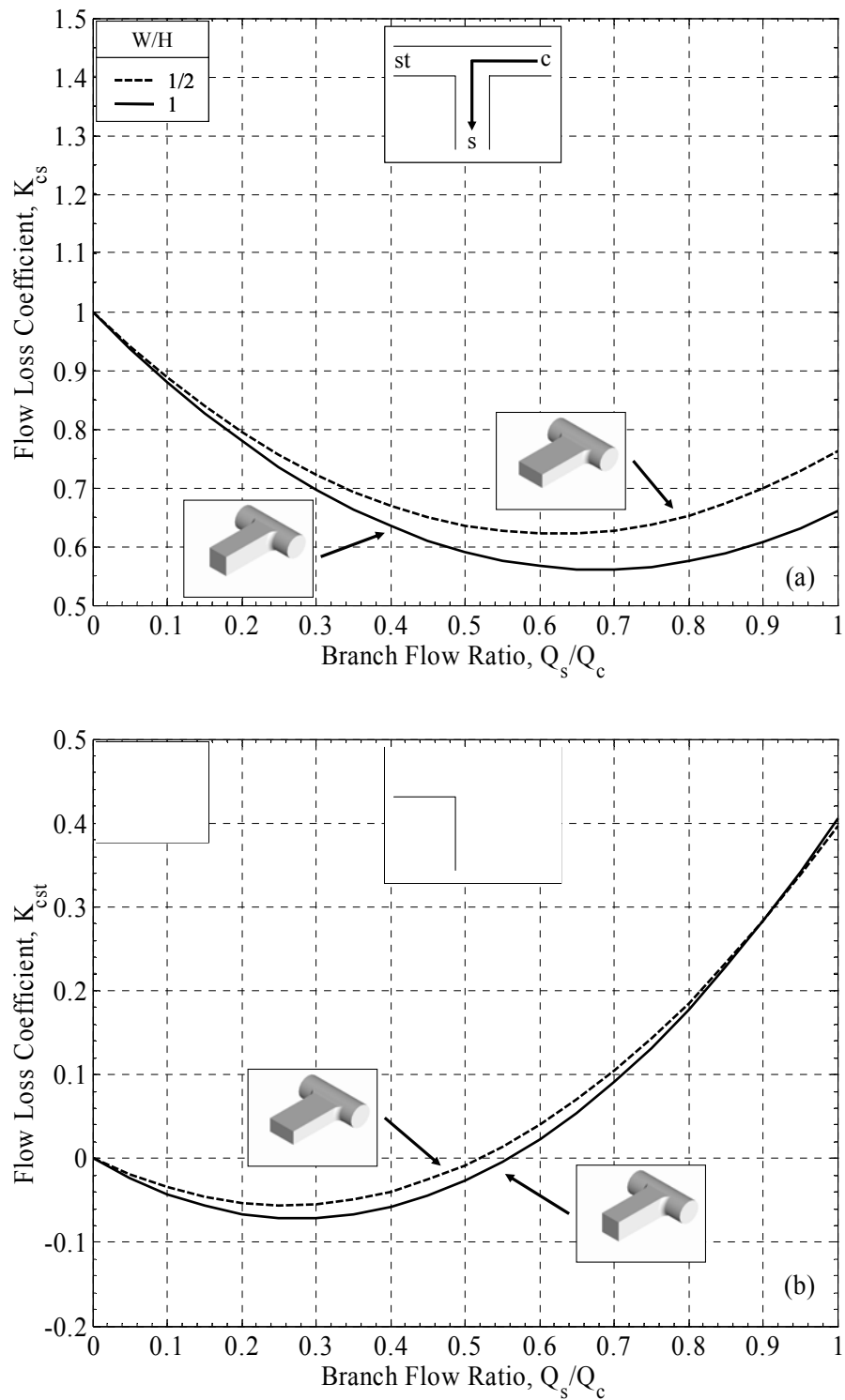


Figure 5.19: Effect of aspect ratio on losses for rectangular junction, $A_c/A_s=1$, $r=0.2 D_s$:
 (a) K_{cs} , (b) K_{cst}

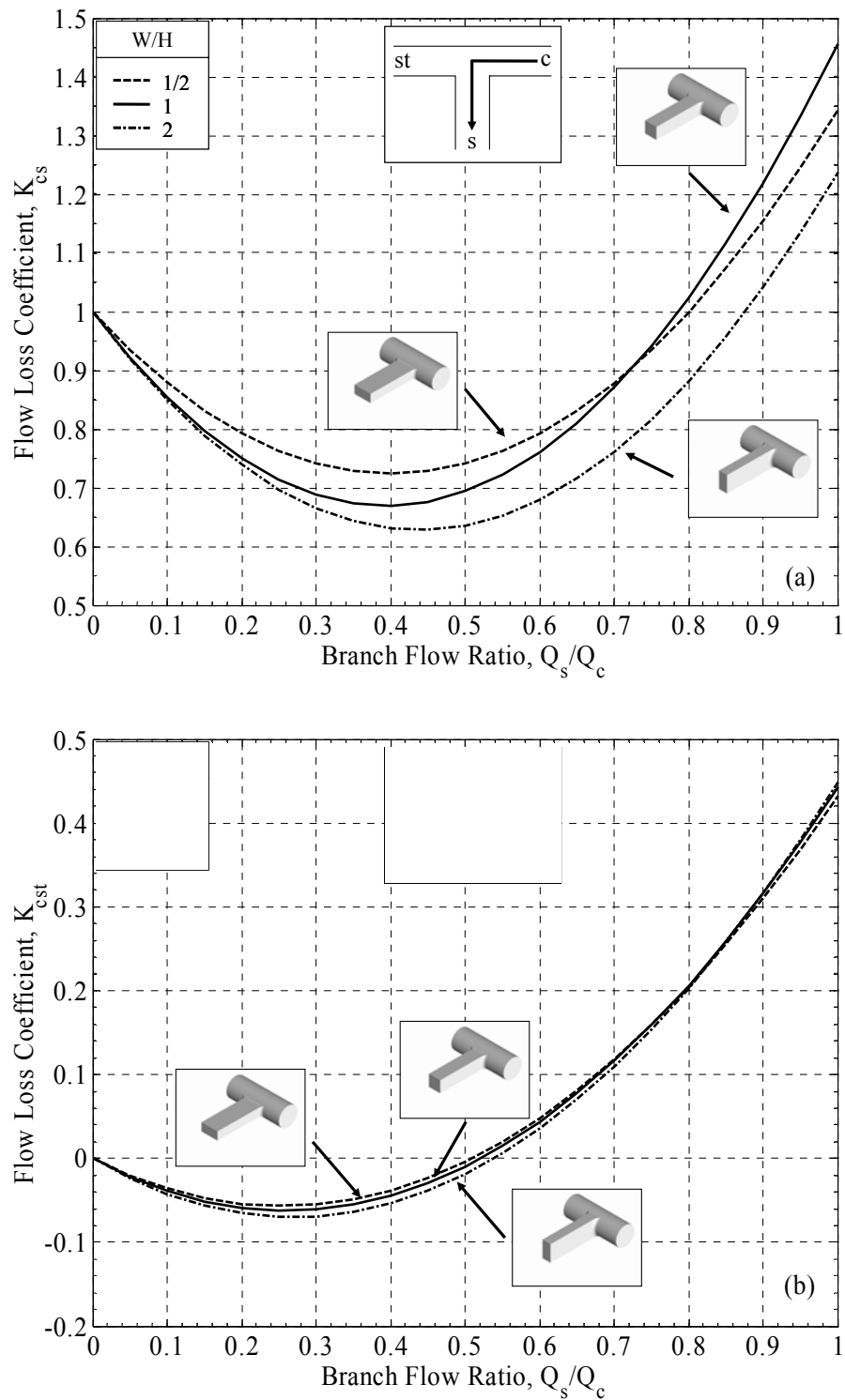


Figure 5.20: Effect of side branch aspect ratio on losses for rectangular junction, $A_c/A_s=2.124$, $r=0.2 D_s$: (a) K_{cs} , (b) K_{cst}

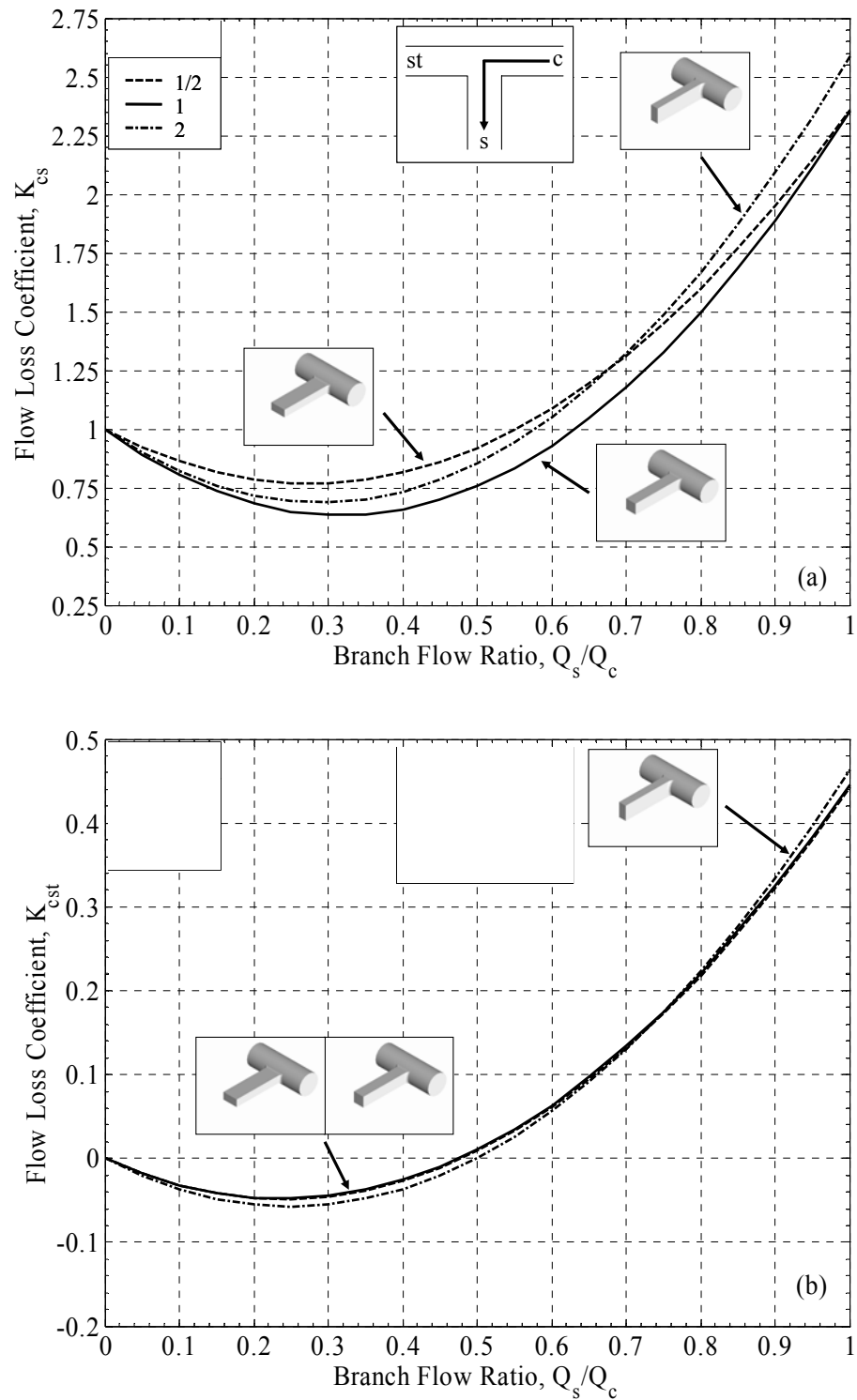


Figure 5.21: Effect of side branch aspect ratio on losses for rectangular junction, $A_c/A_s=3.117$, $r=0.2 D_s$: (a) K_{cs} , (b) K_{cst}

base for the flow to turn about, but the centerline radius of the turning flow is increased. In spite of these differences, the effect of W/H is minor in comparison to those of r and A_c/A_s for all geometries tested. In Figures 5.19a and 5.20a the overall trend appears to be that K_{cs} is reduced with increasing W/H . The effect of W/H on K_{cs} seems to diminish quickly with increasing A_c/A_s . In Figure 5.21a the results for $W/H=2$ and $1/2$ are very similar. This is possibly due to the decreasing magnitude of U_c relative to U_s with increasing A_c/A_s . When $U_s > U_c$ the losses associated with accelerating the flow into the side duct become greater than those due to the loss of combined duct kinetic energy.

The results of K_{cs} for the square junction in Figures 5.20a and 5.21a do not fall between the extents represented by the rectangular junctions in the current experiments. While the junctions with $W/H=1/2$ and 2 used the same side duct by simply rotating by 90° on its longitudinal axis, those with $W/H=1$ required a separate duct. As a result, comparisons between the square and rectangular junctions include additional measurement error due to the tolerances in duct fabrication, while comparisons between rectangular junctions of equal A_c/A_s are free of this particular source of error.

Because the same combined and straight ducts were used for all junctions, measurements aspect ratio effects on K_{cst} are free from error due to duct fabrication inaccuracies. The effect of increasing W/H on K_{cst} in Figures 5.19b, 5.20b, and 5.21b for $A_c/A_s=1, 2.124,$ and $3.117,$ respectively, is rather small, however it appears that K_{cst} is also reduced with increasing W/H . The effect diminishes quickly with increasing $A_c/A_s,$ however, and is within experimental error for $A_c/A_s=3.117$ in Figure 5.21b.

Figures 5.22-5.24 show the effects of side duct cross-sectional shape on loss coefficients K_{cs} and K_{cst} for varying A_c/A_s . The results for K_{cs} in junctions with oval side

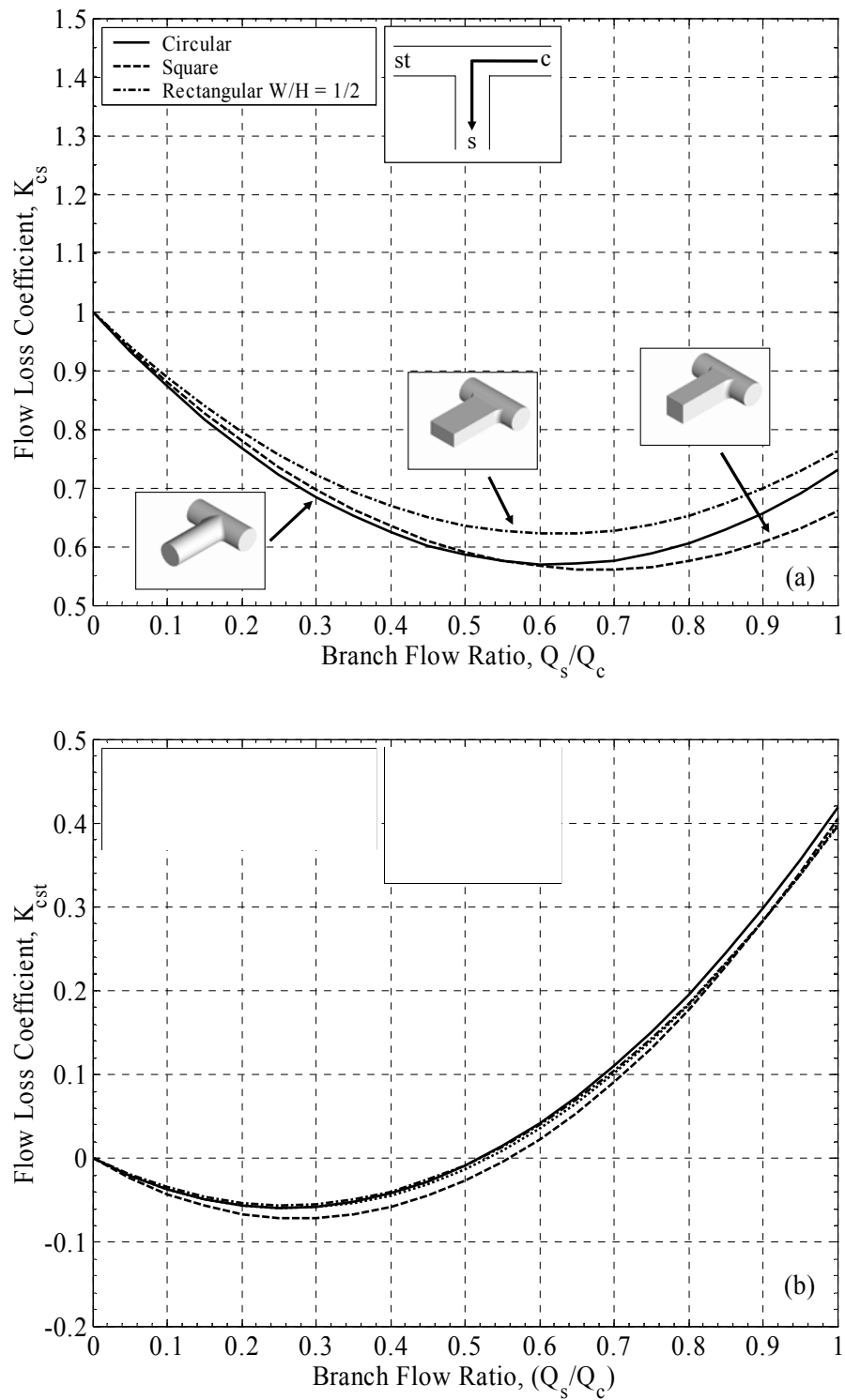


Figure 5.22: Effect of side branch shape on losses for all junctions with $A_c/A_s=1$ and $r=0.2 D_s$: (a) K_{cs} , (b) K_{cst}

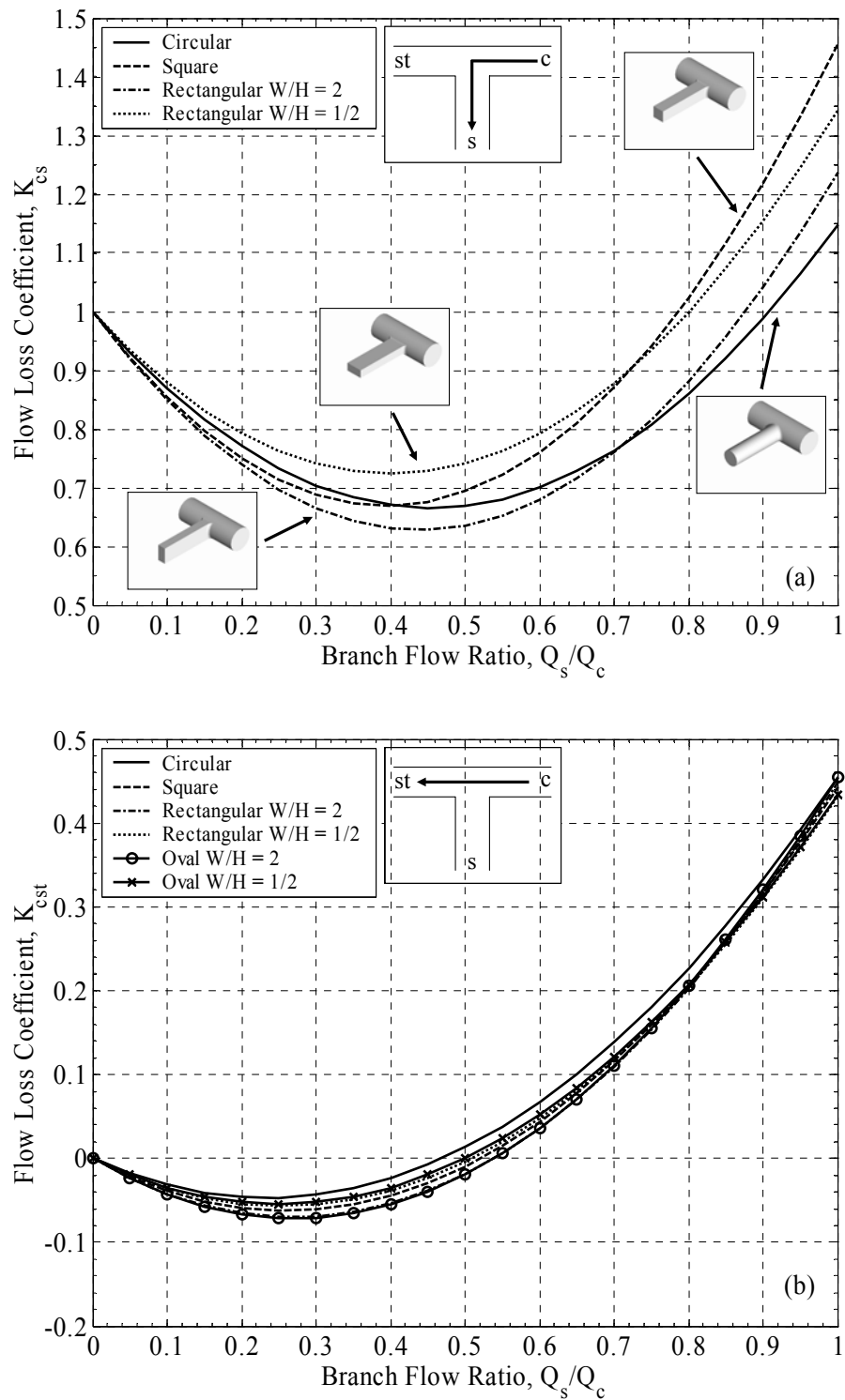


Figure 5.23: Effect of side branch shape on losses for all junctions with $A_c/A_s=2.124$ and $r=0.2 D_s$: (a) K_{cs} , (b) K_{cst}

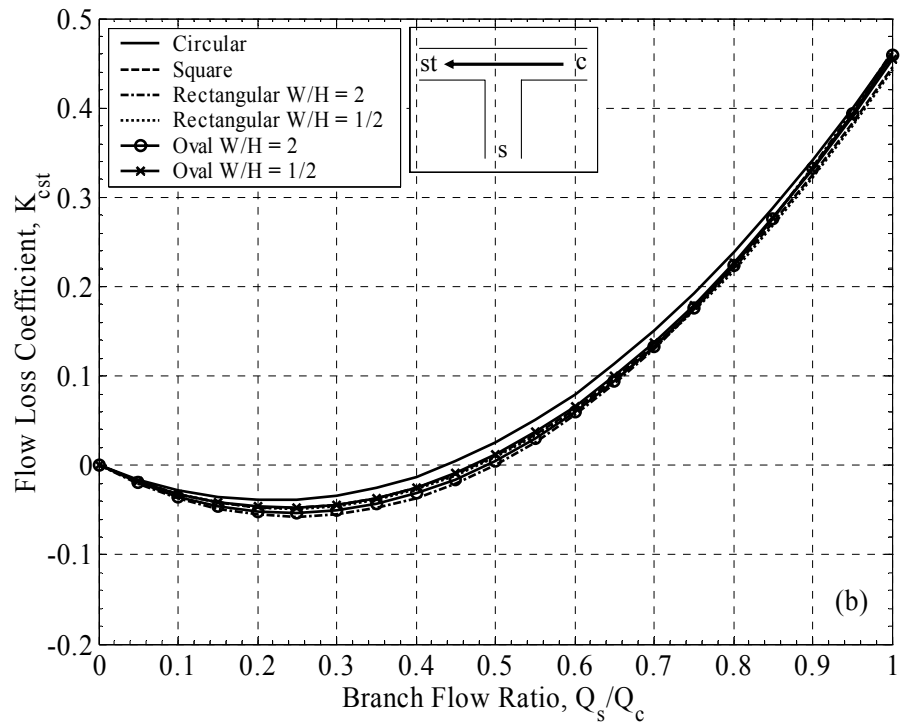
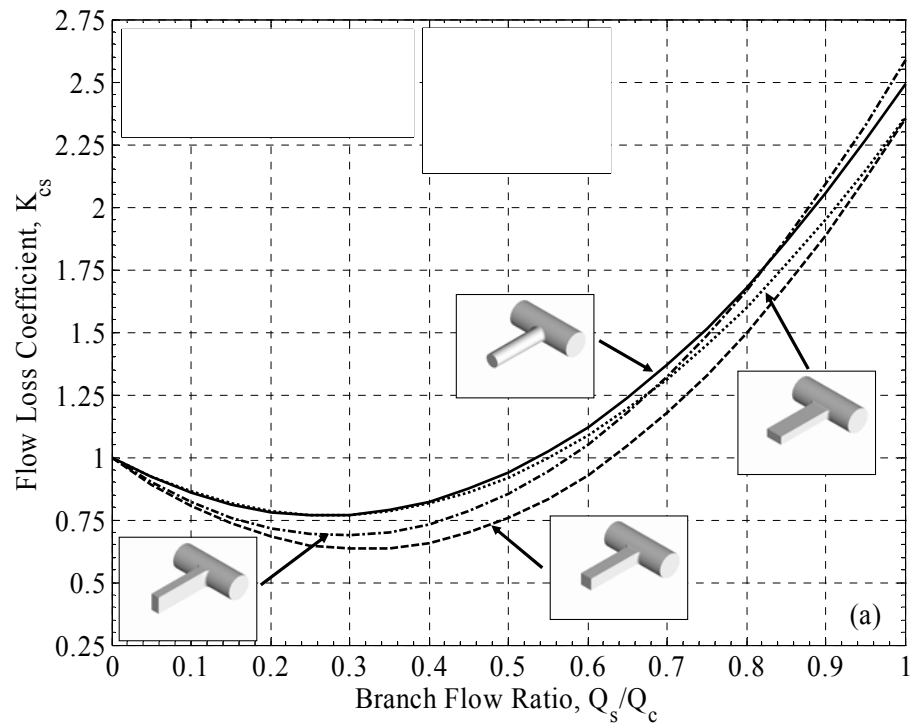


Figure 5.24: Effect of side branch shape on losses for all junctions with $A_c/A_s=3.117$ and $r=0.2 D_s$: (a) K_{cs} , (b) K_{cst}

ducts are not included, (Figures 5.22a, 5.23a, and 5.24a) due to the deformation of the side ducts described in Section 5.1. Since K_{cst} is unaffected by the side duct deformation present in the oval ducts, it is included in Figures 5.22b, 5.23b, and 5.24b. The results of all noncircular junctions lie about those of the circular junctions, with no discernable pattern in relative performance. The spread in K_{cs} is greatest in the case of $A_o/A_s=2.124$ (Figure 5.23a), with a variation of approximately 23% at $Q_s/Q_c=1$.

CHAPTER 6

CONCLUDING REMARKS

The loss coefficients have been determined experimentally for dividing type 1 flows in T-junctions with varying interface radius, through to side duct area ratio, side duct taper, and side duct shape. Losses develop quickly in the straight duct, requiring less than five duct diameters after the junction interface to become essentially fully developed. The development length for flow between the combined and straight ducts is the same for all junctions and combined-duct flow rates tested. For junctions with $A_c/A_s=1$, the majority of flow loss between the combined and side ducts is realized within five diameters of the junction interface. Losses in the side duct of junctions with $A_c/A_s > 1$ and $U_s \leq U_c$ are also fully developed within five diameters of the junction interface. Up to 20 diameters can be required, however, when $U_s > U_c$.

Loss coefficients are nearly independent of combined duct Reynolds number over the range tested in all junctions with the exception of junctions with $A_c/A_s=1$ and $r=0.2$ D_s , where K_{cs} is independent only at $Re_c > 2 \times 10^5$. The assumption of incompressibility made in the flow loss coefficient formulation is valid for flow velocities up to the maximum tested of $M=0.3$ and 0.5 in the combined and side ducts, respectively.

Measurements of both loss coefficients are within the bounds of available data in the literature. Both loss coefficients are represented well as second-order functions of Q_s/Q_c with y-intercepts of unity and zero for K_{cs} and K_{cst} , respectively.

K_{cs} is significantly reduced with the addition of a relatively small radius at the junction interface, and the reduction increases with radius. A reduction in K_{cs} of approximately 40% is possible with an interface radius equal to $0.2 D_s$. K_{cs} increases strongly with A_c/A_s , more than tripling between $A_c/A_s=1$ and 3.117. The effect of A_c/A_s can be greatly reduced with the use of a tapered side branch. For $Q_s/Q_c < 1$ junctions with $A_c/A_s > 1$ and tapered side ducts can actually outperform junctions with $A_c/A_s=1$.

K_{cs} reduces with increasing side duct aspect ratio (W/H), however, the effect diminishes rapidly with increasing A_c/A_s . While there is some variation in K_{cs} with side duct shape, it is relatively small compared to the effects of A_c/A_s and r , and there is no easily discernable pattern in the shapes examined. Although K_{cs} could not be measured accurately in junctions with oval side ducts due to deflections in the duct walls, the results are likely within the spread of measurements made for junctions with circular, rectangular, and square side ducts.

K_{cst} increases slightly with increasing A_c/A_i , quickly converging to a single curve for high A_c/A_i . There is a slight reduction in K_{cst} with increasing W/H . The effect quickly diminishes with increasing A_c/A_s , becoming negligible at $A_c/A_s=3.117$. K_{cst} becomes negative at low to mid flow ratios. This has been attributed to the drawing of slower near-wall flow from the combined duct into side branch, combined with the assumption of uniform velocity made in the formulation of Eq. (2.30).

Although a large amount of information is presented in the current work, it represents only one of four possible flow configurations in T-junctions. All four configurations must be studied to have a complete picture of junction performance. With the construction of the experimental setup complete and measurement approach defined, however, the measurement of the other three configurations will require far less time and effort.

Several lessons have been learned during the current work that should be shared with future researchers. The importance of accurate duct friction measurements cannot be understated. In the case of $A_c/A_s=3.117$ and $Q_s/Q_c=1$, for instance, approximately 35% of the total measured pressure drop between the combined and side ducts at a distance of only $27.5 D_s$ from the junction interface is due to friction alone. Initially, an attempt was made to measure the friction factor in the fully developed region directly during T-junction experiments. The combination of flow measurement error, residual development effects, and the relatively short distance over which the measurements were made, rendered this approach unacceptable. Far superior results were attained by measuring duct friction in separate experiments, and then using these values to subtract frictional effects from T-junction experiments. Loss coefficient measurements should be made as close to the junction interface as possible, while still being in fully developed flow. This approach minimizes junction flow loss measurement error due to that of duct friction measurements.

Once the approach of measuring the friction factor for each duct in a separate experiment was adopted, a new source of error was discovered. The relative effect of duct cross-sectional area variation on friction measurements was underestimated when

dimensional tolerance targets for duct fabrication were determined. The variation in static pressure measurements due to duct area variation was found to have a significant impact on measured duct friction factors. This necessitated the implementation of a correction for static pressure measurements based on the actual duct cross-sectional area at each tap location.

It is important that the pressure taps are made as small and burr-free as possible. During preliminary experiments it was found that a small burr in only one of four pressure taps used to make a piezometric ring caused a change in measured K_{cs} of approximately 20% in a junction with $A_c/A_s=3.117$. In the current work, care was taken to chase all pressure tap holes and deburr the hole to duct inner surface interface with fine sand paper and steel wool. Each duct was then connected to the flow bench and the static pressure gradient measured to find any tap locations that required further smoothing.

In light of the current results, some modifications to the test matrix may be desirable for future experiments. The primary parameters effecting T-junction performance include: (1) interface radius, (2) through to side duct area ratio, (3) side branch taper. One of the strengths of the current work is in the measurement of junction losses with noncircular side ducts. Although the importance of side branch shape has been found to be small, some other parameters have shown interesting trends. In comparing the results of the current work for $A_c/A_s > 1$ and $r > 0$ with other researchers with $r=0$, it appears that the effect of junction interface radius may also be dependent on A_c/A_s . The reduction of K_{cs} in junctions with tapered side branches is significant for the two geometries studied. Although it is desirable to complete the data set for the current test matrix by measuring loss coefficients for the remaining three flow configurations, it

would also be interesting to see a systematic study of both interface radius and side branch taper effects for circular junctions only. A final important parameter that was not investigated in the current work is the side branch angle. Although a systematic investigation of side branch angle combined with interface radius, through to side duct area ratio, and the side branch taper could exceed 100 junction configurations, the task remains feasible because of the experimental setup and analysis techniques developed in this work.

APPENDIX A

MEASURED LOSS COEFFICIENTS FOR JUNCTIONS WITH NONCIRCULAR OR TAPERED SIDE DUCTS

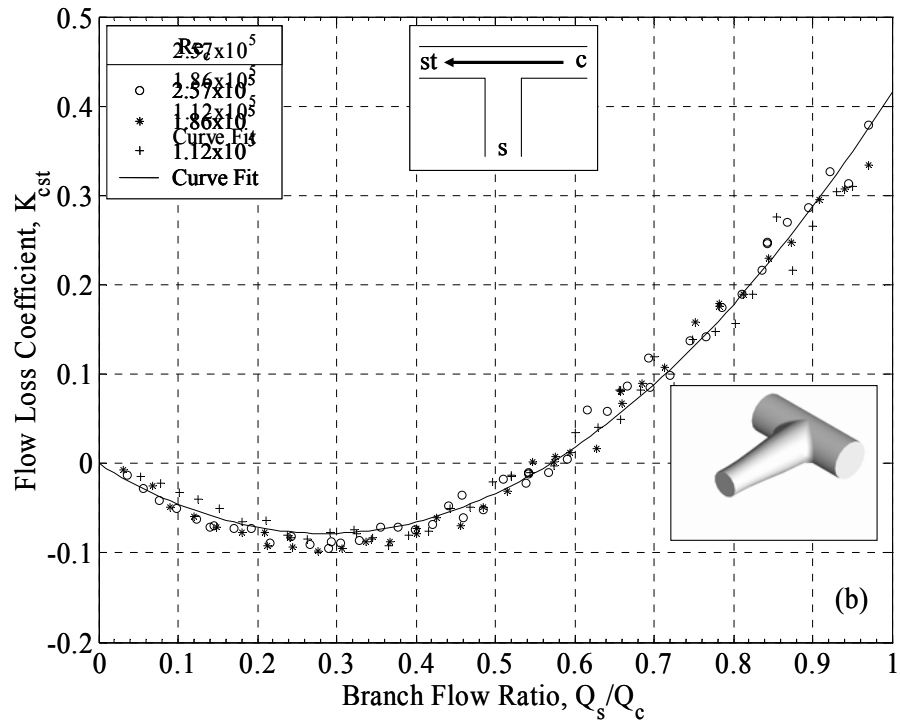
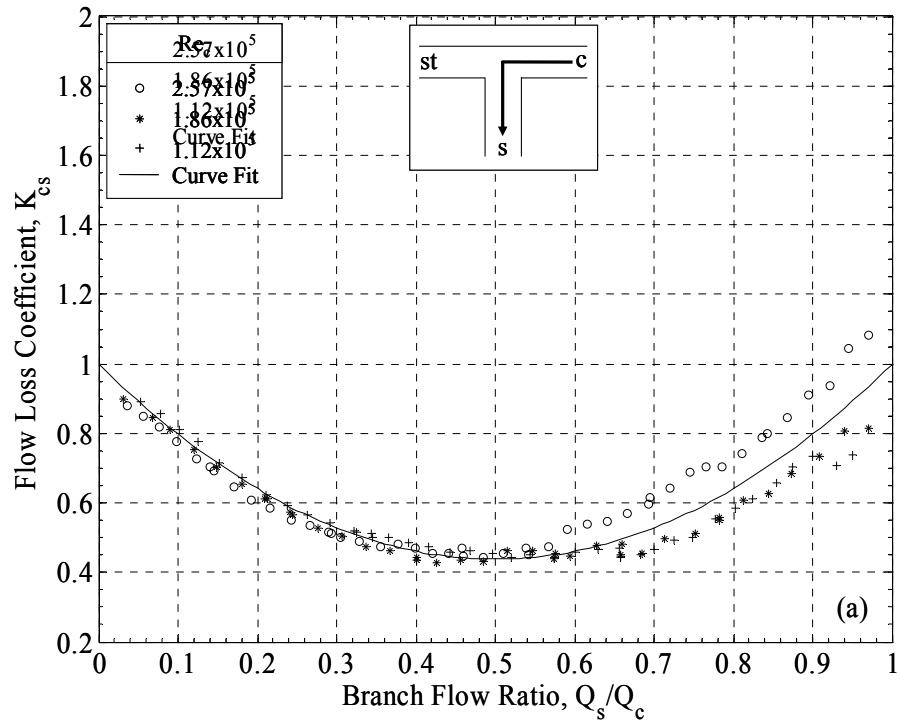


Figure A.1: Losses for tapered circular junction, $A_c/A_i=1$, $A_c/A_s=2.124$, $r=0.2 D_s$:
 (a) K_{cs} , (b) K_{cst}

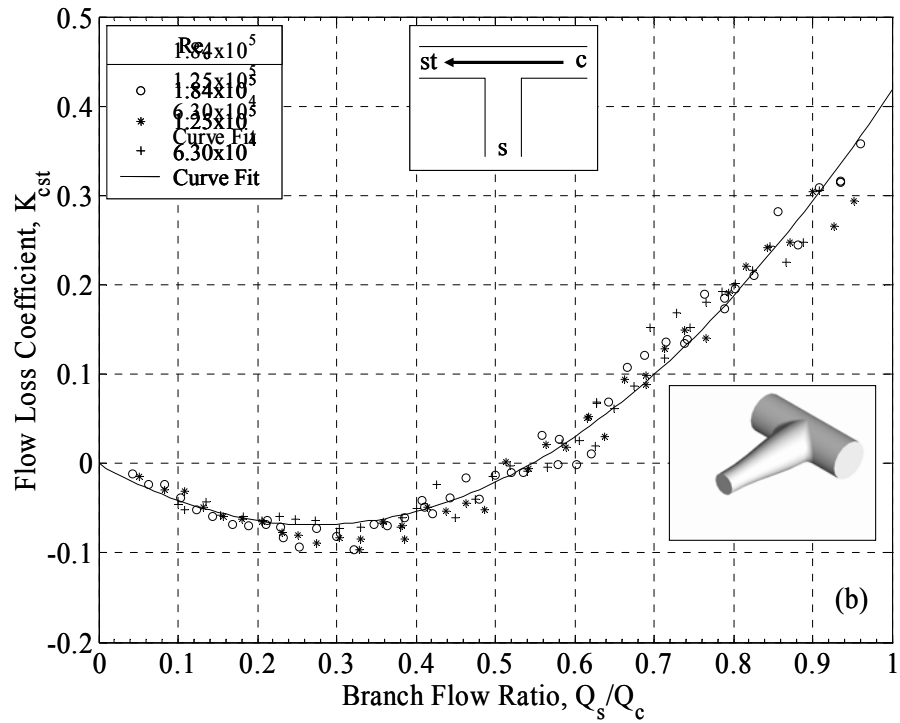
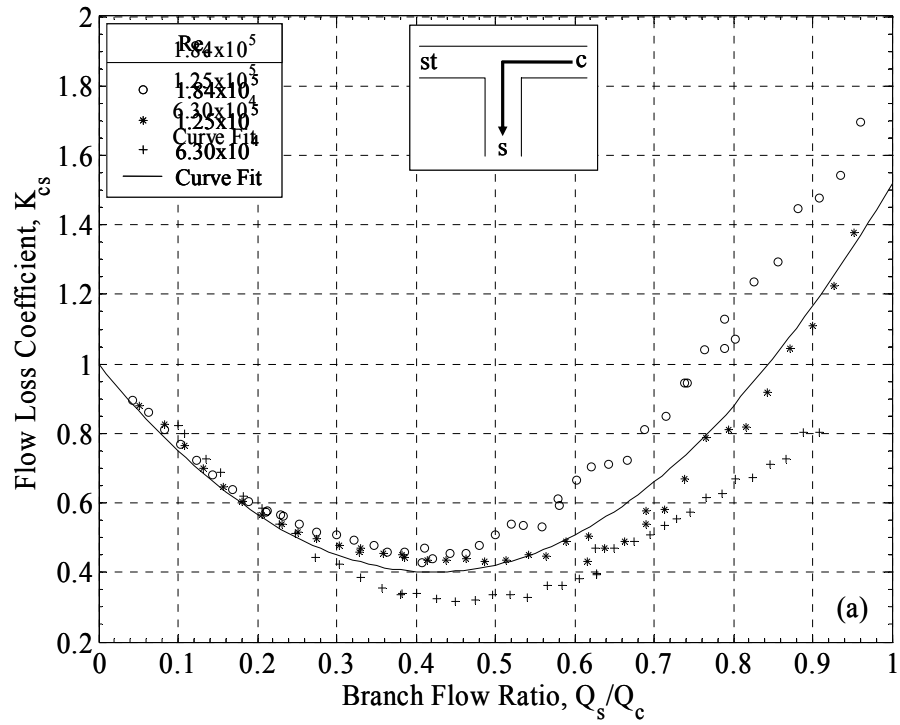


Figure A.2: Losses for tapered circular junction, $A_c/A_i=1$, $A_c/A_s=3.117$, $r=0.2 D_s$:
 (a) K_{cs} , (b) K_{cst}

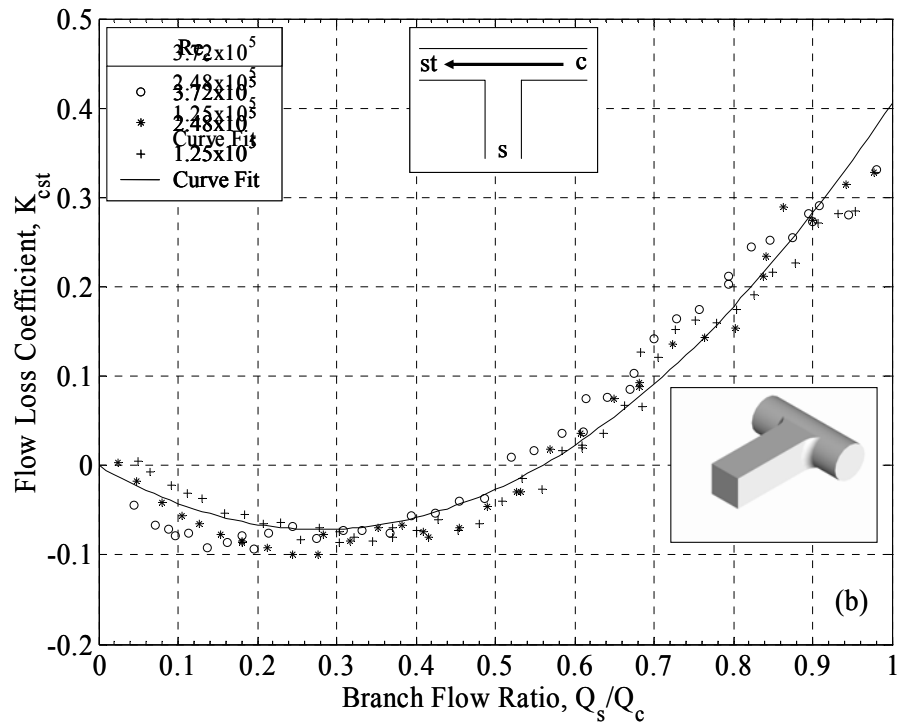
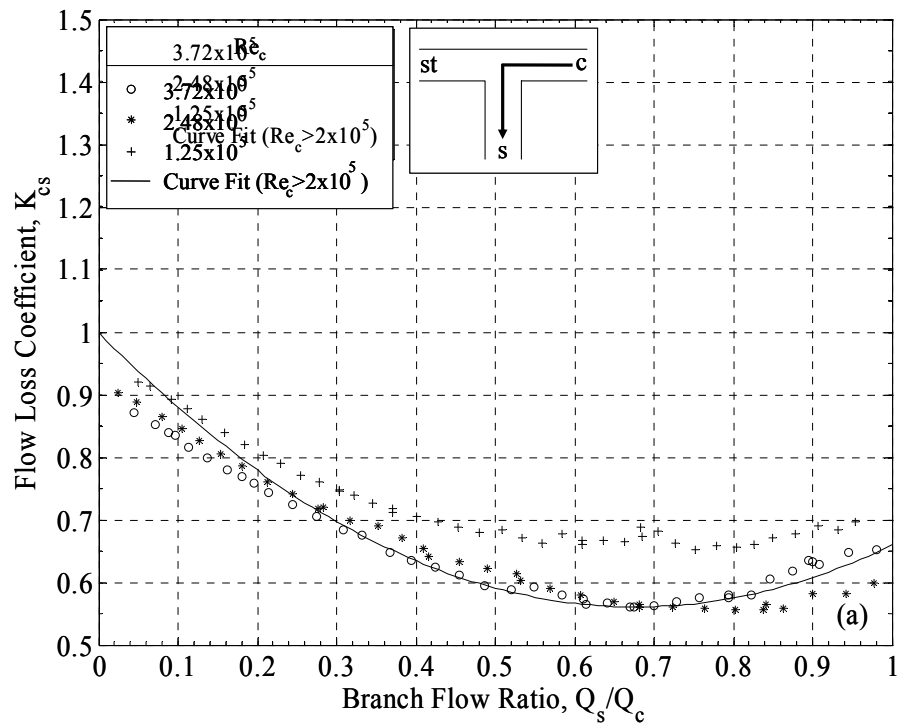


Figure A.3: Losses for square junction, $A_c/A_s=1$, $r=0.2 D_s$: (a) K_{cs} , (b) K_{cst}

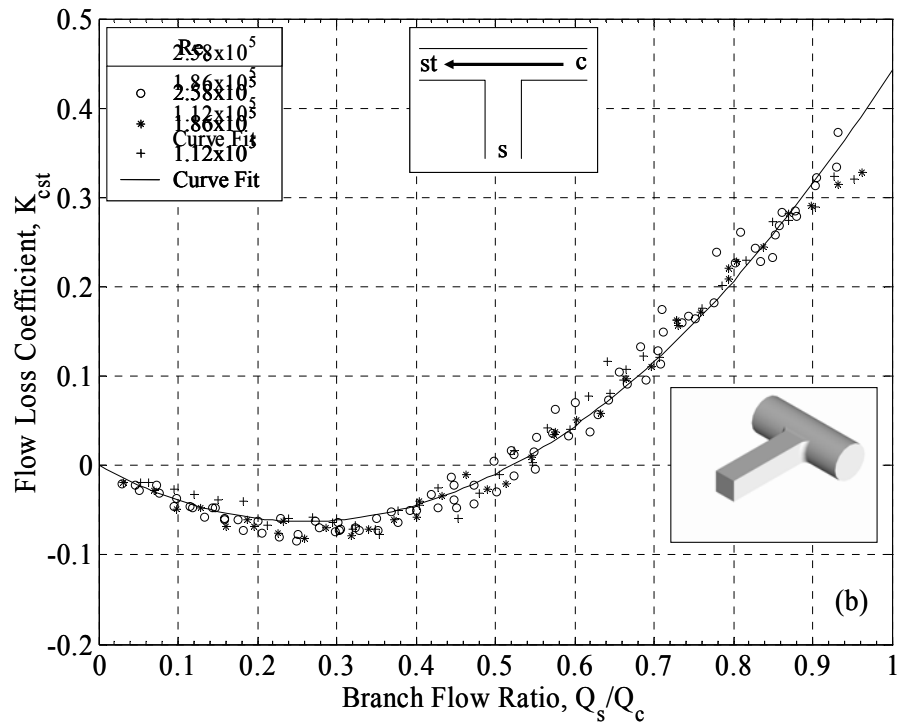
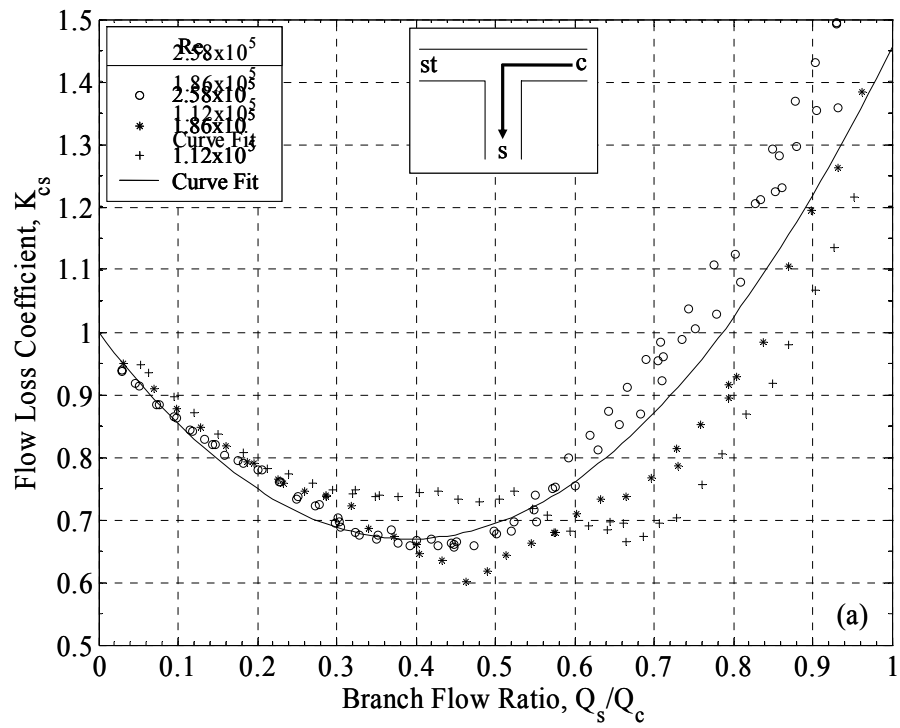


Figure A.4: Losses for square junction, $A_c/A_s=2.124$, $r=0.2 D_s$: (a) K_{cs} , (b) K_{cst}

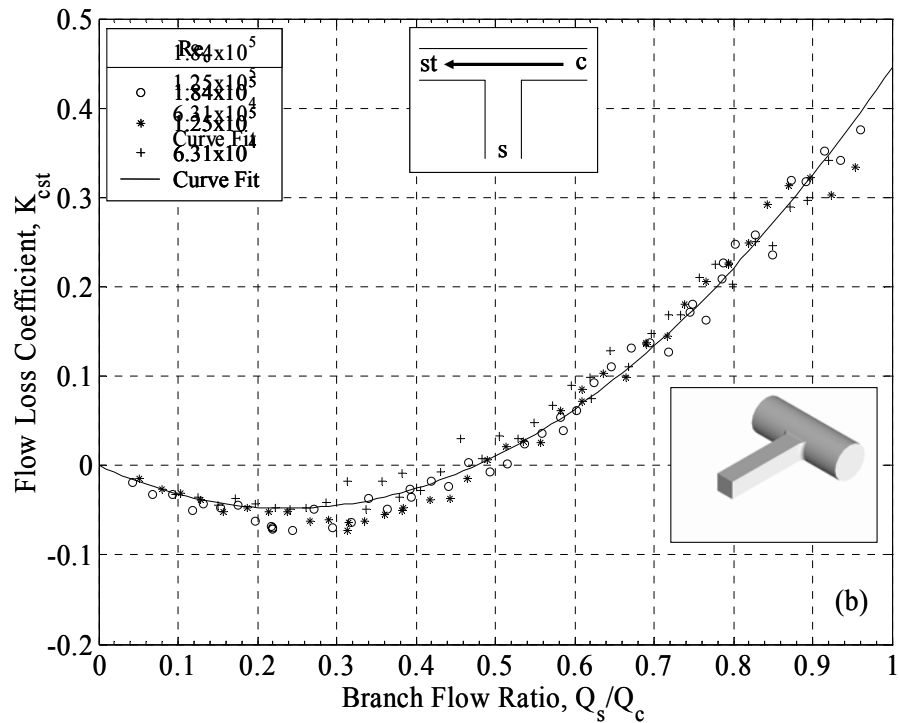
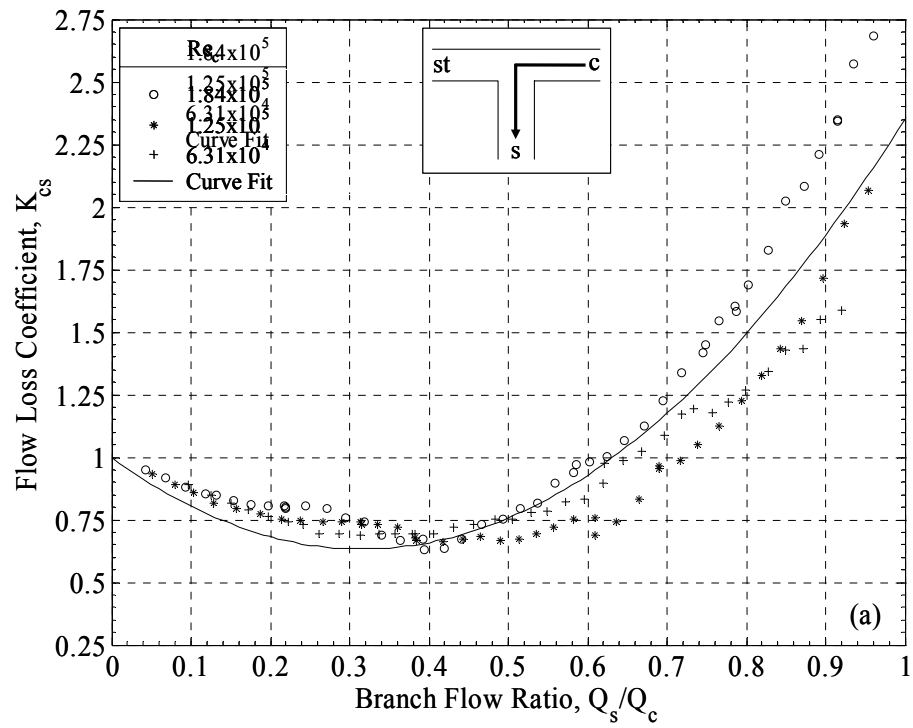


Figure A.5: Losses for square junction, $A_c/A_s=3.117$, $r=0.2 D_s$: (a) K_{cs} , (b) K_{cst}

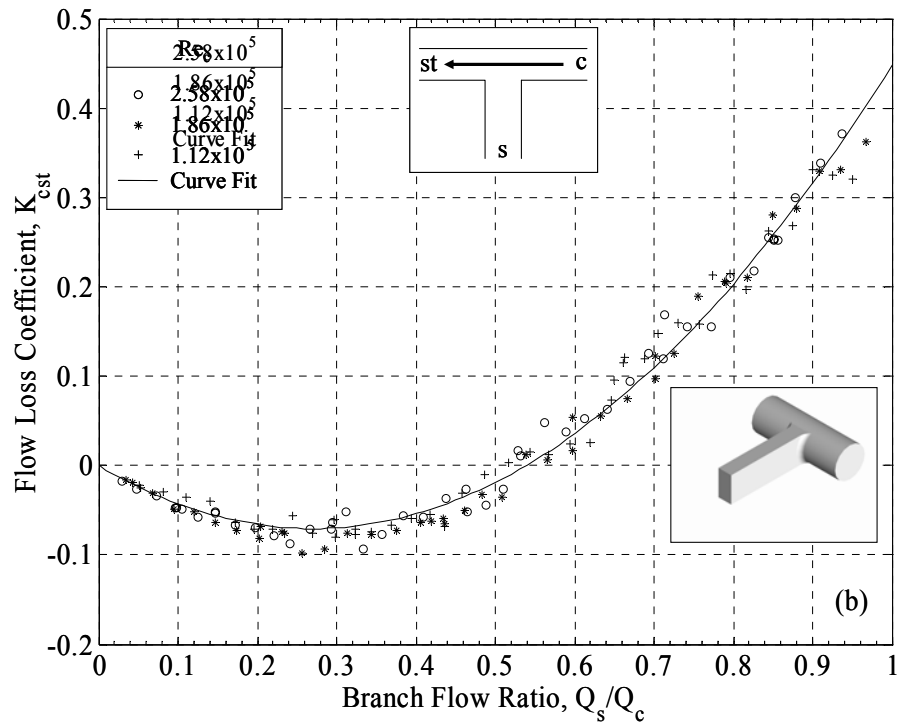
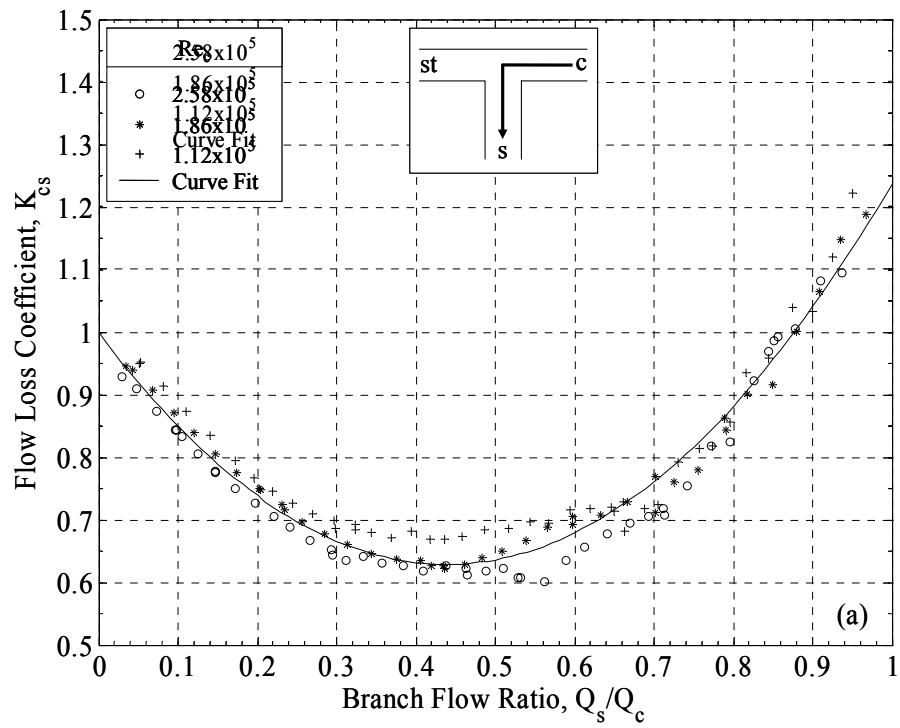


Figure A.6: Losses for rectangular junction, $A_c/A_s=2.124$, $W/H=2$, $r=0.2 D_s$: (a) K_{cs} , (b) K_{cst}

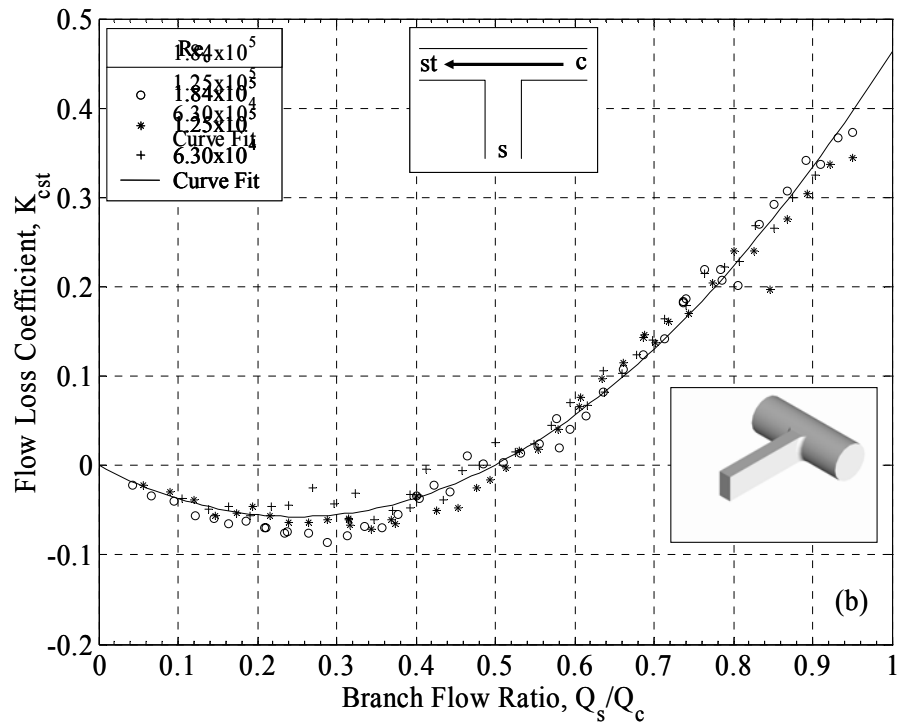
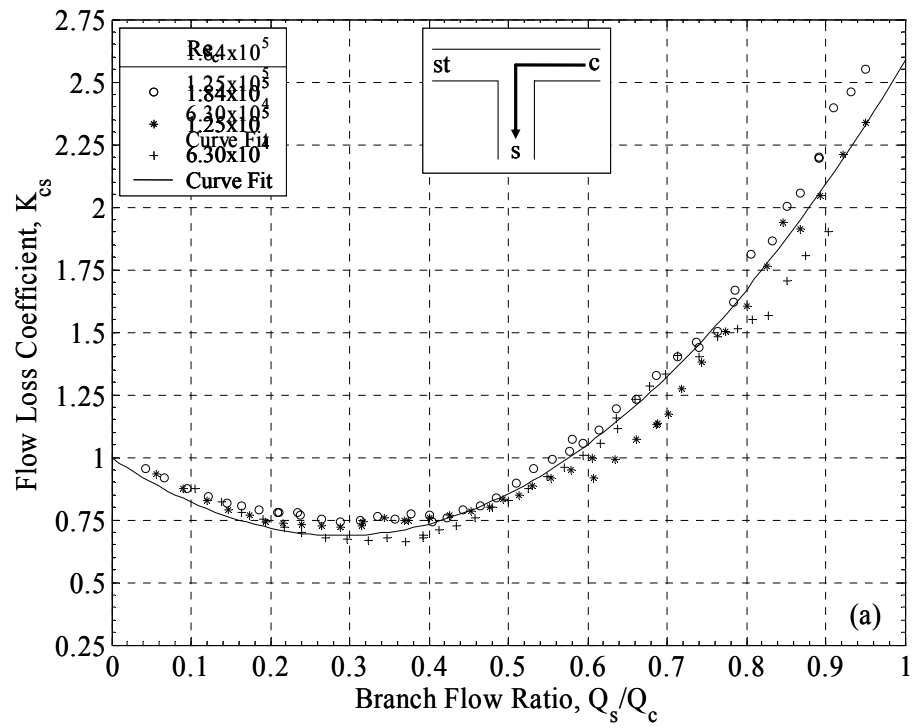


Figure A.7: Losses for rectangular junction, $A_c/A_s=3.117$, $W/H=2$, $r=0.2 D_s$: (a) K_{cs} , (b) K_{cst}

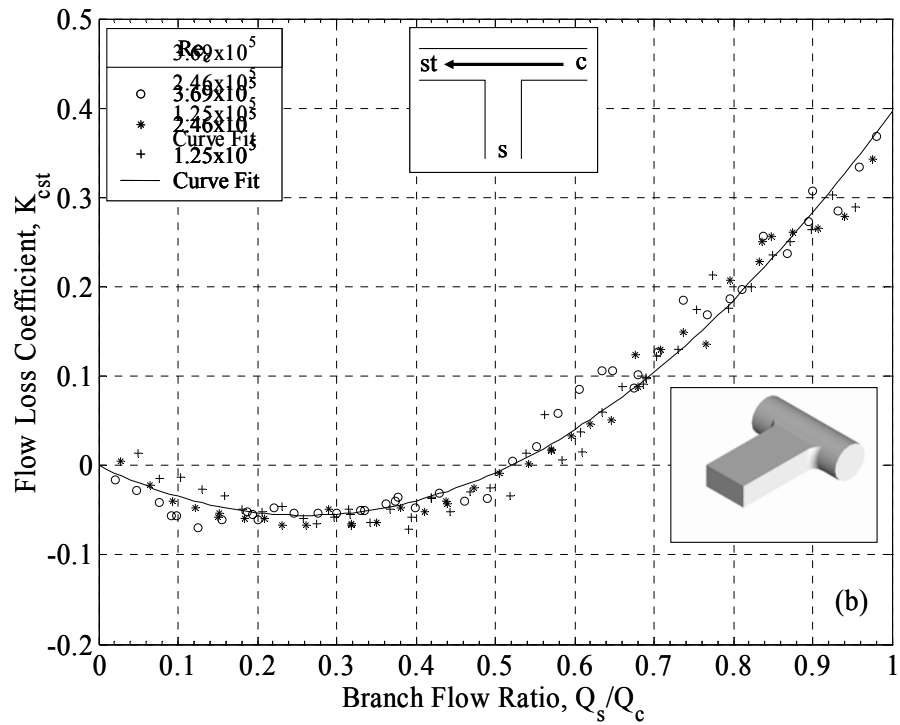
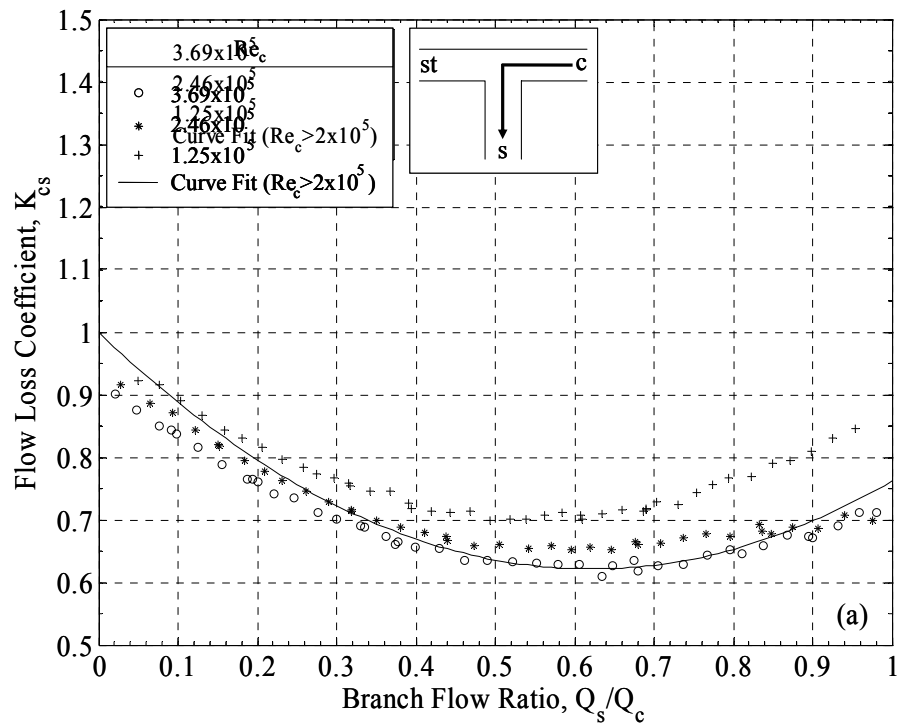


Figure A.8: Losses for rectangular junction, $A_c/A_s=1$, $W/H=1/2$, $r=0.2 D_s$: (a) K_{cs} , (b) K_{cst}

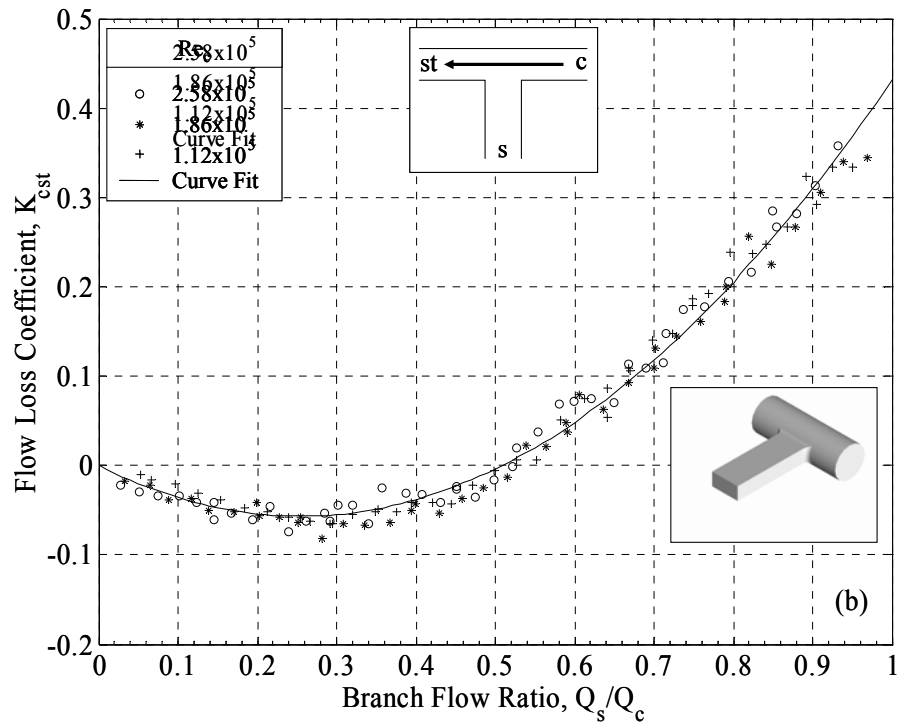
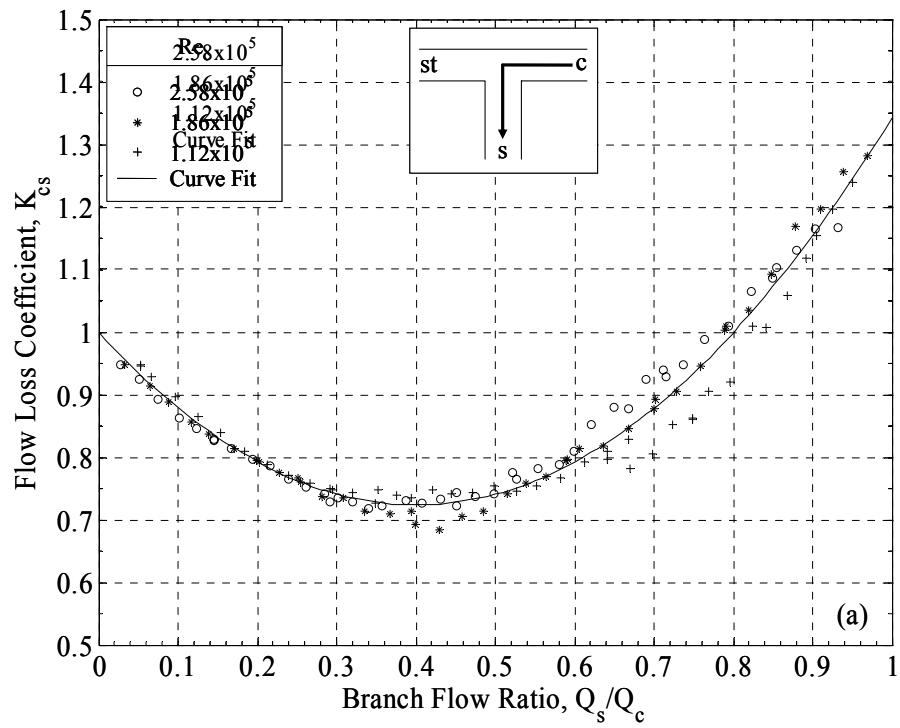


Figure A.9: Losses for rectangular junction, $A_c/A_s=2.124$, $W/H=1/2$, $r=0.2 D_s$: (a) K_{cs} , (b) K_{cst}

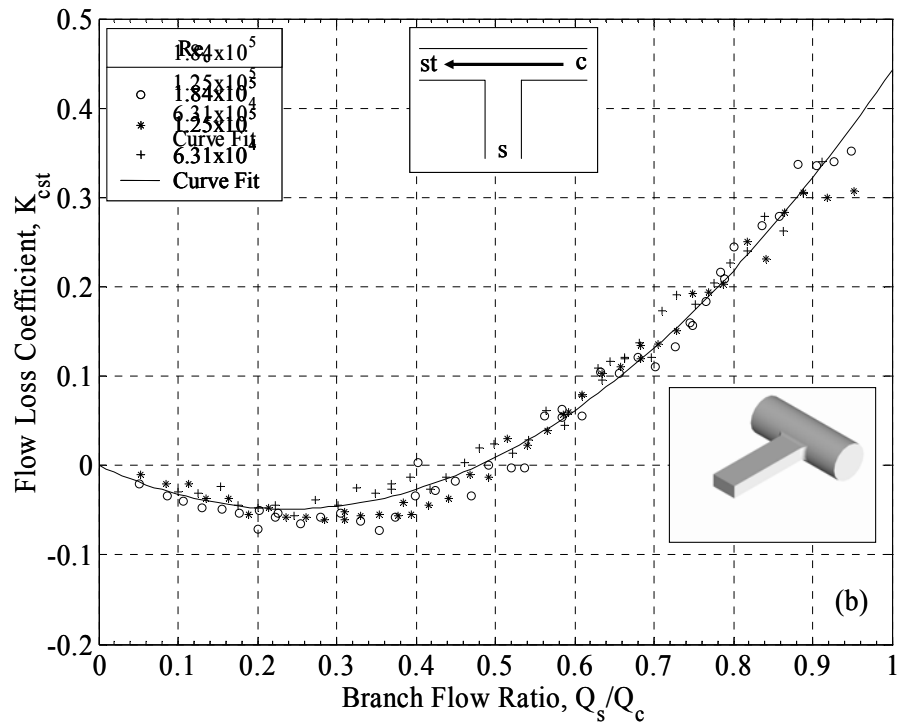
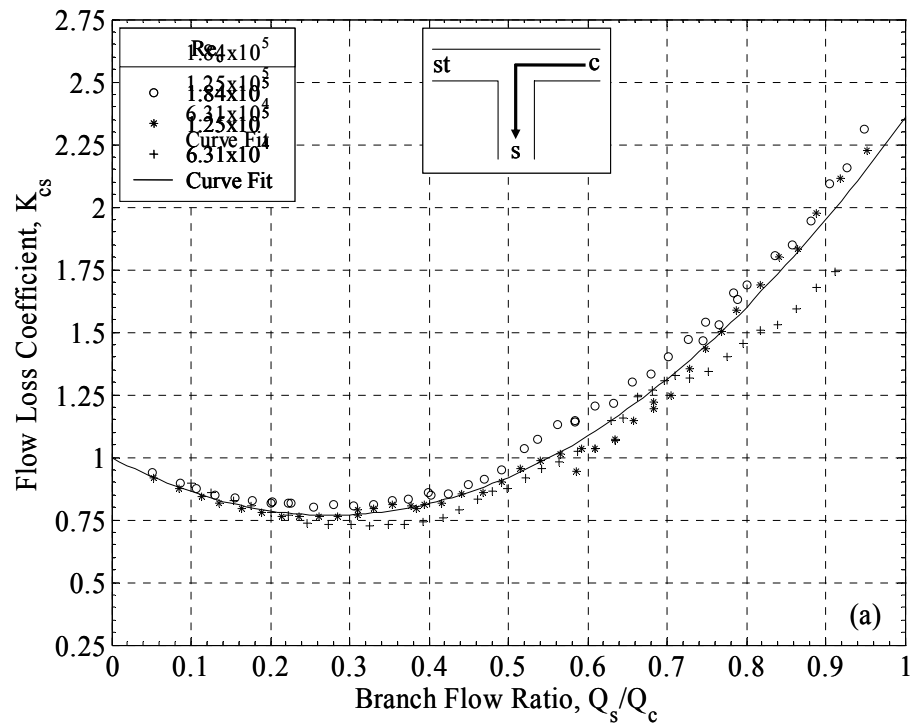


Figure A.10: Losses for rectangular junction, $A_c/A_s=3.117$, $W/H=1/2$, $r=0.2 D_s$: (a) K_{cs} , (b) K_{cst}

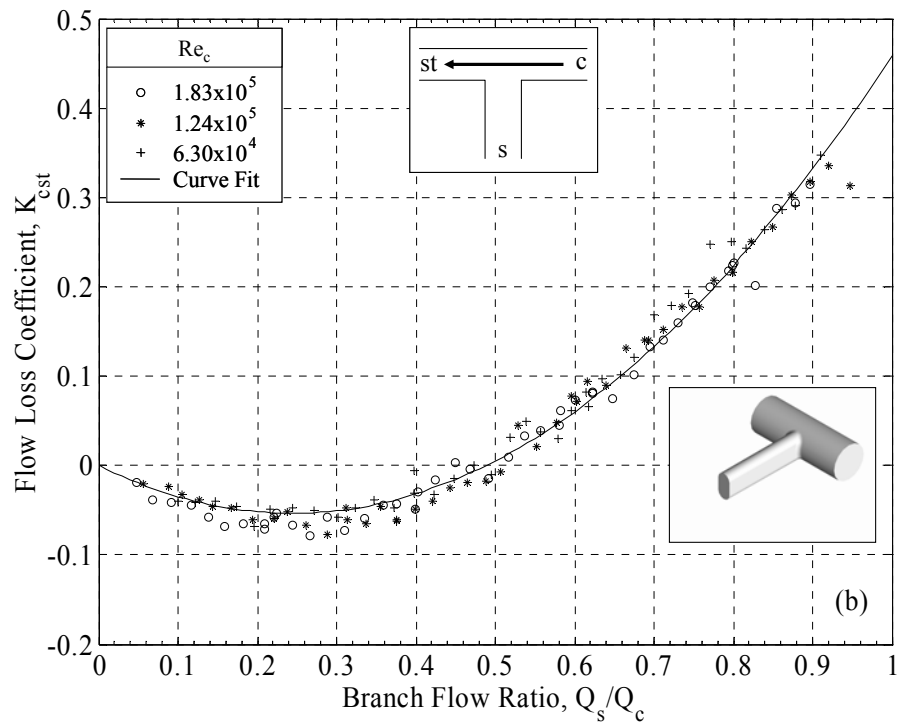
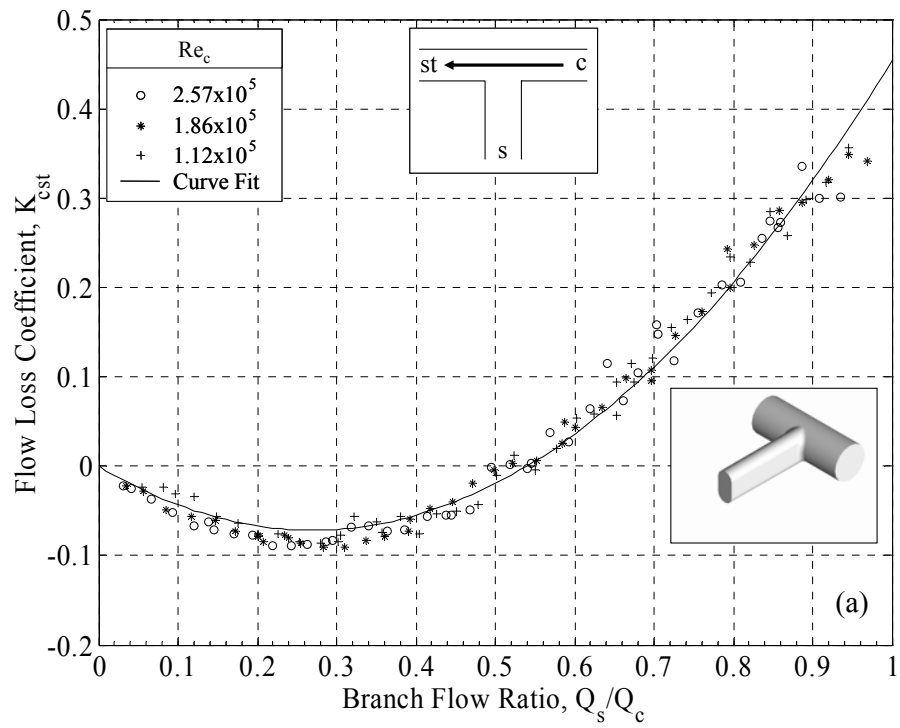


Figure A.11: K_{cst} for oval junction, $W/H=2$, $r=0.2 D_s$: (a) $A_c/A_s=2.124$, (b) $A_c/A_s=3.117$

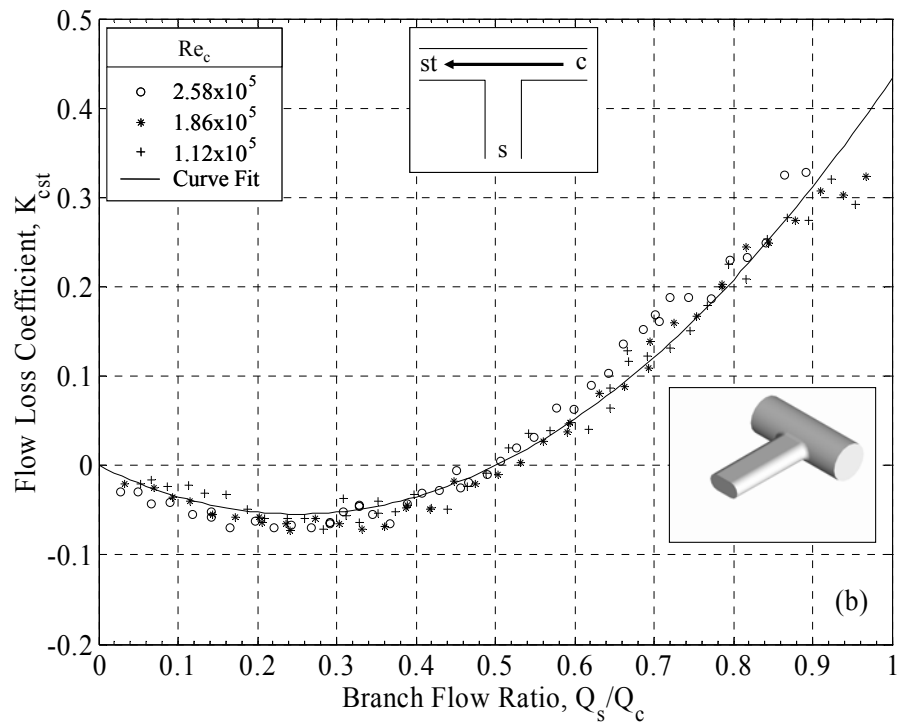
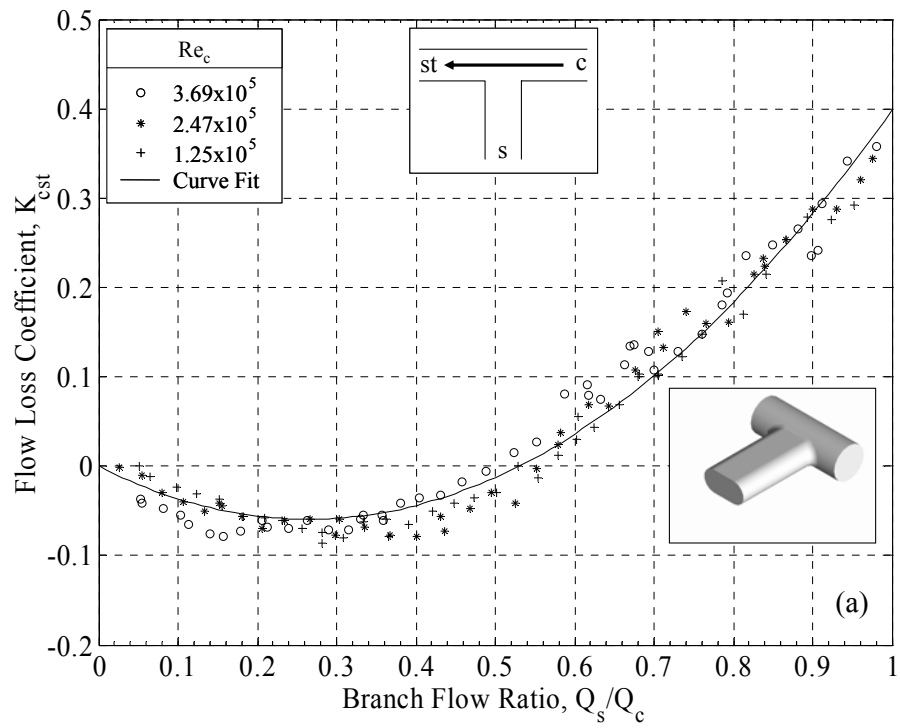


Figure A.12: K_{cst} for oval junction, $W/H=1/2$, $r=0.2 D_s$: (a) $A_c/A_s=1$, (b) $A_c/A_s=2.124$

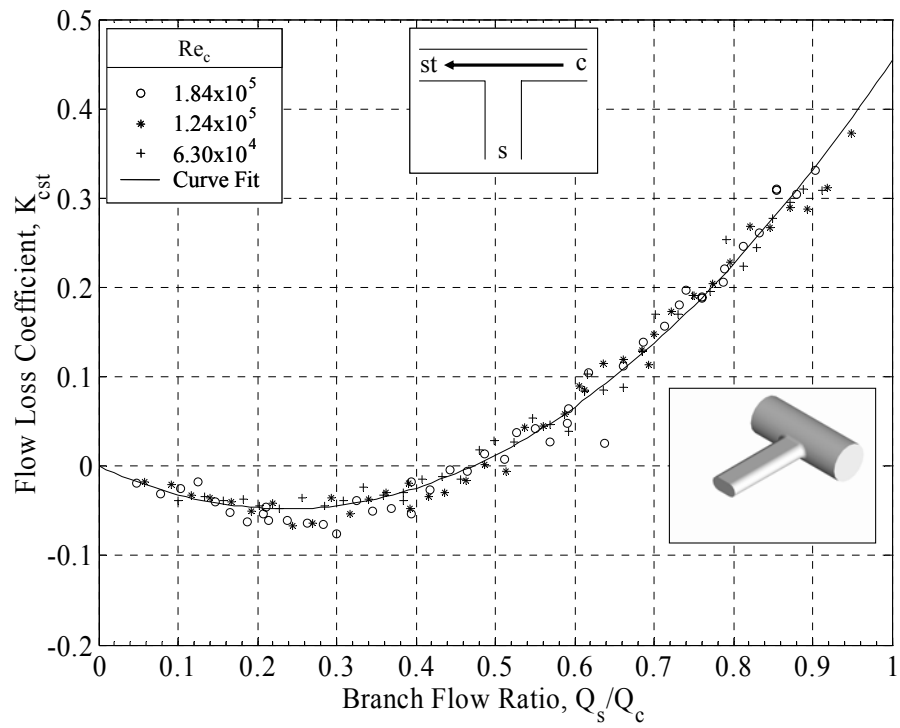


Figure A.13: K_{cst} for oval junction, $A_o/A_s=3.117, W/H=1/2, r=0.2 D_s$

APPENDIX B

CURVE FIT COEFFICIENTS

Least-squares curve fits of measured loss coefficients are used in Chapter 5 for comparison and discussion purposes. The fits are second order functions of Q_s/Q_c with y-intercepts of unity and zero for K_{cs} and K_{cst} , respectively. Thus, for the losses between the combined and side duct:

$$K_{cs} = c_1 \left(\frac{Q_s}{Q_c} \right)^2 + c_2 \left(\frac{Q_s}{Q_c} \right) + 1, \quad (\text{B.1})$$

and between the combined and straight duct:

$$K_{cst} = c_3 \left(\frac{Q_s}{Q_c} \right)^2 + c_4 \left(\frac{Q_s}{Q_c} \right). \quad (\text{B.2})$$

Tables B.1-B.5 list the coefficients c_1 - c_4 in Eqs (B.1) and (B.2) for all junction geometries examined.

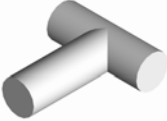
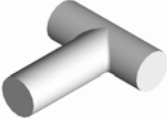
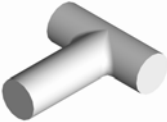


Tee	A_c/A_s	r/D_s	c_1	c_2	c_3	c_4	
	1	0	1.1483	-0.9508	0.8937	-0.4715	
		0.1	1.0281	-1.0624	0.9116	-0.4935	
		0.2		1.118	-1.3876	0.8729	-0.4536
	2.124			1.6207	-1.472	0.8575	-0.4024
	3.117			3.2311	-1.7368	0.8212	-0.3595

Table B.1: Curve fit coefficients for junctions with circular side branches



Tee	A_c/A_i	A_c/A_s	r/D_i	c_1	c_2	c_3	c_4
	1	2.124	0.2	2.2467	-2.2466	0.9656	-0.5497
		3.117		3.3549	-2.8345	0.921	-0.5026

Table B.2: Curve fit coefficients for junctions with tapered circular side branches



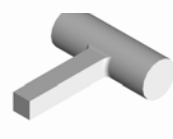
Tee	A_c/A_s	r/D_s	c_1	c_2	c_3	c_4
	1	0.2	0.9563	-1.2963	0.9203	-0.5143
	2.124		2.138	-1.681	0.9232	-0.4804
	3.117		3.6783	-2.3239	0.8505	-0.4043

Table B.3: Curve fit coefficients for junctions with square side branches


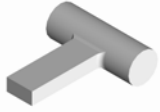
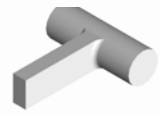
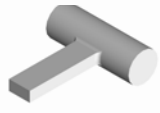
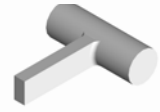
Tee	A_c/A_s	W/H	r/D_s	c_1	c_2	c_3	c_4
	1	1/2	0.2	0.9818	-1.2193	0.8259	-0.4288
	2.124	1/2		1.724	-1.3802	0.8787	-0.4467
	2.124	2		1.9325	-1.6943	0.9723	-0.5238
	3.117	1/2		3.0372	-1.6791	0.8501	-0.4071
	3.117	2		3.7551	-2.168	0.924	-0.4603

Table B.4: Curve fit coefficients for junctions with rectangular side branches



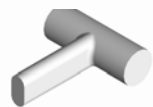

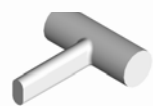
Tee	A_c/A_s	W/H	r/D_s	c_1	c_2	c_3	c_4
	1	$\frac{1}{2}$	0.2	-	-	0.8483	-0.4494
	2.124	$\frac{1}{2}$		-	-	0.8678	-0.4344
	2.124	2		-	-	0.9858	-0.5316
	3.117	$\frac{1}{2}$		-	-	0.8592	-0.4048
	3.117	2		-	-	0.8966	-0.4379

Table B.5: Curve fit coefficients for junctions with oval side branches

BIBLIOGRAPHY

- Bajura, R. A., 1971, "A Model for Flow Distribution in Manifolds," *ASME Journal of Engineering for Power*, 7-12, (Jan. 1971).
- Barbin, A. R., and Jones, J. B., 1963, "Turbulent Flow in the Inlet Region of a Smooth Pipe," *Transactions of the American Society of Engineers, Journal of Basic Engineering*, 85:29-34.
- Bassett, M. D., Pearson, R. J., and Winterbone, D.E., 1999, "Steady-Flow Loss-Coefficient Estimation for Exhaust Manifold Pulse-Converter Type Junctions," *SAE 1999-01-0213*.
- Benedict, R.P., 1980, "Fundamentals of Pipe Flow," John Wiley & Sons, New York.
- Bingham, J. F. and Blair, G. P., 1985, "An Improved Branched Pipe Model for Multi-Cylinder Automotive Engine Calculations," *Proceedings of the Institution of Mechanical Engineers*, 199(D1):65-77.
- Blake, K. A., 1976, "The Design of Piezometer Rings," *Journal of Fluid Mechanics*, 78(2):415-428.
- Butlay, T. and Widenhorn, M., 1993, "Unsteady Flow Calculation of Sophisticated Exhaust Systems Using a Multibranch Junction Model," *Transactions of the ASME*, 115:756-760, (Oct. 1993).
- Chapman, M., Novak, J. M., and Stein, R. A., 1982, "Numerical Modeling of Inlet and Exhaust Flows in Multi-Cylinder Internal Combustion Engines," in *Flows in Internal Combustion Engines*, Uzkan, T., editor. ASME WAM, Phoenix, AZ.
- Fox, Robert W., and McDonald, Alan T., 1998, "Introduction to Fluid Mechanics," John Wiley & Sons, Inc.
- Gardel, A., 1957, "Les Pertes de Charge dans les Ecoulements au Travers de Branchements en Te," Publication No. 44, Ecole Polytechnique de l'Universite de Lausanne. Lausanne, Switzerland.

Gardel, A., and Rechsteiner, G. F., 1971, "Les Pertes de Charge dans les Branchements en Te des Conduites de Section Circulaire," Publication No. 118, Ecole Polytechnique Federale de Lausanne, Lausanne, Switzerland.

Hager, W. H., 1984, "An Approximate Treatment of Flow in Branches and Bends," *Proceedings of the Institution of Mechanical Engineers*, 198C(4):63-69.

Hartnett, J. P., Koh, J. C. Y., and McComas, S. T., 1962 "A Comparison of Predicted and Measured Friction Factors for Turbulent Flow Through Rectangular Ducts," *Transactions of the American Society of Mechanical Engineers, Journal of Heat Transfer* :82-88

Heywood, John B., 1988, "Internal Combustion Engine Fundamentals," McGraw-Hill, New York.

Ito, H., and Imai, K., 1973, "Energy Losses at 90° Pipe Junctions," *Proceedings of the American Society of Civil Engineers, Journal of the Hydraulics Division*, 99(HY9):1353-1368.

Ito, H., Sato, M., and Oka, K., 1984, "Energy Losses Due to Division and Combination of Flow at 90° Wyes," *Bulletin of JSME*, 27(232):2152-2159.

Kinne, E., 1931, "Beitrage zur Kenntnis der hydraulischen Verluste in Abzweigstucken," *Mitteilungen des Hydraulischen Instituts der Technischen Hochschule Munchen*, Heft 4:70-93.

McNown, J. S., 1954, "Mechanics of Manifold Flow," *Transactions of the American Society of Civil Engineers*, 119:1103-1142.

Miller, D. S., 1971, "Internal Flow, A Guide to Losses in Pipe and Duct Systems," BHRA.

Miller, D.S., 1990, "Internal Flow Systems," second edition, BHRA (Information Services) (1990)

Petermann, F., 1929,"Der Verlust in schiefwinkligen Rohrverzweigungen," *Mitteilungen des Hydraulischen Instituts der Technischen Hochschule Munchen*, Heft 3:99-117. (Translation: 'Loss in Oblique-Angled Pipe Branches" *ASME Transactions of the Hydraulic Institute of the Munich Technical University*, No. 3:65-77, (1935)).

Ramamurthy, A. S., 1997, "Combining Flows in 90° Junctions of Rectangular Closed Conduits," *American Society of Civil Engineers, Journal of Hydraulic Engineering*, 1012-1019, (Nov. 1997).

Tallio, K. V., Tobis, B. J., and Selamet, A., 1993, "The Application of Steady-Flow Loss Correlations to Intake Manifold Design," *SAE 930608*.

Vogel, G., 1926, "Untersuchungen über den Verlust in rechtwinkligen Rohrverzweigungen," *Mitteilungen des Hydraulischen Instituts der Technischen Hochschule München*, Heft 1:75-90.

Vogel, G., 1928, "Untersuchungen über den Verlust in rechtwinkligen Rohrverzweigungen," *Mitteilungen des Hydraulischen Instituts der Technischen Hochschule München*, Heft 2:61-64.

Wang, J-S., and Tullis, J. P., 1974, "Turbulent Flow in the Entry Region of a Rough Pipe," *Transactions of the American Society of Mechanical Engineers, Journal of Fluids Engineering*, Ser. I, 96:62-68.